INSTITUTO FEDERAL DE EDUCAÇÃO, CIÊNCIA E TECNOLOGIA GOIANO
CAMPUS RIO VERDE
PROGRAMA DE PÓS-GRADUAÇÃO EM CIÊNCIAS AGRÁRIAS – AGRONOMIA

Marlus Dias Silva

Agricultura Vertical de Precisão aplicada a Microverdes de Lentilha e Gergelim: Telemetria Auditável, Manejo Luminoso e Eficiência Energética da Produção de Biomassa

RIO VERDE – GO

junho – 2026

INSTITUTO FEDERAL DE EDUCAÇÃO, CIÊNCIA E TECNOLOGIA GOIANO
CAMPUS RIO VERDE
PROGRAMA DE PÓS-GRADUAÇÃO EM CIÊNCIAS AGRÁRIAS – AGRONOMIA

Marlus Dias Silva

Agricultura Vertical de Precisão aplicada a Microverdes de Lentilha e Gergelim: Telemetria Auditável, Manejo Luminoso e Eficiência Energética da Produção de Biomassa

Tese apresentada como parte das exigências para obtenção do título de Doutor em Ciências Agrárias – Agronomia, no Programa de Pós-Graduação em Ciências Agrárias – Agronomia, do Instituto Federal de Educação, Ciência e Tecnologia Goiano – Campus Rio Verde.

Autor: Me. Marlus Dias Silva
Orientador: Prof. Dr. Fabiano Guimarães Silva
Coorientador: Prof. Dr. Adriano Soares de Oliveira Bailão
Coorientador: Prof. Dr. Ítalo Moraes Rocha Guedes

RIO VERDE – GO

junho – 2026

Ficha de identificação da obra elaborada pelo autor, através do
Programa de Geração Automática do Sistema Integrado de Bibliotecas do IF Goiano - SIBi

S586 Silva, Marlus Dias

Agricultura Vertical de Precisão aplicada a Microverdes de Lentilha e Gergelim: Telemetria Auditável, Manejo Luminoso e Eficiência Energética da Produção de Biomassa / Marlus Dias Silva. Rio Verde, 2026.
80 f. il.

Orientador: Prof. Dr. Fabiano Guimarães Silva.
Coorientadores: Prof. Dr. Adriano Soares de Oliveira Bailão; Prof. Dr. Ítalo Moraes Rocha Guedes.
Tese (Doutorado) - Instituto Federal Goiano, curso de Doutorado em Ciências Agrárias - Agronomia - Rio Verde (Campus Rio Verde).
1. Agricultura vertical. 2. Microverdes. 3. Iluminação artificial. 4. Internet das Coisas. 5. Eficiência energética. I. Título.

SERVIÇO PÚBLICO FEDERAL
MINISTÉRIO DA EDUCAÇÃO
SECRETARIA DE EDUCAÇÃO PROFISSIONAL E TECNOLÓGICA
INSTITUTO FEDERAL DE EDUCAÇÃO, CIÊNCIA E TECNOLOGIA GOIANO

Documentos 5/2026 - CMPRV/IFGOIANO

Agricultura Vertical de Precisão aplicada a Microverdes de Lentilha e Gergelim: Telemetria Auditável, Manejo Luminoso e Eficiência Energética da Produção de Biomassa

Autor: Marlus Dias Silva
Orientador: Fabiano Guimarães Silva

TITULAÇÃO: Doutor em Ciências Agrárias - Agronomia - Área de Concentração Produção Vegetal Sustentável no Cerrado

gov.br
Documento assinado digitalmente
KEYNES MASAYOSHI KANNO
Data: 01/07/2026 09:38:25-0300
Verifique em https://validar.iti.gov.br

APROVADO em 30 de junho de 2026.

Prof. Dr. Keynes Masayoshi Kanno
Avaliador extern - Universidade Federal de Uberlândia

Prof. Dr. José Weselli de Sá Andrade
Avaliador externo - IF Goiano / Campus Rio Verde

Prof. Dra. Paula Sperotto Alberto Faria
Avaliador externo - IF Goiano / Campus Rio Verde

Prof. Dr. Marconi Batista Teixeira
Avaliador interno - IF Goiano / Campus Rio Verde

Prof. Dr. Fabiano Guimarães Silva
Presidente da Banca - IF Goiano / Campus Rio Verde

Documento assinado eletronicamente por:

- **Fabiano Guimaraes Silva**, **PROFESSOR ENS BASICO TECN TECNOLOGICO** , em 01/07/2026 09:13:44.
- **Paula Sperotto Alberto Faria**, **PROFESSOR ENS BASICO TECN TECNOLOGICO** , em 01/07/2026 09:16:26.
- **Marconi Batista Teixeira**, **COORDENADOR(A) DE CURSO - FUC1 - CCMDAGRO-R**, em 01/07/2026 09:24:24.
- **Jose Weselli de Sa Andrade** , **PROFESSOR ENS BASICO TECN TECNOLOGICO** , em 01/07/2026 09:31:21.

Este documento foi emitido pelo SUAP em 01/07/2026. Para comprovar sua autenticidade, faça a leitura do QRCode ao lado ou acesse https://suap.ifgoiano.edu.br/autenticar-documento/ e forneça os dados abaixo:

Código Verificador: 836579
Código de Autenticação: 5162cb360e

INSTITUTO FEDERAL
Goiano

Repositório Institucional do IF Goiano - RIIF Goiano
Sistema Integrado de Bibliotecas

TERMO DE CIÊNCIA E DE AUTORIZAÇÃO

PARA DISPONIBILIZAR PRODUÇÕES TÉCNICO-CIENTÍFICAS NO REPOSITÓRIO INSTITUCIONAL DO IF GOIANO

Com base no disposto na Lei Federal nº 9.610, de 19 de fevereiro de 1998, AUTORIZO o Instituto Federal de Educação, Ciência e Tecnologia Goiano a disponibilizar gratuitamente o documento em formato digital no Repositório Institucional do IF Goiano (RIIF Goiano), sem ressarcimento de direitos autorais, conforme permissão assinada abaixo, para fins de leitura, download e impressão, a título de divulgação da produção técnico-científica no IF Goiano.

IDENTIFICAÇÃO DA PRODUÇÃO TÉCNICO-CIENTÍFICA

- [x] Tese (doutorado)
- [ ] Dissertação (mestrado)
- [ ] Monografia (especialização)
- [ ] TCC (graduação)
- [ ] Artigo científico
- [ ] Capítulo de livro
- [ ] Livro
- [ ] Trabalho apresentado em evento
- [ ] Produto técnico e educacional - Tipo:

Nome completo do autor: Marlus Dias Silva

Matrícula: 2022202320140007

Título do trabalho: Agricultura Vertical de Precisão aplicada a Microverdes de Lentilha e Gergelim: Telemetria Auditável,

RESTRIÇÕES DE ACESSO AO DOCUMENTO

Documento confidencial: [x] Não [ ] Sim, justifique:

Informe a data que poderá ser disponibilizado no RIIF Goiano: 2 / 7 / 202

O documento está sujeito a registro de patente? [ ] Sim [x] Não

O documento pode vir a ser publicado como livro? [x] Sim [ ] Não

DECLARAÇÃO DE DISTRIBUIÇÃO NÃO-EXCLUSIVA

O(a) referido(a) autor(a) declara:

• Que o documento é seu trabalho original, detém os direitos autorais da produção técnico-científica e não infringe os direitos de qualquer outra pessoa ou entidade;

• Que obteve autorização de quaisquer materiais inclusos no documento do qual não detém os direitos de autoria, para conceder ao Instituto Federal de Educação, Ciência e Tecnologia Goiano os direitos requeridos e que este material cujos direitos autorais são de terceiros, estão claramente identificados e reconhecidos no texto ou conteúdo do documento entregue;

• Que cumpriu quaisquer obrigações exigidas por contrato ou acordo, caso o documento entregue seja baseado em trabalho financiado ou apoiado por outra instituição que não o Instituto Federal de Educação, Ciência e Tecnologia Goiano.

Rio Verde (Local) — 1 / 7 / 202 (Data)

Documento assinado digitalmente
gov.br
MARLUS DIAS SILVA
Data: 01/07/2026 14:51:30-0300
Verifique em https://validar.iti.gov.br

Assinatura do autor e/ou detentor dos direitos autorais

Ciente e de acordo:

Documento assinado digitalmente
gov.br
FABIANO GUIMARAES SILVA
Data: 01/07/2026 15:47:50-0300
Verifique em https://validar.iti.gov.br

Assinatura do(a) orientador(a)

SERVIÇO PÚBLICO FEDERAL
MINISTÉRIO DA EDUCAÇÃO
SECRETARIA DE EDUCAÇÃO PROFISSIONAL E TECNOLÓGICA
INSTITUTO FEDERAL DE EDUCAÇÃO, CIÊNCIA E TECNOLOGIA GOIANO

Ata nº 51/2026 - DPGPI-RV/CMPRV/IFGOIANO

ATA Nº/176

BANCA EXAMINADORA DE DEFESA DE TESE

Ao trigésimo dia do mês de junho do ano de dois mil e vinte e seis, às 14:00h, reuniram-se os componentes da Banca Examinadora: sob a presidência do primeiro, Prof. Dr. Fabiano Guimarães Silva (Presidente); Prof. Dr. Marconi Batista Teixeira (Avaliador Interno); Prof. Dr. Keynes Masayoshi Kanno (Avaliador Externo); Prof. Dr. José Weselli de Sá Andrade (Avaliador Externo) e Profa. Dra. Paula Sperotto Alberto Faria (Avaliadora Externa) em sessão pública realizada no auditório da DPGPI do IF Goiano – Campus Rio Verde, para procederem a avaliação da defesa de Tese, em nível de Doutorado, de autoria de **Marlus Dias Silva,** discente do Programa de Pós-Graduação em Ciências Agrárias – Agronomia do Instituto Federal Goiano – Campus Rio Verde. A sessão foi aberta pelo presidente da Banca Examinadora, Prof. Dr. Fabiano Guimarães Silva, que fez a apresentação formal dos membros da Banca. A palavra, a seguir, foi concedida ao autor da Tese para, em 40 min., proceder à apresentação de seu trabalho. Terminada a apresentação, cada membro da banca arguiu o examinado, tendo-se adotado o sistema de diálogo sequencial. Terminada a fase de arguição, procedeu-se a avaliação da defesa. Tendo-se em vista as normas que regulamentam o Programa de Pós-Graduação em Ciências Agrárias – Agronomia, e procedidas às correções recomendadas, a Tese foi **APROVADA**, considerando-se integralmente cumprido este requisito para fins de obtenção do título de **DOUTOR EM CIÊNCIAS AGRÁRIAS-AGRONOMIA,** na área de concentração Produção Vegetal Sustentável no Cerrado, pelo Instituto Federal Goiano – Campus Rio Verde. A conclusão do curso dar-se-á quando da entrega na secretaria do PPGCA-AGRO da versão definitiva da Tese, com as devidas correções. Assim sendo, esta ata perderá a validade se não cumprida essa condição, em até **60** (sessenta) dias da sua ocorrência. Cumpridas as formalidades da pauta, a presidência da mesa encerrou esta sessão de defesa de Tese de Doutorado, e para constar, eu, Marconi Batista Teixeira, coordenador do PPGCA-AGRO, lavrei a presente Ata, que, após lida e achada conforme, será assinada pelos membros da Banca Examinadora.

Prof. Dr. Fabiano Guimarães Silva (Presidente)

Prof. Dr. Marconi Batista Teixeira (Avaliador Interno)

Prof. Dr. Keynes Masayoshi Kanno (Avaliador Externo)

gov.br Documento assinado digitalmente
KEYNES MASAYOSHI KANNO
Data: 01/07/2026 09:11:49-0300
Verifique em https://validar.iti.gov.br

Prof. Dr. José Weselli de Sá Andrade (Avaliador Externo)

Profa. Dra. Paula Sperotto Alberto Faria (Avaliadora Externa)

Documento assinado eletronicamente por:

- **Paula Sperotto Alberto Faria**, **PROFESSOR ENS BASICO TECN TECNOLOGICO** , em 30/06/2026 17:23:00.
- **Fabiano Guimaraes Silva**, **DIRETOR(A) GERAL - CD2 - CMPRV**, em 30/06/2026 17:27:56.
- **Jose Weselli de Sa Andrade** , **PROFESSOR ENS BASICO TECN TECNOLOGICO** , em 30/06/2026 19:13:17.
- **Marconi Batista Teixeira**, **COORDENADOR(A) DE CURSO - FUC1 - CCMDAGRO-R** , em 30/06/2026 20:53:10.

Este documento foi emitido pelo SUAP em 30/06/2026. Para comprovar sua autenticidade, faça a leitura do QRCode ao lado ou acesse https://suap.ifgoiano.edu.br/autenticar-documento/ e forneça os dados abaixo:

Código Verificador: 836406
Código de Autenticação: d768d4d4ab

INSTITUTO FEDERAL GOIANO
Campus Rio Verde
Rodovia Sul Goiana, Km 01, Zona Rural, 01, Zona Rural, RIO VERDE / GO, CEP 75901-970
(64) 3624-1000

DECLARAÇÃO DE CORREÇÃO ORTOGRÁFICA E GRAMATICAL

Eu, **Samylla Tássia Ferreira de Freitas**, certifico que realizei as correções ortográficas e gramaticais na tese intitulada **"Agricultura Vertical de Precisão aplicada a Microverdes de Lentilha e Gergelim: Telemetria Auditável, Manejo Luminoso e Eficiência Energética da Produção de Biomassa"**, de autoria do estudante **Marlus Dias Silva**. A tese foi revisada em conformidade com as normas da língua portuguesa, com ajustes voltados para a adequação ortográfica, gramatical e de estilo.

Rio Verde, 01 de julho de 2026.

gov.br
Documento assinado digitalmente
SAMYLLA TASSIA FERREIRA DE FREITAS
Data: 01/07/2026 12:28:43-0300
Verifique em https://validar.iti.gov.br

_____

Profa. Dra. Samylla Tássia Ferreira de Freitas

Revisora

Agradecimentos

À minha família, pelo apoio, incentivo, paciência e compreensão ao longo de toda esta trajetória. Em especial, aos meus pais, Martinho Romualdo da Silva e Marli Hozoria Dias Silva, por todo amor, ensinamentos, apoio e por serem base fundamental da minha formação pessoal e profissional. À minha irmã, Marliane Dias Silva, pelo carinho, incentivo e presença ao longo desta caminhada.

Às minhas filhas, Clara Maia Dias e Lívia Maia Dias, que representam uma das maiores motivações da minha vida. Que esta conquista possa servir como exemplo de dedicação, persistência e fé na construção dos sonhos.

Ao Instituto Federal Goiano – Campus Rio Verde e ao Programa de Pós-Graduação em Ciências Agrárias – Agronomia (PPGCA-Agro), pela formação acadêmica, pela estrutura institucional e pelas oportunidades oferecidas durante o desenvolvimento desta tese.

Ao Conselho Nacional de Desenvolvimento Científico e Tecnológico (CNPq), pelo apoio à pesquisa e pelo incentivo à formação científica, que contribuíram para a realização deste trabalho e para o desenvolvimento das atividades vinculadas ao doutorado.

Ao meu orientador, Prof. Dr. Fabiano Guimarães Silva, pela orientação, confiança, incentivo e contribuições fundamentais ao desenvolvimento desta tese. Aos meus coorientadores, Prof. Dr. Ítalo Moraes Rocha Guedes e Prof. Dr. Adriano Soares de Oliveira Bailão, pelas contribuições científicas, técnicas e acadêmicas, que foram essenciais para a consolidação dos resultados apresentados.

Aos coautores dos artigos que compõem esta tese, Dra. Jaqueline Martins Vasconcelos, Dra. Fábia Barbosa da Silva, Prof. Dr. Adriano Soares de Oliveira Bailão, Dr. Ítalo Moraes Rocha Guedes, Prof. Dr. Márcio da Silva Vilela, Prof. Dr. Adriano Carvalho Costa, Prof. Dr. Márcio Rosa, Dr. Lucas Loram Lourenço e Prof. Dr. Fabiano Guimarães Silva, pelas contribuições diretas na construção científica, experimental, tecnológica e analítica dos trabalhos desenvolvidos. A participação de cada um foi importante para transformar as ideias iniciais em resultados concretos, artigos científicos e produtos tecnológicos associados à agricultura vertical de precisão.

Ao Engenheiro Mecânico Bruno Antunes Martins, pela contribuição no desenvolvimento do hardware do ambiente controlado utilizado nesta pesquisa. Sua colaboração foi importante para a estruturação física e funcional do sistema experimental, contribuindo para a execução dos estudos em agricultura vertical de precisão.

Aos colegas, colaboradores e parceiros que contribuíram direta ou indiretamente para a condução dos experimentos, para o desenvolvimento dos sistemas computacionais, para a análise dos dados e para a consolidação dos registros de software apresentados nesta tese.

Por fim, agradeço a todos que, de alguma forma, participaram desta caminhada, seja pelo apoio técnico, científico, institucional ou humano. Cada contribuição foi importante para a realização deste trabalho e para a construção desta etapa da minha formação acadêmica e profissional.

BIOGRAFIA DO AUTOR

Marlus Dias Silva é professor do Instituto Federal de Educação, Ciência e Tecnologia Goiano – Campus Rio Verde, atuando na área de Ciência da Computação. É mestre em Ciências pela Faculdade de Engenharia Elétrica da Universidade Federal de Uberlândia e desenvolve atividades acadêmicas, científicas e tecnológicas na interface entre Computação, Internet das Coisas, sistemas embarcados, automação, análise de dados e Agricultura Digital.

No âmbito da pós-graduação em Ciências Agrárias – Agronomia, sua pesquisa concentrou-se na aplicação de infraestrutura digital aberta, telemetria auditável e estratégias de iluminação artificial para sistemas de agricultura vertical de precisão. A tese integrou experimentos com microverdes cultivados em ambiente controlado, análise de resposta fisiológica e produtiva, eficiência energética, rastreabilidade dos protocolos luminosos e desenvolvimento de produtos tecnológicos associados à automação e ao monitoramento de sistemas de cultivo *indoor*.

Ao longo da pesquisa, participou do desenvolvimento de soluções computacionais aplicadas à agricultura vertical, incluindo arquitetura IoT, aplicações híbridas, monitoramento ambiental e energético, integração de sensores e validação operacional de protocolos experimentais, contribuindo para aproximar Ciência da Computação, Agronomia e Agricultura de Precisão em ambientes controlados.

Sumário

ÍNDICE DE TABELAS

ÍNDICE DE FIGURAS

SUPLEMENTAR Figure 7. Supplementary characterization of chamber microclimate during Constant and Gaussian windows.

LISTA DE SÍMBOLOS, SIGLAS, ABREVIAÇÕES E UNIDADES

Símbolo/Sigla	**Significado**	**Unidade**
%	Porcentagem	%
$\pm$	Mais ou menos	–
α	Nível de significância estatística	–
AEC	*Areal Energy Consumption*; consumo de energia por área	kWh m^{-2}
ANOVA	Análise de variância	–
API	*Application Programming Interface*; interface de programação de aplicações	–
Cart/CART	Carotenoides	μg g^{-1}
CE	Condutividade elétrica	dS m^{-1}
CHL	Comprimento do hipocótilo	cm
Chla	Clorofila *a*	μg g^{-1}
Chlb	Clorofila *b*	μg g^{-1}
CO_2	Dióxido de carbono	ppm
CTLA/TLA	Área foliar total	cm^2
CV	Coeficiente de variação	%
DLI	*Daily Light Integral*; integral diária de luz	mol m^{-2} d^{-1}
EEMS	*Energy-to-Mass Efficiency*; eficiência energia–massa	g kWh^{-1}
EnE	Eficiência energética	g W^{-1}
ESP32	Microcontrolador utilizado em sistemas embarcados e IoT	–
ETR	Taxa de transporte de elétrons	–
Fv/Fm	Rendimento quântico máximo do fotossistema II	–
HFW	Massa fresca do hipocótilo	g
HMD	Massa seca do hipocótilo	g
IoT	*Internet of Things*; Internet das Coisas	–
LED	*Light Emitting Diode*; diodo emissor de luz	–
LFW	Massa fresca da folha	g
LMD	Massa seca da folha	g
LPFI	*Light Profile Fidelity Index*; índice de fidelidade do perfil luminoso	–

MAE	Erro absoluto médio	–
MQTT	*Message Queuing Telemetry Transport*; protocolo de mensagens para IoT	–
NPQ	Extinção não fotoquímica	–
PCA	Análise de Componentes Principais	–
PFAL	*Plant Factory with Artificial Lighting*; fábrica de plantas com iluminação artificial	–
pH	Potencial hidrogeniônico	–
PPFD	*Photosynthetic Photon Flux Density*; densidade de fluxo de fótons fotossintéticos	μmol m^{-2} s^{-1}
PVFS	*Precision Vertical Farming System*; sistema de agricultura vertical de precisão	–
qP	Coeficiente de extinção fotoquímica	–
QA/QC	Controle e garantia da qualidade dos dados	–
RBW	Combinação espectral vermelho–azul–branco	–
RH/UR	Umidade relativa do ar	%
RMSE	Raiz do erro quadrático médio	–
RTC	*Real-Time Clock*; relógio de tempo real	–
SEC	*Specific Energy Consumption*; consumo específico de energia	kWh g^{-1}
TMD/TDM	Massa seca total	g
TOST	*Two One-Sided Tests*; teste de equivalência	–
UART	*Universal Asynchronous Receiver/Transmitter*; interface serial assíncrona	–
Y(II)	Rendimento quântico efetivo do fotossistema II	–

Resumo

Esta tese investigou estratégias de iluminação artificial e infraestrutura digital aplicada à agricultura vertical de precisão, com ênfase em microverdes cultivados em ambiente controlado. O trabalho integrou dois eixos principais: a avaliação dos efeitos de espectros luminosos e regimes temporais de iluminação sobre o desempenho fisiológico e produtivo de microverdes, e o desenvolvimento de uma arquitetura IoT aberta e auditável para controle, monitoramento e registro de experimentos em sistemas de cultivo indoor. No estudo com microverdes de lentilha, verificou-se que regimes constantes, especialmente sob luz vermelha, branca e RBW, favoreceram a produção de biomassa e a eficiência energética, enquanto o regime gaussiano apresentou maior potencial para estimular o acúmulo de carotenoides. No estudo com microverdes de gergelim, foi desenvolvido e validado o *Precision Vertical Farming System* (PVFS), capaz de executar perfis dinâmicos de PPFD, registrar telemetria ambiental e elétrica e integrar métricas como *Areal Energy Consumption* (AEC), *Specific Energy Consumption* (SEC) e *Energy-to-Mass Efficiency* (EEMS). Os resultados demonstraram que a equivalência de DLI não garante equivalência de desempenho energético, destacando o tratamento Red–Constant como mais eficiente na relação energia–biomassa. A tese contribui ao demonstrar que a agricultura vertical de precisão deve integrar resposta biológica, eficiência energética e rastreabilidade digital para alcançar maior robustez experimental, reprodutibilidade e racionalidade operacional.

Palavras-chave: agricultura vertical. microverdes. iluminação artificial. internet das coisas. eficiência energética. telemetria.

Abstract

This thesis investigated artificial lighting strategies and digital infrastructure applied to precision vertical farming, with emphasis on microgreens cultivated under controlled environment conditions. The work integrated two main axes: the evaluation of light spectra and temporal lighting regimes on the physiological and productive performance of microgreens, and the development of an open and auditable IoT architecture for control, monitoring, and experimental data recording in indoor cultivation systems. In the study with lentil microgreens, constant lighting regimes, especially under red, white, and RBW light, favored biomass production and energy efficiency, whereas the Gaussian regime showed greater potential to stimulate carotenoid accumulation. In the study with sesame microgreens, the *Precision Vertical Farming System* (PVFS) was developed and validated, enabling the execution of dynamic PPFD profiles, environmental and electrical telemetry recording, and the integration of metrics such as *Areal Energy Consumption* (AEC), *Specific Energy Consumption* (SEC), and *Energy-to-Mass Efficiency* (EEMS). The results demonstrated that DLI equivalence does not guarantee equivalent energy performance, with the Red–Constant treatment showing the best energy–biomass relationship. This thesis contributes by demonstrating that precision vertical farming must integrate biological response, energy efficiency, and digital traceability to achieve greater experimental robustness, reproducibility, and operational rationality.

Keywords: vertical farming. microgreens. artificial lighting. internet of things. energy efficiency. telemetry.

1 Introdução

A agricultura vertical tem se consolidado como uma alternativa promissora para a produção de alimentos em ambientes urbanos e controlados, especialmente diante da urbanização crescente, da limitação de áreas agricultáveis e da demanda por sistemas produtivos mais intensivos, resilientes e sustentáveis (Van Gerrewey; BOON; GEELEN, 2022; BANTIS et al., 2024; KABIR et al., 2023). Nesse contexto, as *Plant Factories with Artificial Lighting* (PFALs) destacam-se por possibilitarem o controle preciso de variáveis ambientais como temperatura, umidade, nutrição e iluminação, favorecendo maior previsibilidade produtiva, padronização da qualidade e uso mais racional dos recursos (BANTIS et al., 2024; KABIR et al., 2023).

Entre os fatores de manejo em sistemas de cultivo *indoor*, a luz ocupa posição central, pois afeta diretamente a fotossíntese, a morfogênese, o crescimento, a composição bioquímica e o desempenho produtivo das plantas (BUDAVÁRI et al., 2024; SHIBAEVA et al., 2022). O avanço das tecnologias de iluminação por LEDs ampliou significativamente a capacidade de ajuste da intensidade luminosa, do fotoperíodo e da composição espectral, tornando possível adaptar as condições de cultivo a objetivos agronômicos específicos (BUDAVÁRI et al., 2024; SHIBAEVA et al., 2022). Além disso, a resposta vegetal em ambientes controlados depende não apenas do espectro empregado, mas também da duração da exposição luminosa e da forma temporal com que a radiação é distribuída ao longo do período de iluminação. Assim, a modulação do perfil de densidade de fluxo de fótons fotossintéticos (*Photosynthetic Photon Flux Density*, PPFD) torna-se um componente relevante para interpretar o desempenho fisiológico, produtivo e energético das plantas (BUDAVÁRI et al., 2024; SHIBAEVA et al., 2022; SILVA et al., 2024).

No caso dos microverdes, essa discussão torna-se ainda mais importante. Esses produtos apresentam ciclo curto, alta densidade de cultivo, elevado valor agregado e crescente interesse comercial, características que os tornam especialmente adequados para PFALs e outros sistemas de agricultura vertical (DUBEY et al., 2024; BUDAVÁRI et al., 2024). Além do interesse produtivo, os microverdes se destacam pelo teor de compostos funcionais e pelo potencial nutricional, o que reforça a necessidade de estratégias de cultivo capazes de conciliar produtividade, qualidade fisiológica e eficiência no uso da energia (DUBEY et al., 2024; SHIBAEVA et al., 2022). Portanto, em sistemas de ambiente controlado, não basta produzir biomassa; é necessário compreender quanto de energia foi necessário para produzi-la e se esse custo é compatível com a finalidade agronômica, econômica e tecnológica do sistema.

Apesar do avanço da literatura sobre qualidade espectral da luz, ainda persistem lacunas quanto ao efeito do perfil temporal de fornecimento da radiação ao longo do período de iluminação. Muitos estudos concentram-se em regimes constantes ou em comparações entre diferentes durações de luz, enquanto ainda são menos frequentes investigações que avaliem, sob a mesma

integral luminosa diária (*Daily Light Integral*, DLI), como diferentes perfis de PPFD influenciam simultaneamente crescimento, fotossíntese, biomassa e desempenho energético (BUDAVÁRI et al., 2024; SILVA et al., 2024; SILVA et al., 2026). Essa lacuna é particularmente relevante em PFALs, nas quais a iluminação representa uma parcela expressiva do consumo elétrico e, por isso, precisa ser analisada não apenas em termos de resposta biológica, mas também em termos de custo energético por unidade de biomassa produzida.

Sob essa perspectiva, métricas como *Areal Energy Consumption* (AEC), *Specific Energy Consumption* (SEC) e *Energy-to-Mass Efficiency* (EEMS) tornam-se essenciais para interpretar a eficiência real de receitas de luz em agricultura vertical (SILVA et al., 2026). A simples equivalência de DLI não implica, necessariamente, equivalência de desempenho energético, pois diferentes trajetórias temporais de fornecimento de luz podem resultar em diferentes custos elétricos e em diferentes relações entre energia consumida e biomassa gerada (SILVA et al., 2026). Assim, a análise da iluminação em sistemas de cultivo controlado deve avançar de uma abordagem centrada apenas na fotobiologia para uma avaliação integrada entre resposta fisiológica, produção vegetal, consumo energético e eficiência operacional.

Além da dimensão agronômica, o avanço da agricultura vertical depende da consolidação de infraestruturas tecnológicas capazes de executar, registrar e validar, com precisão, os protocolos experimentais adotados. Em muitos estudos conduzidos em PFALs, as condições de cultivo são descritas de forma textual, mas nem sempre são acompanhadas por sistemas que permitam monitorar continuamente a execução do experimento, registrar variáveis ambientais e energéticas em tempo real e assegurar a rastreabilidade dos dados produzidos. Essa limitação compromete a reprodutibilidade, dificulta comparações entre estudos e reduz a robustez metodológica de experimentos envolvendo iluminação dinâmica, sensores ambientais e análise integrada entre desempenho biológico e consumo de energia (KABIR et al., 2023; BANTIS et al., 2024; SILVA et al., 2026).

Nesse cenário, esta tese foi concebida a partir da integração entre dois eixos centrais. O primeiro está relacionado à compreensão de como diferentes estratégias de iluminação artificial afetam o crescimento, a fisiologia, a biomassa e a qualidade de microverdes cultivados em ambiente controlado. O segundo está associado ao desenvolvimento de uma infraestrutura digital aberta e auditável para agricultura vertical de precisão, capaz de transformar protocolos de cultivo em rotinas executáveis, monitoráveis e rastreáveis, ampliando a confiabilidade experimental e o potencial de aplicação dos resultados.

O primeiro eixo é desenvolvido no Capítulo 2, correspondente ao artigo publicado na *Frontiers in Plant Science*. Nesse estudo, foram avaliados os efeitos de diferentes espectros e regimes temporais de iluminação sobre microverdes de lentilha (*Lens culinaris*) cultivados em sistema de agricultura vertical (SILVA et al., 2024). Os resultados demonstraram que regimes constantes, especialmente sob luz vermelha, branca e RBW, favoreceram a produção de biomassa e a eficiência energética, enquanto o regime gaussiano promoveu maior acúmulo de carotenoides.

Além disso, variações em pigmentos e parâmetros fisiológicos, como clorofilas, rendimento fotoquímico e coeficiente de extinção fotoquímica, evidenciaram que a modulação temporal da luz afeta não apenas o rendimento, mas também a qualidade funcional e o desempenho fotossintético das plantas (SILVA et al., 2024). Esses achados mostram que a estratégia luminosa ideal não é única, devendo ser definida de acordo com a finalidade produtiva: maximização de biomassa, melhoria da qualidade fisiológica, estímulo ao acúmulo de compostos bioativos ou maior racionalidade energética.

Entretanto, identificar respostas biológicas promissoras não é suficiente quando o objetivo é estabelecer protocolos robustos, reproduzíveis e tecnicamente auditáveis para sistemas de produção vegetal *indoor*. Torna-se necessário integrar sensores, automação, telemetria, controle programável e armazenamento estruturado de dados em uma arquitetura que permita não apenas aplicar os tratamentos planejados, mas também verificar se tais tratamentos foram efetivamente executados ao longo de todo o ciclo experimental (SILVA et al., 2026). Em outras palavras, além de responder qual estratégia luminosa produz melhor desempenho, é necessário garantir que essa estratégia seja operacionalmente confiável e experimentalmente rastreável.

Essa perspectiva é aprofundada no Capítulo 3, correspondente ao artigo aceito para publicação na *Smart Agricultural Technology*. Nesse estudo, foi desenvolvido e validado um *Precision Vertical Farming System* (PVFS) de arquitetura aberta, aplicado ao cultivo de microverdes de gergelim sob perfis temporais constantes e gaussianos, com fotoperíodo fixo de 12 h e DLI equalizado em 10,8 mol m^{-2} d^{-1} (SILVA et al., 2026). O sistema foi projetado para executar perfis dinâmicos de PPFD, registrar telemetria ambiental e elétrica com alta regularidade temporal e elevada completude de dados, além de integrar métricas como AEC, SEC e EEMS à análise agronômica (SILVA et al., 2026). Essa abordagem responde a uma limitação recorrente em experimentos com iluminação dinâmica: a ausência de dados operacionais auditáveis que permitam verificar se o protocolo planejado foi efetivamente executado durante o cultivo (SILVA et al., 2026).

Os resultados do Capítulo 3 evidenciam a relevância da integração entre agronomia, energia e arquitetura computacional. Mesmo sob DLI equivalente, o perfil gaussiano elevou o custo energético por biomassa gerada na maior parte dos espectros, sem produzir ganhos proporcionais de massa seca. O tratamento Red–Constant apresentou a maior eficiência energética, expressa por maior EEMS e menor SEC, enquanto a luz branca exibiu o maior custo energético por unidade de biomassa (SILVA et al., 2026). Dessa forma, a equivalência da luz total fornecida ao longo do dia não garante equivalência de retorno produtivo por unidade de energia consumida. O trabalho, portanto, amplia a discussão clássica sobre desempenho vegetal ao incorporar, simultaneamente, gestão energética, rastreabilidade de dados e validação operacional dos protocolos de iluminação.

A principal contribuição desta tese não reside apenas na comparação entre tratamentos luminosos, mas na articulação entre resposta biológica, desempenho energético e infraestrutura digital. Ao reunir avaliação fisiológica de microverdes, controle programável da iluminação,

monitoramento contínuo e métricas explícitas de energia por biomassa, a tese propõe uma abordagem integrada para agricultura vertical de precisão, com potencial de aplicação tanto em pesquisa quanto no desenvolvimento de soluções tecnológicas voltadas à produção vegetal em ambiente controlado.

Com base nessa articulação, o objetivo geral desta tese foi investigar como diferentes estratégias de iluminação artificial influenciam o desempenho fisiológico, produtivo e energético de microverdes em sistemas de agricultura vertical, bem como desenvolver uma arquitetura aberta e auditável capaz de sustentar experimentalmente essa investigação. Especificamente, buscou-se: (i) avaliar os efeitos de regimes temporais de iluminação e diferentes espectros sobre o crescimento, a biomassa, a fotossíntese e a qualidade fisiológica de microverdes; (ii) quantificar o custo energético associado à geração de biomassa, por meio de métricas como AEC, SEC e EEMS; (iii) desenvolver e validar uma infraestrutura IoT de agricultura vertical de precisão apta a executar protocolos dinâmicos de iluminação com rastreabilidade operacional e suporte à análise integrada entre energia e produção; e (iv) consolidar os produtos tecnológicos derivados da pesquisa, com ênfase nos registros de software associados ao desenvolvimento da arquitetura proposta.

Em razão de sua natureza interdisciplinar, esta tese foi estruturada em formato de artigos, de modo a organizar de forma clara os diferentes produtos científicos e tecnológicos gerados ao longo da pesquisa. Além deste capítulo introdutório, o Capítulo 2 apresenta o artigo publicado na *Frontiers in Plant Science*, com foco nos efeitos de espectros e regimes de iluminação sobre microverdes de lentilha. O Capítulo 3 apresenta o artigo aceito para publicação na *Smart Agricultural Technology*, centrado no desenvolvimento e na validação do *Precision Vertical Farming System* (PVFS) e na análise integrada entre telemetria, energia e biomassa em microverdes de gergelim. O Capítulo 4 reúne os registros de software associados ao desenvolvimento da tese, evidenciando os produtos tecnológicos derivados da arquitetura proposta e sua relevância para a consolidação da pesquisa. Por fim, o Capítulo 5 apresenta a conclusão geral, na qual são integrados os principais resultados agronômicos, energéticos e tecnológicos obtidos ao longo do trabalho, bem como suas implicações para o avanço da agricultura vertical de precisão.

Referências da Introdução

BANTIS, F. et al. Vegetable production in PFALs: Control of micro-environmental factors, principal components and automated systems. *Agriculture*, v. 14, n. 4, p. 642, 2024. Disponível em: <https://doi.org/10.3390/agriculture14040642>. Citado 2 vezes nas páginas 20 e 21.

BUDAVÁRI, N. et al. An overview on the use of artificial lighting for sustainable lettuce and microgreens production in an indoor vertical farming system. *Horticulturae*, v. 10, n. 9, p. 938, 2024. Disponível em: <https://doi.org/10.3390/horticulturae10090938>. Citado 2 vezes nas páginas 20 e 21.

DUBEY, S. et al. Microgreens production: Exploiting environmental and cultural factors for enhanced agronomical benefits. *Plants*, v. 13, n. 18, p. 2631, 2024. Disponível em: <https://doi.org/10.3390/plants13182631>. Citado na página 20.

KABIR, M. S. N. et al. Technological trends and engineering issues on vertical farms: A review. *Horticulturae*, v. 9, n. 11, p. 1229, 2023. Disponível em: <https://doi.org/10.3390/horticulturae9111229>. Citado 2 vezes nas páginas 20 e 21.

SHIBAEVA, T. G. et al. Continuous LED lighting enhances yield and nutritional value of four genotypes of brassicaceae microgreens. *Plants*, v. 11, n. 2, p. 176, 2022. Disponível em: <https://doi.org/10.3390/plants11020176>. Citado na página 20.

SILVA, M. D. et al. An open-architecture precision vertical farming system for sesame microgreens: Audit-ready telemetry for dynamic lighting and energy–biomass benchmarking. *Smart Agricultural Technology*, p. 102105, 2026. ISSN 2772-3755. Disponível em: <https://www.sciencedirect.com/science/article/pii/S2772375526003266>. Citado 2 vezes nas páginas 21 e 22.

SILVA, M. D. et al. Growing in red: impact of different light spectra and lighting conditions on lentil microgreens growth in vertical farming. *Frontiers in Plant Science*, v. 15, p. 1515457, 2024. Disponível em: <https://doi.org/10.3389/fpls.2024.1515457>. Citado 3 vezes nas páginas 20, 21 e 22.

Van Gerrewey, T.; BOON, N.; GEELEN, D. Vertical farming: The only way is up? *Agronomy*, v. 12, n. 1, p. 2, 2022. Disponível em: <https://doi.org/10.3390/agronomy12010002>. Citado na página 20.

2 Crescendo no vermelho: impacto de diferentes espectros de luz e condições de iluminação no crescimento de microverdes de lentilha em agricultura vertical

Este capítulo apresenta o artigo intitulado *Growing in red: impact of different light spectra and lighting conditions on lentil microgreens growth in vertical farming*, publicado no periódico *Frontiers in Plant Science*.

Título em português: Crescendo no vermelho: impacto de diferentes espectros de luz e condições de iluminação no crescimento de microverdes de lentilha em agricultura vertical.

DOI: <https://doi.org/10.3389/fpls.2024.1515457>

Periódico: *Frontiers in Plant Science*.

Indicadores do periódico: Impact Factor 4.8 e CiteScore 8.8.

O artigo avalia os efeitos de diferentes regimes temporais de iluminação, constante e gaussiano, associados a diferentes qualidades espectrais, branca, azul, vermelha e RBW, sobre o crescimento, a fisiologia, a produção de biomassa, os pigmentos fotossintéticos e a eficiência energética de microverdes de lentilha cultivados em sistema de agricultura vertical. Os resultados demonstram que a escolha da estratégia luminosa deve considerar o objetivo produtivo, uma vez que regimes constantes favoreceram o acúmulo de biomassa e a eficiência energética, enquanto o regime gaussiano contribuiu para o aumento de carotenoides.

frontiers | Frontiers in Plant Science

TYPE Original Research
PUBLISHED 23 December 2024
DOI 10.3389/fpls.2024.1515457

OPEN ACCESS

EDITED BY
Stefania De Pascale,
University of Naples Federico II, Italy

REVIEWED BY
Martina Puccinelli,
University of Pisa, Italy
Aušra Brazaitytė,
Lithuanian Research Centre for Agriculture and Forestry, Lithuania

*CORRESPONDENCE
Fabiano Guimarães Silva
fabiano.silva@ifgoiano.edu.br

RECEIVED 22 October 2024
ACCEPTED 27 November 2024
PUBLISHED 23 December 2024

CITATION
Silva MD, Vasconcelos JM, Silva FB, Bailão ASO, Guedes IMR, Vilela MS, Costa AC, Rosa M and Silva FG (2024) Growing in red: impact of different light spectra and lighting conditions on lentil microgreens growth in vertical farming.
Front. Plant Sci. 15:1515457.
doi: 10.3389/fpls.2024.1515457

Growing in red: impact of different light spectra and lighting conditions on lentil microgreens growth in vertical farming

Marlus Dias Silva[1], Jaqueline Martins Vasconcelos[1], Fábia Barbosa da Silva[1], Adriano Soares de Oliveira Bailão[2], Ítalo Moraes Rocha Guedes[3], Márcio da Silva Vilela[4], Adriano Carvalho Costa[1], Márcio Rosa[5] and Fabiano Guimarães Silva[1]*

[1]Laboratory of Advanced Studies in Vertical Agriculture, Goiano Federal Institute of Education, Science and Technology, Rio Verde, Brazil, [2]Laboratory of Computational Intelligence, Goiano Federal Institute of Education, Science and Technology, Rio Verde, Brazil, [3]Brazilian Agricultural Research Corporation (EMBRAPA), Embrapa Hortaliças, Brasília, Brazil, [4]Laboratory of Automation, Simulation and Control, Goiano Federal Institute of Education, Science and Technology, Rio Verde, Brazil, [5]Graduate Program in Plant Production, University of Rio Verde, Rio Verde, Brazil

Vertical Farming Systems (VFS) emerge as an approach to optimize plant growth in urban and controlled environments, by enabling sustainable and intensive production in reduced spaces. VFS allow for greater control over growing conditions, such as light, temperature and humidity, resulting in higher quality crops and with less use of resources, such as water and fertilizers. This research investigates the effects of different lighting regimes (Constant and Gaussian) and spectral qualities (white, RBW, blue and red) on the growth, photosynthesis, and biomass accumulation of lentil microgreens (*Lens culinaris*) in VFS. The results demonstrate that constant lighting regimes, particularly under red, white, and RBW lights, significantly increase biomass production and energy efficiency. On the other hand, the Gaussian regime promotes the accumulation of bioactive compounds such as carotenoids, especially under red light. Chlorophyll content and the photochemical coefficient (qP) also varied across treatments, with significant variations between lighting regimes and spectral combinations. Tailored lighting strategies, adjusted to specific production goals, have the potential to enhance both productivity and nutritional quality in VFS. The analysis contained in the research provides relevant information for optimizing lighting management in controlled agricultural environments, providing practical applications to improve harvest performance.

KEYWORDS

vertical farming, lighting regimes, *Lens culinaris*, microgreens, constant light, gaussian curve, photosynthetic efficiency, artificial lighting

1 Introduction

Vertical farming, also known as the Vertical Farming System (VFS), has gained prominence as an innovative approach to plant cultivation in urban and controlled environments, optimizing space usage and enabling efficient food production in areas with land limitations Bantis and Koukounaras (2024). The precise control of factors such as lighting, temperature, and humidity enhances plant growth, improving not only productivity but also the nutritional and biochemical quality of the cultivated plants. VFS are particularly advantageous in regions where natural resources are limited, promoting a more sustainable and efficient form of agriculture van Delden et al. (2021).

One of the main obstacles in vertical farming is managing artificial lighting conditions, as light plays a fundamental role in the process of photosynthesis and plant development. The use of LEDs (Light Emitting Diodes) has proven to be a good alternative for cultivation, allowing fine-tuning of the intensity, duration, and spectrum of light, factors that directly influence photosynthesis and biomass accumulation Yudina et al. (2023). Light spectra such as red and blue, for instance, have been widely recognized for their beneficial effects on plant growth. Monochromatic red light can stimulate cell elongation, while blue light promotes compactness and the production of photosynthetic pigments. However, the combination of different spectra, such as RBW (red, blue, and white), has also shown good results, regulating photosynthesis to enhance plant growth and quality Budavári et al. (2024); Ciriello et al. (2023); Zhang et al. (2022).

The selection of light spectrum is essential for optimizing photosynthetic efficiency, growth, and biomass accumulation in controlled cultivation systems. Research has shown that variations in UV-A LED wavelengths and exposure durations can significantly enhance bioactive compounds production in mustard microgreens without compromising growth Brazaitytė et al. (2019). Furthermore, a balanced combination of red, green, and blue light has been found to optimize growth and metabolite accumulation in radish microgreens, while UV-A and far-red light improve antioxidant properties in a cultivar-specific manner Garegnani et al. (2024). Light intensity also plays a critical role in agronomic traits and phytochemical composition: lower intensities promote chlorophyll content and cotyledon expansion, whereas higher intensities enhance antioxidant activity and total phenolic content, influencing microgreen quality and productivity Flores et al. (2024).

Thus, it can be seen that the choice of light spectrum is essential for optimizing photosynthetic efficiency, growth, and biomass accumulation in controlled cultivation systems. Therefore, the use of differentiated light spectra, tailored to the needs of each crop and stage of development, is crucial for optimizing production in vertical farming systems, ensuring healthy growth and higher quality agricultural products Nájera et al. (2022); Boucher et al. (2023).

Microgreens, in particular, stand out in the context of VFS due to their short growth cycle, ranging from 5 to 10 days from germination to harvest Bantis and Koukounaras (2024). Due to their high added value, these vegetables are becoming increasingly common in plant factories with artificial lighting (PFAL) in urban areas Kozai and Niu (2020); Orsini et al. (2020); Boonmee et al. (2024). Furthermore, the high sowing density and low height of these plants make them ideal for cultivation in small spaces, allowing for continuous production throughout the year, regardless of the seasons Cowden et al. (2024).

In this context, lentils (*Lens culinaris*), a widely cultivated legume valued for its high nutritional content and ease of cultivation, are an advantageous crop for studying the effects of different light regimes and qualities on biomass accumulation, photosynthetic efficiency, and pigment production Preiti et al. (2024). Studies have shown that lentils are highly responsive to changes in environmental conditions, including variations in light quality, which directly influence their carbohydrate metabolism and overall yield. These characteristics make them an ideal candidate for optimization in vertical cultivation systems Bhandari et al. (2016). Additionally, lentil microgreens have been highlighted for their nutritional value and adaptability to controlled environments Priti et al. (2021), for example, observed higher levels of flavonoids, carotenoids, and ascorbic acid in lentil microgreens grown under semi-controlled conditions. These findings align with the growing interest in microgreens due to their distinct flavor profiles and high nutrient content Dubey et al. (2024). Furthermore, lentils' ability to regulate antioxidant and photoprotective metabolism under stress conditions reinforces their suitability for controlled environments Saini et al. (2024).

Although several studies have assessed the impact of different light spectra on the quality of microgreens, most focus exclusively on constant lighting regimes—i.e., on how light is provided over time. Furthermore, the works are limited to investigating variations in photoperiods. However, could it be possible that different lighting regimes also influence the growth of microgreens in diverse ways? Constant regimes, which provide a uniform light intensity, and modulated regimes, such as Gaussian curves that simulate natural light variations throughout the day, could affect the development of these vegetables? These adjustments could promote the optimization of photosynthesis and biomass accumulation? It is hypothesized that the lighting regimes constant light and modulation with Gaussian curves combined with variations in light spectrum, may distinctly influence the growth, photosynthesis, and biomass production of lentils cultivated in vertical farming systems. Thus, this research seeks to explore the impact of lighting regimes (constant and Gaussian), in association with spectral variations (white light, RBW, blue, and red), on the growth and quality of lentils cultivated in vertical farming environments. A detailed understanding of these lighting effects may provide important information for optimizing cultivation practices in these systems, ensuring greater productivity and quality of harvests.

2 Materials and methods

2.1 Experimental setup and cultivation conditions

The experiment was conducted at the Laboratory of Advanced Studies in Vertical Agriculture, Goiano Federal Institute of Education, Science and Technology, Rio Verde, Brazil. Thirteen

grams (13 g) of lentil seeds (*Lens culinaris*) Yoki® (Brazil, BR), approximately 200 seeds for each technical replicate, were distributed in plastic containers measuring 20 cm in length, 14 cm in width, and 6.5 cm in height, containing 100 g of the commercial substrate *Bioplant Plus*®, previously moistened with 25 mL of water and kept in the dark for 12 hours. Subsequently, the containers were placed in a growth chamber (Spectral Int®, Rio Verde, Brazil) (Figure 1) that is 1.80 meters tall and 65 cm wide, equipped with four shelves containing luminaires measuring 45×55cm, with 55 LEDs evenly distributed and installed at a distance of 22 cm between shelves. The luminaires were programmed to provide a distinct spectral composition of light: cool white 6500 K (400-700 nm), red (600-700 nm, peak at 660 nm), blue (400-500 nm, peak at 440 nm), and RBW (Red: Blue : White - spectral composition: 70.5% red, 8.5% green, and 21.0% blue).

Lentil microgreens were cultivated under a photoperiod of 12 hours (06:30 to 18:30) in two lighting regimes: constant and Gaussian curve (Supplementary Figure S11). In the constant regime, the light intensity was maintained at 250 μmol m^{-2} s^{-1}, while in the Gaussian regime, using an automatic dimming system, the intensity varied from 85 to 500 μmol m^{-2} s^{-1}. In both regimes, a supply of 10.80 mol m^{-2} day^{-1} of DLI (*Daily Light Integral*) was ensured. Light intensity and spectral composition were measured using a LI-180 light spectrometer (LI-COR, Nebraska, USA). Cultivation in the constant regime took place from March 8 to 18, 2024, followed by the Gaussian regime from March 21 to April 1, 2024, with a duration of 10 days each.

Irrigation was adjusted throughout the experiment according to the growth of the seedlings and the water needs of the substrate. Each experimental unit corresponded to a replicate, represented by a plastic tray containing approximately 200 lentil seeds treated with a specific combination of lighting regime and spectral quality. In the first 7 days, 25 mL of water was applied daily to each experimental unit. From the eighth day onwards, the amount of water was increased to 35 mL per day due to the greater development of the seedlings and the consequent reduction in substrate moisture. The average air temperature in the growth chamber was maintained at 24°C ± 0.5, with relative humidity controlled at 60% ± 0.5 during the cultivation period (Supplementary Figures S9, S10).

The design was completely randomized in a 2x4 factorial scheme with two lighting regimes (Constant and Gaussian) and four spectral qualities of light (white, blue, red, and RBW), with six repetitions, totaling 48 experimental units. After 10 days of sowing, fluorescence assessment of chlorophyll *a*, photosynthetic pigments, growth, and biomass was conducted.

2.2 Growth and biomass assessment of lentils

The planning of the analysis to evaluate plant growth consists of multiple replicates. Each replicate includes 15 plants selected for measuring hypocotyl length (CHL), number of leaves (3), and average leaf area. The measurements of these variables were

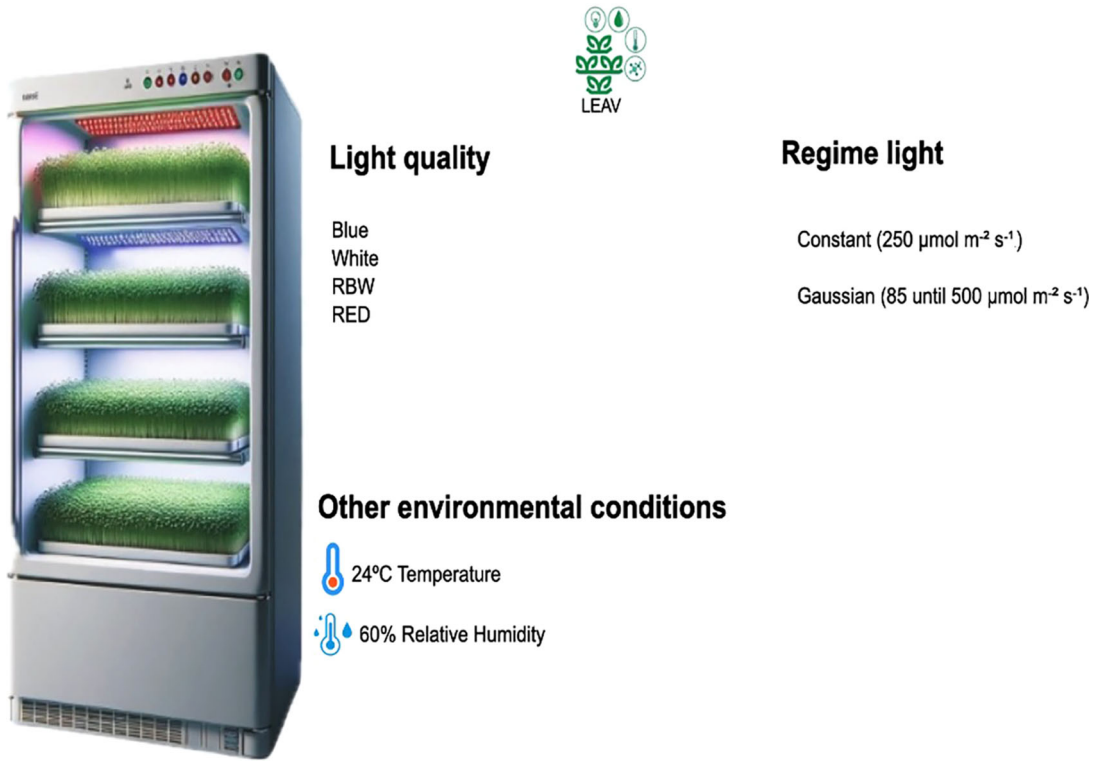

FIGURE 1
Representation of the cultivation environment.

obtained from photographs of the plants, analyzed using the ImageJ software, as highlighted by Schneider et al. (2012).

The remaining plants from each replicate were used to determine the fresh and dry mass of the hypocotyl and leaves. Samples were weighed on an analytical balance to obtain the fresh mass and then dried in an oven (Tecnal, TE-394/1, Brazil) at a temperature of 65°C for 48 hours to determine the dry mass.

2.3 Chlorophyll *a* fluorescence

The chlorophyll *a*fluorescence parameters were obtained using the IMAGING PAM modulated fluorometer (MAXI version) and the Imaging Win software (Heinz Walz GmbH, Effeltrich, Germany). The seedlings were individually fixed in a holder at a distance of 18.5 cm from a charge-coupled device (CCD) camera connected to a fluorescence device. Measurements were taken from the adaxial portion of the leaves, adapted to the dark for 30 minutes, so that the reaction centers were fully open. Under this condition, the leaf tissues were exposed to low-intensity light (0.03 μmol m^{-2} s^{-1}) to determine the initial fluorescence (Fo). Then, a saturating light pulse (> 6000 μmol m^{-2} s^{-1}) was applied for 0.8 s to determine the maximum fluorescence (Fm), from which the maximum quantum yield of photosystem II was calculated (*Fv*/*Fm* = (Fm - Fo)/Fm) Genty et al. (1989).

After illuminating the sample for 40 seconds, light-adapted fluorescence was determined to measure the light-acclimated variables such as the effective quantum yield of PSII Y(II), and the non-photochemical quenching (NPQ) Kramer et al. (2004). The electron transport rate (ETR) was calculated as ETR = Y(II) × PAR × Aleaf × 0.5 Bilger et al. (1995), where PAR is the photon flux density; Aleaf is the fraction of the incident light absorbed by the leaves; and 0.5 is the fraction of excitation energy presumed to be equally distributed between PSII and PSI Laisk and Loreto (1996). Data were obtained from processing images of the median region of the leaves.

2.4 Photosynthetic pigments

The concentrations of the pigments were determined after extraction with dimethyl sulfoxide (DMSO) saturated with calcium carbonate ($CaCO_3$) de Castro et al. (2019). The concentrations of chlorophyll *a* (Chl*a*), chlorophyll *b* (Chl*b*), and carotenoids (Cart) were determined using a UV-VIS spectrophotometer (Evolution 60S, Thermo Fisher Scientific Inc., MA, USA) at wavelengths of 665, 649, and 480 nm, respectively. The calculations were performed using the equations proposed by Wellburn (1994), and the results were expressed in $\mu g\ g^{-1}$ of fresh leaf weight.

2.5 Calculation of energy consumption per gram of dry matter

In the experiment, the seedlings were placed at a distance of 22 cm from the luminaires, covering an illuminated area of 0.247 m^2. Based on the electric power of the luminaires and the illuminated area, energy consumption per square meter was calculated. For each light spectrum, the total power of the luminaires was measured as follows: 0.167653 kWh/m^2 for white light, 0.099832 kWh/m^2 for RBW light, 0.18536 kWh/m^2 for blue light, and 0.075324 kWh/m^2 for red light. This value was then divided by the estimated dry matter mass per square meter, resulting in the energy consumption per gram of dry matter. The total dry matter mass per square meter was obtained by multiplying the average dry matter mass per seedling by the total number of seedlings per square meter (1,428 seedlings), a density close to that recommended by recent studies, which indicate three seeds per square centimeter as ideal for lentil microgreens Dubey et al. (2024).

The formula for calculating energy consumption per gram of dry matter is given by:

$$E_g = \frac{P_{tot} \cdot A}{M_{sec} \cdot N_m}$$

where $-E_g$ is the energy consumption per gram of dry matter (kWh/g), $-P_{tot}$ is the total power of the luminaires (kWh/m^2), - A is the illuminated area (m^2), $-M_{sec}$ is the average dry matter mass per seedling (g), $-N_m$ is the number of seedlings per square meter.

2.6 Statistical analysis

The data analysis was carried out using the R computer program. Initially, exploratory analysis was performed considering the effects of light supply regimes, spectral light composition, and the interaction between these factors, with residual analysis conducted and outliers removed when necessary. The normality of the residuals was checked using the Shapiro-Wilk test, the homogeneity of variances was tested using the Levene test (using the car package), and the correlation of the residuals was analyzed using the Durbin-Watson test (via the lmtest package).

A two-way analysis of variance (ANOVA) was conducted to evaluate the effects of lighting regimes and spectral compositions, as well as their interaction, on the measured variables. Subsequently, analysis of variance (ANOVA) was conducted, and when effects were significant, the Tukey test at a 5% probability level was applied using the ExpDes.pt package. Aiming to expand the data analysis, Pearson linear correlation analyzes were carried out between the variables and principal components analysis (PCA). The ExpDes.pt, MVar.pt, FactoMineR, factoextra, tidyverse, corrplot, viridis, and RColorBrewer packages were utilized.

3 Results

The interaction between lighting regime (constant and Gaussian) and spectral qualities of light (white, RBW, blue, and red) was significant for the variables: chlorophyll *a* (Chl*a*), chlorophyll *b* (Chl*b*), carotenoid content (Cart), average leaf area (CALA), total leaf area (CTLA), hypocotyl length (CHL), hypocotyl fresh weight (HF), leaf fresh weight (LFW), leaf dry mass (LMD), total dry mass (TDM), photochemical quenching coefficient (qP),

and energy efficiency (EnE) (Figures 2–4). These variables indicate how plants utilize light to convert energy into biomass and thus directly reflect photosynthetic efficiency and plant growth.

When breaking down the lighting regime in relation to the light spectrum, it was found that for chlorophyll *a* (Chl*a*), the constant regime was statistically superior to the Gaussian regime in all spectral qualities of light (white, RBW, blue, and red) (Figure 2A). For total leaf area (TLA), hypocotyl fresh weight (HFW), leaf dry mass (LMD), total dry mass (TDM), and energy efficiency (EnE), the constant regime was also statistically superior to the Gaussian regime under the spectra of white, RBW, and red light (Figures 3C, D, F, G, 4B). For these variables, there was no statistical difference between the regimes when cultivated under blue light, except for total leaf area (TLA) and leaf dry mass (LMD), where the Gaussian regime was statistically superior to the constant regime (Figures 3C, F).

For average leaf area (CALA), the constant regime was superior to the Gaussian regime when seedlings were cultivated under white and RBW light. In red light, there was no significant difference between the regimes; however, when cultivated under blue light, the Gaussian regime was statistically superior to the constant regime (Figure 3B).

For chlorophyll *b* and hypocotyl length (CHL), the constant regime was statistically superior to the Gaussian only in the RBW light quality (Figures 2B, 3A). However, the Gaussian regime had statistically higher means than the constant regime under blue and red lights for chlorophyll *b*, and there was no statistical difference between the lighting regimes in the white light spectrum. For hypocotyl length, the Gaussian regime was superior to the constant regime only under blue light (Figures 2B, 3A).

For leaf fresh weight (LFW), seedlings cultivated under white and red light in the constant regime were statistically superior to the Gaussian regime. The opposite was observed in blue light cultivation, where the Gaussian regime was superior to the constant regime, and no difference between the regimes was observed under RBW light (Figure 3E). The carotenoid content was significantly higher in the Gaussian regime across all light types (Figure 2C). The photochemical quenching coefficient was also statistically superior in the Gaussian regime under RBW and red lights, with no differences between the regimes in the other light types (Figure 4A).

When breaking down the lighting regime within the types of light spectra, it was found that for chlorophyll *a* (Chl*a*), the constant regime was statistically superior to the Gaussian regime in all light qualities (white, RBW, blue, and red) (Figure 2A).

Through the breakdown of the light spectrum within each lighting regime, it was verified that there was no effect of the light spectrum in the Gaussian regime for average leaf area (CALA). In the constant regime, the white, RBW, and red colors showed higher values than blue light (Figure 3B). For chlorophyll *b* (Chl*b*), the different light spectra showed no statistical differences when cultivation was conducted in the Gaussian regime. In the constant regime, RBW and white did not differ from each other and were superior to blue and red (Figure 2B).

In the Gaussian regime for chlorophyll *a* (Chl*a*), there was a difference only between blue and red colors, with higher values for the latter (Figure 2A). In the constant regime, RBW showed higher

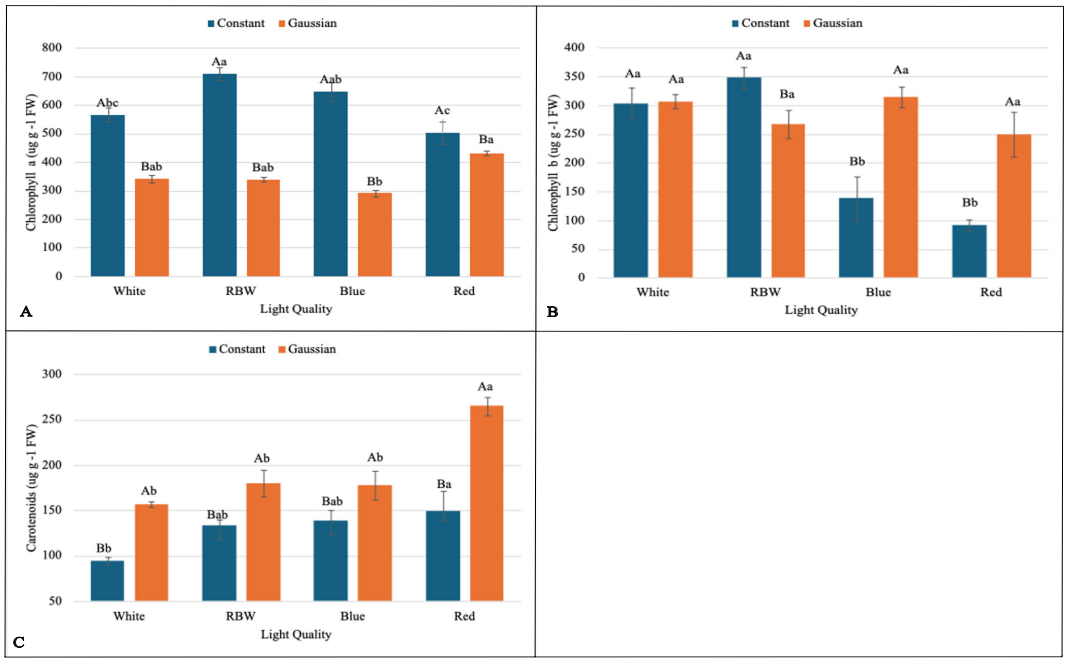

FIGURE 2
Graphs illustrating the main effects and interactions between lighting regimes (constant and Gaussian) and spectral light qualities (white, RBW, blue, and red) on pigment concentration. Values are expressed as means ± standard error, with uppercase letters indicating comparisons between lighting regimes and lowercase letters indicating comparisons between spectral qualities, according to the Tukey test (p<0,05). **(A)** Chlorophyll *a* ($\mu g g^{-1}$ *FW*), **(B)** Chlorophyll *b* ($\mu g g^{-1}$ *FW*), **(C)** Carotenoids ($\mu g g^{-1}$ *FW*).

10.3389/fpls.2024.1515457

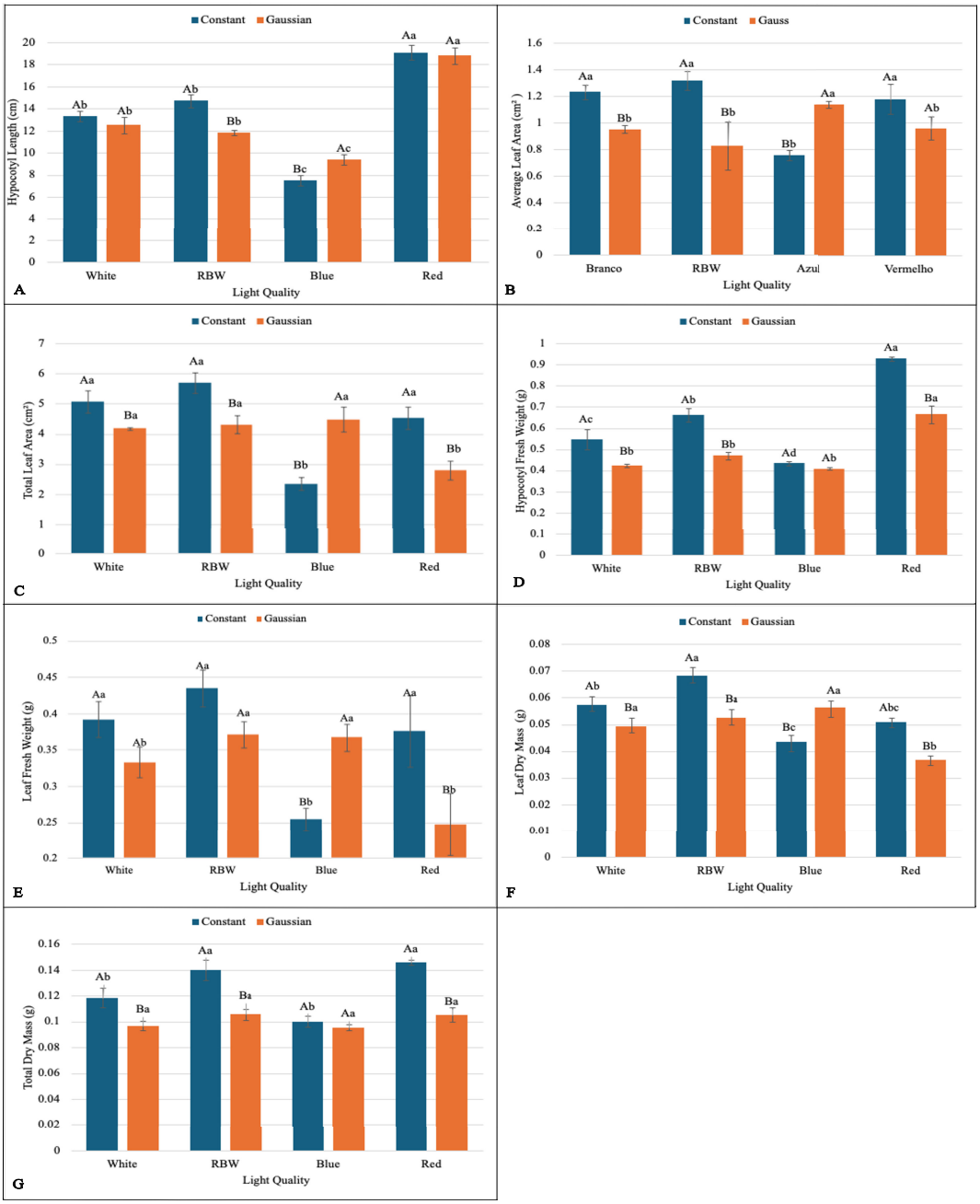

FIGURE 3
Graphs illustrating the main effects and interactions between lighting regimes (constant and Gaussian) and spectral light qualities (white, RBW, blue, and red) on growth and biomass variables. Values are presented as means ± standard error, with uppercase letters indicating comparisons between lighting regimes and lowercase letters indicating comparisons between spectral qualities, according to the Tukey test ($p<0,05$). **(A)** Hypocotyl Length (cm), **(B)** Average Leaf Area (cm^2), **(C)** Total Leaf Area (cm^2), **(D)** Hypocoty Fresh Weight (g), **(E)** Leaf Fresh Weight (g), **(F)** Leaf Dry Mass (g), **(G)** Total Dry Massa (g).

values than white and red light, not differing from blue light, which also presented higher values than red light.

For carotenoids (CART) and hypocotyl fresh weight (HFW) in the Gaussian regime, the red color had a higher value than the other colors, which did not differ among themselves. In the constant regime for carotenoids, there was a difference only between red and white colors, with the latter being lower (Figures 2C, 3D). In the constant regime, HFW indicated that all colors differed from each other, with the highest value for red, followed by RBW, white, and lastly blue.

In hypocotyl length (CHL) in the Gaussian regime, it was found that red light had the highest value and blue the lowest. In CHL, in both regimes, red light had the lowest value (Figure 3A). In energy efficiency (EnE), it was observed that in both regimes, red light had the highest value, while white and blue had lower values (Figure 4B).

For leaf fresh weight (LFW), in the Gaussian regime, higher values were found for RBW and blue, and lower for the other treatments. In the constant regime, blue light had a lower value than the others, which did not differ from each other (Figure 3E).

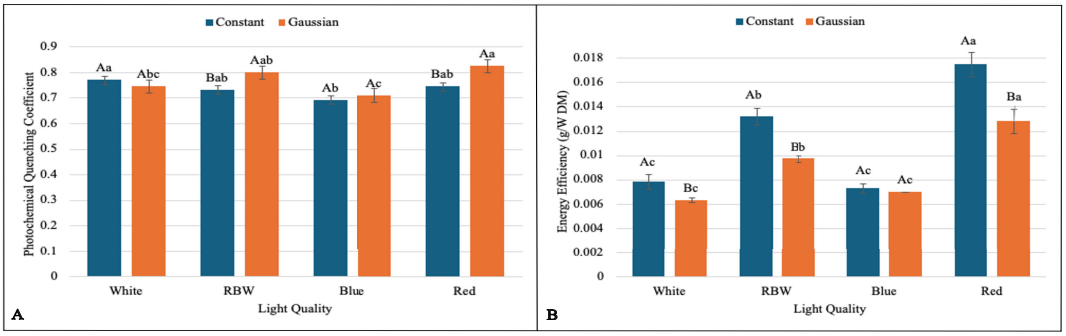

FIGURE 4
Graphs illustrating the main effects and interactions between lighting regimes (constant and Gaussian) and spectral light qualities (white, RBW, blue, and red) on photosynthetic and energy efficiency variables. Values are presented as means ± standard error, with uppercase letters indicating comparisons between lighting regimes and lowercase letters indicating comparisons between spectral qualities, according to the Tukey test (p<0,05). **(A)** Photochemical Quenching Coefficient, **(B)** Energy Efficiency (g/W DM).

In total leaf area (CTLA), white, RBW, and blue lights were superior to red light in the Gaussian regime. In the constant regime, blue light showed lower values than the others, which did not differ from each other (Figure 3C).

For the photochemical quenching coefficient (qP) in the Gaussian regime, it was found that red light had higher values than white and blue lights. RBW light did not differ from white and was superior to blue. In the constant regime, there was a significant difference only between white and blue light, with the latter being lower (Figure 4A).

Total dry mass (TDM) showed higher averages under red and RBW lights compared to blue and white lights under the constant regime, which had the lowest means and were statistically equal among themselves. There was no statistical difference between the spectral light qualities in the Gaussian regime (Figure 3G).

When analyzing energy consumption per gram of dry matter (Table 1), it was observed that white light in the constant regime consumed 0.167653 $\frac{kWh}{g}$, while in the Gaussian regime the consumption was 0.210675 $\frac{kWh}{g}$. For RBW light, the consumption was 0.099832 $\frac{kWh}{g}$ under constant lighting and 0.135709 $\frac{kWh}{g}$ in the Gaussian regime. Blue light in the constant regime consumed 0.18536 $\frac{kWh}{g}$, while in the Gaussian regime the consumption was 0.197157 $\frac{kWh}{g}$. Under red light in the constant regime, the consumption was 0.075324 $\frac{kWh}{g}$, while in the Gaussian regime it was 0.106168 $\frac{kWh}{g}$.

Finally, for leaf dry mass (LMD), in the Gaussian regime, white, RBW, and blue lights did not differ from each other and showed higher values than red light. In the constant regime, RBW showed higher values than the other treatments, while the blue treatment had the lowest value, not differing from the red treatment (Figure 3F).

For the variables NPQ, Y(II), HDM, and ETR, there was no interaction effect (Supplementary Tables S3, S4), with a significant simple effect of the lighting regime and light spectrum observed for all of them. Higher values were found in the constant regime for the NPQ and HDM variables, and lower values for Y(II) and ETR compared to the Gaussian regime. For ETR, white light had lower values than the others, which did not differ from each other. For HDM, higher values were found for red light and lower for white. The Y(II) showed higher values for red and RBW and lower for blue. For NPQ, higher values were found for blue and lower for red and RBW.

In summary, we can highlight that in the experiment with the breakdown of the light regime, it was observed that the constant regime was statistically superior to the Gaussian regime in several key variables, especially under white, RBW, and red light qualities. This included chlorophyll *a* (Chl*a*), total leaf area (TLA), hypocotyl fresh weight (HFW), leaf dry mass (LMD), total dry mass (TMD), and energy efficiency (EnE). However, under blue light, there was no significant difference between the regimes, except for TLA and LMD, where the Gaussian regime surpassed the constant one. In terms of carotenoids (CART), the Gaussian regime was consistently superior regardless of light quality. Interestingly, the photochemical quenching coefficient (qP) was also higher in the Gaussian regime under RBW and red lights. For the other variables, there was variation between the regimes depending on the light quality, with the Gaussian regime performing better under blue light for some measurements.

From the principal component analysis, it was found that the first four components jointly explained 82.76% of the total variation in the data (Table 2; Figure 5). It was found that the first component (PC1) explained 32.70% of the variation in the data, showing a high positive correlation (—$|r|$ > 0.70—) with variables such as HFW, HMD, TMD, CHL, and EnE. This indicates that these variables have the highest variability within the dataset and are directly related to each other, meaning that an increase in one causes an

TABLE 1 Energy consumption per gram of dry matter (kWh/m^2) under different light spectra and lighting regimes.

Light Spectrum	Constant (kWh/m^2)	Gaussian (kWh/m^2)
White	0.167653	0.210675
RBW	0.099832	0.135709
Blue	0.185360	0.197157
Red	0.075324	0.106168

The bolded words highlight the light treatments used in each lighting regime presented.

TABLE 2 Correlation coefficients of the first four principal components (PC1, PC2, PC3, PC4) resulting from Principal Component Analysis (PCA) for different physiological and production variables.

Variables	cp1	cp2	cp3	cp4
HFW Hypocotyl Fresh Weight (g)	0,9	0,16	-0,34	-0,05
LFW Leaf Fresh Weight (g)	0,39	0,58	0,55	-0,3
HMD Hypocotyl Dry Mass (g)	0,84	0,18	-0,46	-0,15
LMD Leaf Dry Mass (g)	0,23	0,71	0,53	-0,12
FvFm Maximum Quantum Yield of PSII (Fv/Fm)	0,04	0,31	-0,19	0,88
Y(II) Effective Quantum Yield of PSII	0,65	-0,63	0,30	0,14
NPQ Non-Photochemical Quenching	-0,65	0,60	-0,33	-0,09
qP Photochemical Quenching Coefficient	0,51	-0,59	0,38	-0,42
ETR Electron Transport Rate)	0,51	-0,63	0,35	0,35
Chla Chlorophyll *a* ($\mu g\ g^{-1} FW$)	0,17	0,59	-0,42	-0,10
Chlb Chlorophyll *b* ($\mu g\ g^{-1} FW$)	-0,19	0,12	0,74	0,11
Cart Carotenoids ($\mu g\ g^{-1} FW$)	0,17	-0,77	-0,06	-0,09
TDM Total Dry Mass (g)	0,81	0,50	-0,09	-0,18
EnE Energy Efficiency (g/W DM)	0,90	0,08	-0,31	-0,01
CTLA Total Leaf Area (cm^2)	0,32	0,61	0,53	0,24
CALA Average Leaf Area (cm^2)	0,41	0,56	0,30	0,18
CHL Hypocotyl Length (cm)	0,80	-0,15	-0,16	0,27
Eigenvalue	5,559	4,412	2,643	1,455
Variance (%)	32,70%	25,95%	15,55%	8,56%
Cumulative Variance (%)	32,70%	58,65%	74,20%	82,76%

The bold acronyms correspond to the physiological and production variables evaluated in the experiment, indicating their respective correlation coefficients for the four main principal components (PC1, PC2, PC3, and PC4).

increase in the other. This direct relationship among the variables and their importance can be graphically observed in (Figure 5), where the smaller angle between the arrows indicates greater correlation, and the greater the shift in the horizontal direction, the more important the variable is within the first component.

The second principal component explained 25.95% of the variation in the data, showing a high positive correlation with LMD and a negative correlation with Cart, indicating that this group of variables is also relevant and has an inverse correlation. The third component explained 15.55% of the variation in the data, showing a high positive correlation with chlorophyll *b*. The fourth component (PC4) explained 8.56% of the variation in the data, correlating highly with the variable F*v*F*m*.

Through the principal component analysis, it was possible to globally understand the behavior of treatments based on the evaluated variables, verifying that in the first principal component, it was possible to discriminate the treatments, showing a greater effect of light color, with a greater contrast of blue light compared to red. Red light showed higher values for the variables associated with this component, as also verified in the univariate analysis, although some variables may not have been significant.

The second principal component (PC2) indicated that the light regime (constant versus Gaussian) has an additional impact, especially within each light color, except blue. The scores close to 0 for blue light suggest that the variation in the lighting regime (constant versus dynamic) has a limited effect in this specific color, possibly due to the way blue light is absorbed and utilized in plants. In contrast, for white, RBW, and red lights, PC2 shows a trend of higher values for negatively associated variables, such as carotenoid content (CART), and lower values for positively associated variables, such as leaf dry mass (LMD), highlighting how different light regimes affect resource distribution and use in plants.

Through correlation analysis and principal component analysis (Figure 6), it was possible to verify the formation of groups of variables that have moderate to high positive correlations within the same group.

Group a) HFW, HMD, TMD, CHL, and EnE; b) TMD, CALA, LFW, CTLA, and LMD; c) CART, ETR, qP, and Y(II); d) NPQ. The variables in group a have moderate to low correlations with those in group b. The NPQ variable has high negative correlations with ETR, qP, and Y(II).

4 Discussion

Light quality and illumination regime are key environmental factors influencing in the growth, yield, and production of bioactive compounds in microgreens. However, the interactions between the light spectrum and the light regime has received less attention in the literature. Exploring these interactions offers a more comprehensive undertanding of how to optimize cultivation practices in vertical farming systems for microgreens, emphasizing their implications for growth, photosynthetic efficiency, and biomass production.

This research shows that cultivating lentil microgreens under constant red LED light (660 nm) can increase yield (Figure 3G), while Gaussian modulation favors carotenoid production (Figure 2C), a functional bioactive compound essential for human health. Similar results regarding seedling yield have been demonstrated in grapevine under constant red light Kong et al. (2024). This result may be linked to the effect of red light, which directly excites photosystem II (PSII), promoting greater efficiency in capturing and converting light into chemical energy (Figure 4A; Supplementary Tables S3, S4), favoring cell growth and biomass accumulation Maxwell and Johnson (2000); Yousef et al. (2021).

These responses may also be associated with the inhibitory effect of red light on the activity of the IAA oxidase enzyme, increasing endogenous auxin levels Jeong and Sivanesan (2015). Moreover, red light has a stimulating effect on endogenous gibberellins, hormones involved in mitosis and cell proliferation Toyomasu et al. (1993); Manivannan et al. (2015). These hormonal changes may contribute to increased cell elongation, resulting in greater biomass production, as shown in previous studies Poorter et al. (2019). Thus, red light, by promoting both greater photosynthetic efficiency and cell growth, proves to be an effective

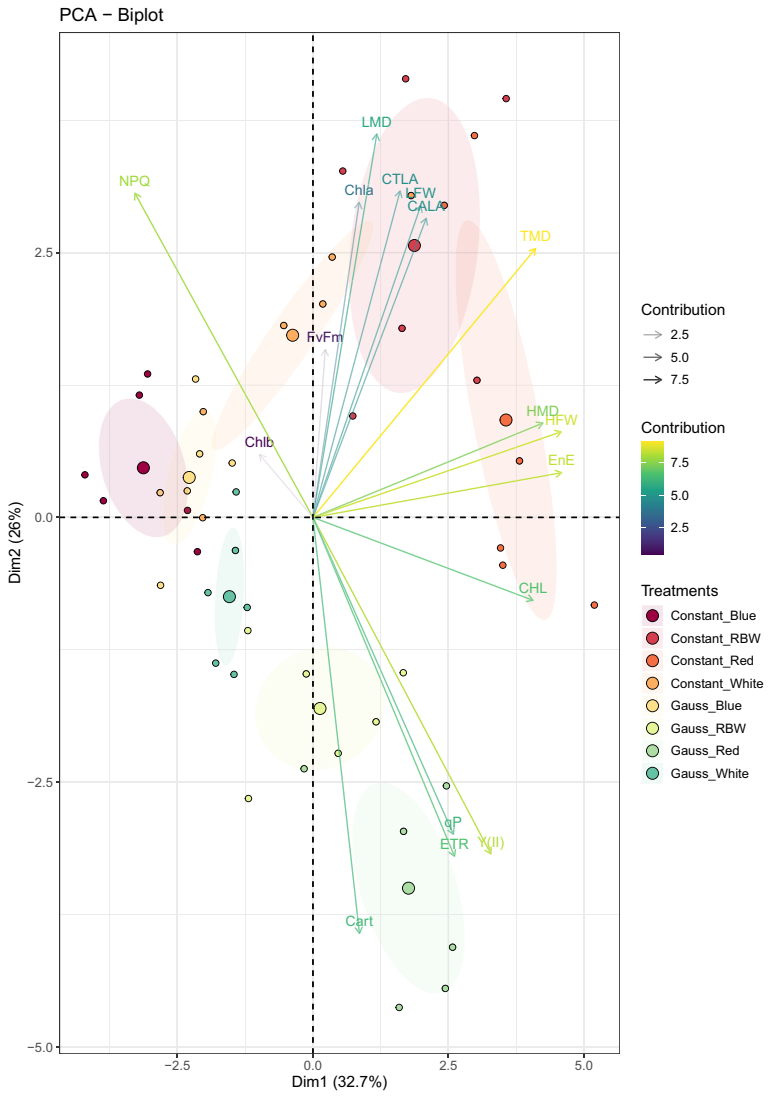

FIGURE 5
Two-dimensional scatter plot of Principal Component Analysis (PCA) representing the scores of the physiological and production variables, observations, and average values. The plot shows how different variables relate to and contribute to the variation observed in the first two principal components (PC1 and PC2). The first two principal components (PC1 and PC2) explain 32.70% and 25.95% of the total variance, respectively, accounting for a total of 58.65% of the explained variance.

tool for optimizing the productive performance of microgreens Li et al. (2023).

However, the interaction between the red light spectrum and illumination regime also resulted in a significant effect, beyond just biomass production (Figures 3A, D, G). In the Gaussian regime, the modulation of photosynthetic responses, as observed in the PCA 5, was due to the greater influence of red light on the variables YII, qP, and ETR, and photoprotective compounds such as carotenoid concentration (Figure 2C). Red light can induce an increase in photoxidative response, triggering greater carotenoid production as a protective mechanism. These pigments play a critical role in photoacclimation by dissipating excess light energy and shielding cellular membranes from damage caused by reactive oxygen species (ROS) Hashimoto et al. (2016); Jahns and Holzwarth (2012); Caferri et al. (2022); Qiao et al. (2021). This adaptive response effectively optimizes light utilization under intensified light conditions (similar to the Gaussian regime), further emphasizing the role of red light in regulating photosynthetic and photoprotective pathways.

Moreover, plant pigments such as carotenoids and chlorophylls also have direct implications for the nutritional quality of plants, especially in microgreens, which are consumed at early developmental stages when the concentration of nutrients and bioactive compounds is maximized Dou et al. (2018); Pennisi et al. (2020). Carotenoids, in particular, are precursors of vitamin A and act as antioxidants, which is crucial for both photoprotection in plants and for promoting functional foods that contribute to human health Teng et al. (2024); Caferri et al. (2022). In this context, red light, which significantly increased carotenoid production, can be explored as a strategy to enhance the nutritional value of microgreens. This is achieved not only through increased biomass accumulation but also by boosting the concentration of bioactive compounds with health benefits, such as carotenoids Llorente et al. (2016).

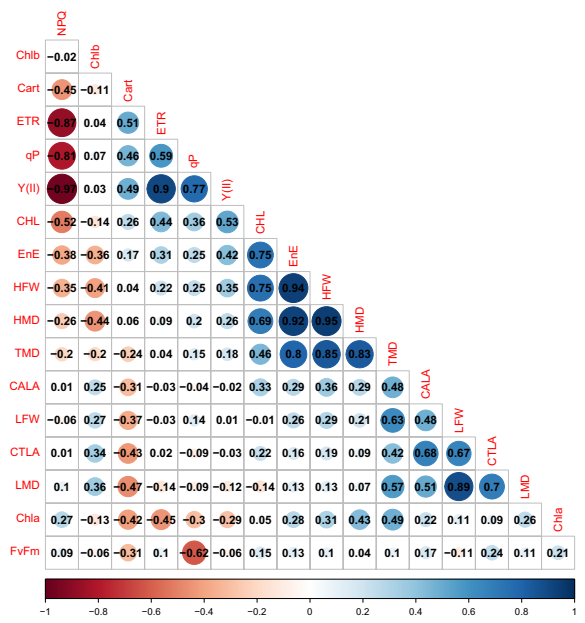

FIGURE 6
Heatmap showing the correlation coefficient (r) between the variables. Non-significant correlations are represented by white backgrounds, while negative and positive correlations are represented by shades of red and blue, respectively. The variables included are: HFW, Hypocotyl Fresh Weight; LFW, Leaf Fresh Weight; HMD, Hypocotyl Dry Mass; LMD, Leaf Dry Mass; FvFm, Maximum Quantum Yield of PSII; Y(II),Effective Quantum Yield of PSII; NPQ, Non-Photochemical Quenching; qP, Photochemical Quenching Coefficient; ETR, Electron Transport Rate); Chla, Chlorophyll *(a)*; Chlb, Chlorophyll *(b)*; Cart, Carotenoids; TDM, Total Dry Mass; EnE,Energy Efficiency; CTLA, Total Leaf Area; CALA, Average Leaf Area; and CHL, (Hypocotyl Length.

The physiological adjustments observed under red light resulted in superior energy efficiency in both lighting regimes (constant and Gaussian), as illustrated in (Figure 4B). This performance is directly related to the greater ability of red light to promote photosynthesis in photosystem II (YII) (Supplementary Tables S3, S4), especially in the constant regime, where an increase in biomass production was noted. This factor is crucial for crops aiming to maximize organic matter.

The data also corroborate the energy efficiency of red light, which had the lowest energy consumption per gram of dry matter in the constant regime (0.075324 kWh/g). In contrast, the highest consumption was recorded with white light in the Gaussian regime (0.210675 kWh/g), indicating a higher energy demand related to light modulation.

These results reinforce the superiority of red light in terms of energy efficiency and biomass production, especially under the constant regime, aligning with previous studies highlighting the effectiveness of red light in optimizing photosynthesis and plant growth in controlled environments Hernández and Kubota (2016). On the other hand, the higher energy consumption of white light in the Gaussian regime may be explained by the additional energy demand to maintain light intensity variation over time, which, while promoting the synthesis of bioactive compounds, compromises efficiency in biomass accumulation Li et al. (2020).

In relation to RBW light in the constant regime, a good performance in biomass accumulation and energy efficiency is observed (Figures 3A–F, 4A, B), comparable to red light. The energy consumption per gram of biomass was 0.099832 $\frac{kWh}{g}$ under constant lighting and 0.135709 $\frac{kWh}{g}$ in the Gaussian regime, trailing behind cultivation under red light and ahead of blue and white light cultivations, regardless of the cultivation type. This suggests that the mixed spectrum provided a balance between different wavelengths, optimizing both growth and the efficient use of light by plants Wang et al. (2024); Toscano et al. (2021); Nie et al. (2024). These results are also corroborated by the data presented on the photochemical efficiency of photosystem II (qP) and relative electron transport rate (ETR) (Supplementary Tables S3, S4), where both are directly linked to the plants' ability to convert light into chemical energy, driving biomass accumulation Fork and Satoh (1986); Guenther et al. (1990); Havaux et al. (1991). These results have important applications for agriculture in controlled environments, where adjusting light regimes, including the strategic use of RBW and red light, can be an effective tool for optimizing photosynthetic efficiency and crop productivity Murchie and Niyogi (2010); Chen et al. (2018); Keller et al. (2022); Tang et al. (2024).

Some positive responses in plants under RBW may be related to the synergy with green radiation, which can promote increases in certain characteristics such as leaf area and fresh leaf mass, as phytochromes and cryptochromes, photoreceptors related to morphogenesis, are also sensitive to this radiation Folta and Maruhnich (2007); Carvalho and Folta (2016).

Blue light, on the other hand, although it demonstrated a lower effect on biomass accumulation, stood out in photosynthetic and photoprotective parameters, especially in the Gaussian regime. The adjustments promoted by blue light resulted in an increase in chlorophyll *a* (CHLA) production (Figure 2A) and a reduction in the effective quantum yield of PSII (Y(II)). In response to the lower YII, photoprotection and adaptation mechanisms were activated, as observed by the increase in non-photochemical quenching (NPQ) (Supplementary Tables S3, S4). This is consistent with studies showing that blue light promotes greater light absorption and efficiency in photosynthesis, but with less leaf growth, corroborating its influence on more compact morphological characteristics adapted for environments with higher light intensity Zhang et al. (2020); Ashenafi et al. (2023). This adaptive response is relevant for plants grown under conditions where light stress is a concern, such as in intensive artificial lighting systems. The ability of blue light to promote photoprotection mechanisms, along with its influence on more compact morphological development, makes it a useful option for optimizing plant resilience against environmental variations.

Despite the opposing effects observed in lentil seedlings cultivated under monochromatic red and blue light, the combination of red and blue lights, widely discussed in the literature, also emerges as an effective strategy to maximize both growth and photosynthesis in controlled systems. Previous studies

have already indicated that red light stimulates stem elongation, while blue light promotes greater leaf development. Studies integrating these characteristics can result in plants with higher efficiency in light capture and, consequently, increased biomass production Fraszczak and Kula-Maximenko (2022). Our results corroborate this synergy between the two spectra, suggesting that the combined use of red and blue light can be explored to optimize both yield and quality of plants in controlled cultivation systems Ashenafi et al. (2023).

Importantly, the responses observed in this study are specific to lentil microgreens, and variations in plant species should be considered when designing light regimes. Studies with other plants, such as lettuce, radish, and spinach, have shown that different combinations of red and blue lights produce diverse effects on growth and biochemical composition Lin et al. (2013); Zukauskas et al. (2011). These interspecies variations underscore the importance of tailoring light spectra to the specific characteristics of each plant, aiming to optimize both yield and nutritional quality, particularly in large-scale cultivation systems Dou et al. (2018); Pennisi et al. (2020).

Furthermore, according to Li et al. (2011); Wei et al. (2023), during the initial seedling stage, cotyledonary reserves provide most of the energy required for growth, limiting the immediate dependence on active photosynthesis. As the seedlings mature and these reserves are depleted, the effects of different light spectra, such as the Gaussian regime, become more evident, impacting growth and photosynthetic efficiency. This has been observed in species like Arabidopsis thaliana and other plants under controlled light. These results suggest that the combination of different spectra may be more effective in later stages of development. Thus, the difference in the response observed under the Gaussian light regime, despite the use of the same DLI and spectra, can be explained by the early activation of photoprotective mechanisms, such as non-photochemical quenching (NPQ), which reduces the efficiency of converting light into chemical energy. This leads to the dissipation of energy as heat instead of being used to increase biomass production.

Despite the better photochemical performance in plants under the Gaussian regime, as evidenced by the chlorophyll a fluorescence data, this did not translate into greater leaf and total dry mass. Vialet-Chabrand et al. (2024) observed negative impacts on the accumulation of edible biomass in lettuce grown under a sinusoidal regime compared to a square wave light regime. These responses need to be further explored; however, much of this response is related to the slow process of photosynthetic induction at the beginning of the photoperiod Kaiser et al. (2014); Lawson et al. (2012).

Thus, unlike a stationary system, the gradual process of photosynthetic induction in the Gaussian or sinusoidal regime can be characterized by a temporary lag in the maximum efficiency of photosynthesis when light increases, due to the need for metabolic and biophysical adjustments in the plant, such as RuBP regeneration, Rubisco activation, and stomatal opening. Only after these processes, does photosynthesis reach an efficient steady state, where CO_2 is assimilated optimally Vialet-Chabrand et al. (2024). According to Stamford et al. (2024), more satisfactory productivity responses in lettuce could be obtained by using the same DLI but with lower PPFD during a longer photoperiod, avoiding exposure to peaks of saturating light, where there is lower quantum efficiency.

This study highlights the importance of optimizing light conditions for lentil microgreen cultivation, emphasizing how the interaction between light regimes and spectral quality can influence both physiological performance and the production of bioactive compounds. Red light under a constant regime promoted greater biomass accumulation, aligning with previous studies emphasizing its role in optimizing photosynthesis and cell elongation in controlled systems Poorter et al. (2019); Hernández and Kubota (2016). The Gaussian regime, particularly under red and blue light, activated photoprotective mechanisms, consistent with findings linking blue light to enhanced stress responses Zhang et al. (2020). The balanced effects of RBW light, supporting growth and nutritional quality, align with literature on the synergistic potential of red and blue light combinations Ashenafi et al. (2023), while the moderate effects of white light may be related to its spectral diversity, characterized by a significantly higher proportion of green light compared to red and blue light. Although green light exhibits high leaf penetration capacity Brodersen and Vogelmann (2010), its effectiveness in activating photoreceptors such as cryptochromes and phytochromes is lower than that of blue and red light, respectively. Furthermore, green light can antagonize the activation of cryptochromes induced by blue light, reversing responses such as blue light-induced stomatal opening Smith et al. (2017), which may negatively affect gas exchange and photosynthetic capacity. In this context, white light can be advantageous in cultivation systems where uniformity and versatility are prioritized over the maximization of specific variables, such as biomass or bioactive compound production. Although the responses to Gaussian white light are subtle, it is evident that the spectral variation in this regime may have induced signaling pathways favoring the allocation of resources toward adaptation and protection mechanisms rather than growth. These findings contribute valuable insights for refining spectral combinations and illumination regimes to optimize production, particularly for high-value crops like microgreens. By advancing the understanding of spectral interactions, this study supports the development of more efficient and sustainable approaches in vertical farming, enhancing yield, nutritional quality, and valorization of these microgreens, which may also positively impact their market value Kozai et al. (2016); Pennisi et al. (2020).

5 Conclusions

As indicated by the obtained results, it is evident that constant and modulated lighting regimes distinctly impact the growth, photosynthesis, and biomass production in lentil microgreens. The constant regime stood out for its greater efficiency in biomass production and energy efficiency, particularly under red, RBW, and white lights. On the other hand, the Gaussian regime was more effective in inducing bioactive compounds, such as carotenoids, especially under red light, demonstrating a greater photoprotective adaptation.

The results indicate that the choice of lighting regime should be based on the cultivation objective. To maximize biomass accumulation and energy efficiency, the constant regime is most suitable. However, if the focus is on nutritional quality and the production of bioactive compounds, such as carotenoids, the Gaussian regime offers advantages.

Therefore, it is observed that the strategic combination of lighting regimes and light spectra can optimize both the yield and quality of harvests.

Data availability statement

The raw data supporting the conclusions of this article will be made available by the authors, without undue reservation.

Author contributions

MS: Conceptualization, Investigation, Software, Writing – original draft, Writing – review & editing. JV: Data curation, Investigation, Writing – original draft, Writing – review & editing. FS: Resources, Supervision, Writing – original draft, Writing – review & editing. AB: Formal analysis, Methodology, Supervision, Writing – original draft, Writing – review & editing. ÍG: Supervision, Writing – original draft, Writing – review & editing. MV: Formal analysis, Writing – original draft, Writing – review & editing. AC: Data curation, Formal analysis, Writing – original draft, Writing – review & editing. MR: Investigation, Writing – original draft, Writing – review & editing. FS: Supervision, Writing – original draft, Writing – review & editing.

Funding

The author(s) declare financial support was received for the research, authorship, and/or publication of this article. The project was funded by the National Council for Scientific and Technological Development (CNPq, Grant # 408285/2021-4; 421052/2023-6 and 153369/2023-0), and by the Financier of Studies and Projects/the Research Support Foundation of the State of Goiás (FINEP/FAPEG Tecnova II Grant # 202010267000346).

Acknowledgments

The authors thank the Goiano Federal Institute of Education, Science and Technology - Rio Verde CAMPUS, the Pro-Rectory of Research, Postgraduate Studies, and Innovation of the Goiano Federal Institute, the National Council for Scientific and Technological Development (CNPq), and the Financier of Studies and Projects (FINEP), as well as the Research Support Foundation of the State of Goiás (FAPEG) for the funding.

Conflict of interest

Author IG was employed by the company Brazilian Agricultural Research Corporation EMBRAPA.

The remaining authors declare that the research was conducted in the absence of any commercial or financial relationships that could be construed as a potential conflict of interest.

Generative AI statement

The author(s) declare that no Generative AI was used in the creation of this manuscript.

Publisher's note

Supplementary material

The Supplementary Material for this article can be found online at: https://www.frontiersin.org/articles/10.3389/fpls.2024.1515457/full#supplementary-material

References

Ashenafi, E. L., Nyman, M. C., Holley, J. M., and Mattson, N. S. (2023). The influence of leds with different blue peak emission wavelengths on the biomass, morphology, and nutrient content of kale cultivars. *Scientia Hortic.* 317, 111992. doi: 10.1016/j.scienta.2023.111992

Bantis, F., and Koukounaras, A. (2024). Microgreen vegetables' production can be optimized by combining the substrate and nutrient solution in a pfal. *Scientia Hortic.* 333, 113277. doi: 10.1016/j.scienta.2024.113277

Bhandari, K., Siddique, K. H. M., Turner, N. C., Kaur, J., Singh, S., and Agrawal, S. K. (2016). Heat stress at reproductive stage disrupts leaf carbohydrate metabolism, impairs reproductive function, and severely reduces seed yield in lentil. *J. Crop Improvement* 30, 118–151. doi: 10.1080/15427528.2015.1134744

Bilger, W., Schreiber, U., and Bock, M. (1995). Determination of the quantum efficiency of photosystem ii and of non-photochemical quenching of chlorophyll fluorescence in the field. *Oecologia* 102, 425–432. doi: 10.1007/BF00341354

Boonmee, C., Watjanatepin, N., Kiatsookkanatorn, P., Sooktang, K., Wannakam, K., and Homjan, J. (2024). "Control of a semi-closed plant factory with artificial lighting-based on two different led with nb-iot," in *ECTI transactions on electrical engineering, electronics, and communications* (Thailand: ECTI Association), 22. doi: 10.37936/ecti-eec.2024221.251491

Boucher, L., Nguyen, T.-T.-A., Brégard, A., Pepin, S., and Dorais, M. (2023). Optimizing light use efficiency and quality of indoor organically grown leafy greens by using different lighting strategies. *Agronomy* 13, 2582. doi: 10.3390/agronomy13102582

Brazaitytė, A., Viršilė, A., Samuolienė, G., Vaštakaitė-Kairienė, V., Jankauskienė, J., Miliauskienė, J., et al. (2019). Response of mustard microgreens to different wavelengths and durations of uv-a leds. *Front. Plant Sci.* 10. doi: 10.3389/fpls.2019.01153

Brodersen, C. R., and Vogelmann, T. C. (2010). Do changes in light direction affect absorption profiles in leaves? *Funct. Plant Biol.* 37, 403–412. doi: 10.1071/FP09262

Budavári, N., Pék, Z., Helyes, L., Takács, S., and Nemeskéri, E. (2024). An overview on the use of artificial lighting for sustainable lettuce and microgreens production in an indoor vertical farming system. *Horticulturae* 10, 938. doi: 10.3390/horticulturae10090938

Caferri, R., Guardini, Z., Bassi, R., and Dall'Osto, L. (2022). "Assessing photoprotective functions of carotenoids in photosynthetic systems of plants and green algae," in *Methods in Enzymology*, Vol. 674. (Academic Press), 53–84. doi: 10.1016/bs.mie.2022.04.006

Carvalho, S., and Folta, K. (2016). Green light control of anthocyanin production in microgreens. *Acta Hortic.* 1134, 11–18. doi: 10.17660/ActaHortic.2016.1134.2

Chen, Z., Tao, X., Khan, A., Tan, D. K. Y., and Luo, H. (2018). Biomass accumulation, photosynthetic traits and root development of cotton as affected by irrigation and nitrogen-fertilization. *Front. Plant Sci.* 9. doi: 10.3389/fpls.2018.00173

Ciriello, M., Formisano, L., Rouphael, Y., De Pascale, S., and Kacira, M. (2023). Effects of daily light integral and photoperiod with successive harvests on basil yield, morpho-physiological characteristics, and mineral composition in vertical farming. *Scientia Hortic.* 322, 112396. doi: 10.1016/j.scienta.2023.112396

Cowden, R. J., Markussen, B., Ghaley, B. B., and Henriksen, C. B. (2024). The effects of light spectrum and intensity, seeding density, and fertilization on biomass, morphology, and resource use efficiency in three species of brassicaceae microgreens. *Plants* 13, 124. doi: 10.3390/plants13010124

de Castro, J. N., Müller, C., Almeida, G. M., and Costa, A. C. (2019). Physiological tolerance to drought under high temperature in soybean cultivars. *Aust. J. Crop Sci.* 13, 976–987. doi: 10.21475/AJCS.19.13.06.P1767

Dou, H., Niu, G., Gu, M., and Masabni, J. G. (2018). Responses of sweet basil to different daily light integrals in photosynthesis, morphology, yield, and nutritional quality. *HortScience* 53, 496–503. doi: 10.21273/HORTSCI12785-17

Dubey, S., Harbourne, N., Harty, M., Hurley, D., and Elliott-Kingston, C. (2024). Microgreens production: exploiting environmental and cultural factors for enhanced agronomical benefits. *Plants* 13, 2631. doi: 10.3390/plants13182631

Flores, M., Hernández-Adasme, C., Guevara, M. J., and Escalona, V. H. (2024). Effect of different light intensities on agronomic characteristics and antioxidant compounds of brassicaceae microgreens in a vertical farm system. *Front. Sustain. Food Syst.* 8. doi: 10.3389/fsufs.2024.1349423

Folta, K. M., and Maruhnich, S. A. (2007). Green light: a signal to slow down or stop. *J. Exp. Bot.* 58, 3099–3111. doi: 10.1093/jxb/erm130

Fork, D. C., and Satoh, K. (1986). The control by state transitions of the distribution of excitation energy in photosynthesis. *Annu. Rev. Plant Biol.* 37, 335–361. doi: 10.1146/annurev.pp.37.060186.002003

Fraszczak, B., and Kula-Maximenko, M. (2022). The biometric parameters of microgreen crops grown under various light conditions. *Agriculture* 12, 576. doi: 10.3390/agriculture12050576

Garegnani, M., Sandri, C., Pacelli, C., Ferranti, F., Bennici, E., Desiderio, A., et al. (2024). Non-destructive real-time analysis of plant metabolite accumulation in radish microgreens under different led light recipes. *Front. Plant Sci.* 14. doi: 10.3389/fpls.2023.1289208

Genty, B., Briantais, J.-M., and Baker, N. R. (1989). The relationship between the quantum yield of photosynthetic electron transport and quenching of chlorophyll fluorescence. *Biochim. Biophys. Acta (BBA) - Gen. Subj.* 990, 87–92. doi: 10.1016/S0304-4165(89)80016-9

Guenther, J. E., Nemson, J. A., and Melis, A. (1990). Development of photosystem ii in dark grown chlamydomonas reinhardtii: A light-dependent conversion of ps iiβ, qb-nonreducing centers to the ps iiα, qb-reducing form. *Photosynthesis Res.* 24, 35–46. doi: 10.1007/BF00032642

Hashimoto, H., Uragami, C., and Cogdell, R. J. (2016). Carotenoids and photosynthesis. *Subcell. Biochem.* 79, 111-139. doi: 10.1007/978-3-319-39126-74

Havaux, M., Strasser, R. J., and Greppin, H. (1991). A theoretical and experimental analysis of the qp and qn coefficients of chlorophyll fluorescence quenching and their relation to photochemical and nonphotochemical events. *Photosynthesis Res.* 27, 41–55. doi: 10.1007/BF00029975

Hernández, R., and Kubota, C. (2016). Physiological responses of cucumber seedlings under different blue and red photon flux ratios using leds. *Environ. Exp. Bot.* 121, 66–74. doi: 10.1016/j.envexpbot.2015.04.001

Jahns, P., and Holzwarth, A. R. (2012). The role of the xanthophyll cycle and of lutein in photoprotection of photosystem ii. *Biochim. Biophys. Acta (BBA) - Bioenergetics* 1817, 182–193. doi: 10.1016/j.bbabio.2011.04.012

Jeong, B. R., and Sivanesan, I. (2015). Direct adventitious shoot regeneration, *in vitro* flowering, fruiting, secondary metabolite content and antioxidant activity of scrophularia takesimensis nakai. *Plant Cell Tissue Organ Culture (PCTOC)* 123, 607–618. doi: 10.1007/s11240-015-0864-6

Kaiser, E., Morales, A., Harbinson, J., Kromdijk, J., Heuvelink, E., and Marcelis, L. F. M. (2014). Dynamic photosynthesis in different environmental conditions. *J. Exp. Bot.* 66, 2415–2426. doi: 10.1093/jxb/eru406

Keller, B., Zimmermann, L., Rascher, U., Matsubara, S., Steier, A., and Muller, O. (2022). Toward predicting photosynthetic efficiency and biomass gain in crop genotypes over a field season. *Plant Physiol.* 188, 301–317. doi: 10.1093/plphys/kiab483

Kong, J., Zhao, Y., Fan, P., Wang, Y., Xu, X., Wang, L., et al. (2024). Far-red light modulates grapevine growth by increasing leaf photosynthesis efficiency and triggering organ-specific transcriptome remodelling. *BMC Plant Biol.* 24, 189. doi: 10.1186/s12870-024-04870-7

Kozai, T., Fujiwara, K., and Runkle, E. S. (2016). "Led lighting for urban agriculture," in *Plant factory: an indoor vertical farming system for efficient quality food production*. Eds. T. Kozai, K. Fujiwara and E. S. Runkle (Singapore: Springer), 277–293. doi: 10.1007/978-981-10-1848-0

Kozai, T., and Niu, G. (2020). "Chapter 2 - role of the plant factory with artificial lighting (pfal) in urban areas," in *Plant factory (Second edition)*. Eds. T. Kozai, G. Niu and M. Takagaki (London, UK: Academic Press), 7–34. doi: 10.1016/B978-0-12-816691-8.00002-9

Kramer, D. M., Johnson, G., Kiirats, O., and Edwards, G. E. (2004). New fluorescence parameters for the determination of qa redox state and excitation energy fluxes. *Photosynthesis Res.* 79, 209–218. doi: 10.1023/B:PRES.0000015391.99477.0d

Laisk, A., and Loreto, F. (1996). Determining photosynthetic parameters from leaf CO2 exchange and chlorophyll fluorescence (Ribulose-1,5-bisphosphate carboxylase/oxygenase specificity factor, dark respiration in the light, excitation distribution between photosystems, alternative electron transport rate, and mesophyll diffusion resistance. *Plant Physiol.* 110, 903–912. doi: 10.1104/pp.110.3.903

Lawson, T., Kramer, D. M., and Raines, C. A. (2012). Improving yield by exploiting mechanisms underlying natural variation of photosynthesis. *Curr. Opin. Biotechnol.* 23, 215–220. doi: 10.1016/j.copbio.2011.12.012

Li, R., He, Y., Chen, J., Zheng, S., and Zhuang, C. (2023). Research progress in improving photosynthetic efficiency. *Int. J. Mol. Sci.* 24, 9286. doi: 10.3390/ijms24119286

Li, Y., Swaminathan, K., and Hudson, M. E. (2011). Rapid, organ-specific transcriptional responses to light regulate photomorphogenic development in dicot seedlings. *Plant Physiol.* 156, 2124–2140. doi: 10.1104/pp.111.179416

Li, L., Xin Tong, Y., Ling Lu, J., Mei Li, Y., and Chang Yang, Q. (2020). Lettuce growth, nutritional quality, and energy use efficiency as affected by red–blue light combined with different monochromatic wavelengths. *HortScience* 55, 613–620. doi: 10.21273/HORTSCI14671-19

Lin, K.-H., Huang, M.-Y., Huang, W.-D., Hsu, M.-H., Yang, Z.-W., and Yang, C.-M. (2013). The effects of red, blue, and white light-emitting diodes on the growth, development, and edible quality of hydroponically grown lettuce (lactuca sativa l. var. capitata). *Scientia Hortic.* 150, 86–91. doi: 10.1016/j.scienta.2012.10.002

Llorente, B., D'Andrea, L., and Rodríguez-Concepción, M. (2016). Evolutionary recycling of light signaling components in fleshy fruits: new insights on the role of pigments to monitor ripening. *Front. Plant Sci.* 7. doi: 10.3389/fpls.2016.00263

Manivannan, A., Soundararajan, P., Halimah, N., Ko, C. H., and Jeong, B. R. (2015). Blue led light enhances growth, phytochemical contents, and antioxidant enzyme activities of rehmannia glutinosa cultured in *vitro*. *Horticulture Environment Biotechnol.* 56, 105–113. doi: 10.1007/s13580-015-0114-1

Maxwell, K., and Johnson, G. N. (2000). Chlorophyll fluorescence—a practical guide. *J. Exp. Bot.* 51, 659–668. doi: 10.1093/jexbot/51.345.659

Murchie, E. H., and Niyogi, K. K. (2010). Manipulation of photoprotection to improve plant photosynthesis. *Plant Physiol.* 155, 86–92. doi: 10.1104/pp.110.168831

Nájera, C., Gallegos-Cedillo, V. M., Ros, M., and Pascual, J. A. (2022). Led lighting in vertical farming systems enhances bioactive compounds and productivity of vegetables crops. *Biol. Life Sci. Forum* 16, 24. doi: 10.3390/IECHo2022-12514

Nie, R., Wei, X., Jin, N., Su, S., and Chen, X. (2024). Response of photosynthetic pigments, gas exchange and chlorophyll fluorescence parameters to light quality in *Phoebe bournei* seedlings. *Plant Growth Regul.* 103, 675–687. doi: 10.1007/s10725-024-01131-3

Orsini, F., Pennisi, G., Zulfiqar, F., and Gianquinto, G. (2020). Sustainable use of resources in plant factories with artificial lighting (pfals). *Eur. J. Hortic. Sci.* 85, 297–309. doi: 10.17660/eJHS.2020/85.5.1

Pennisi, G., Pistillo, A., Orsini, F., Cellini, A., Spinelli, F., Nicola, S., et al. (2020). Optimal light intensity for sustainable water and energy use in indoor cultivation of lettuce and basil under red and blue leds. *Scientia Hortic.* 272, 109508. doi: 10.1016/j.scienta.2020.109508

Poorter, H., Niinemets, Ü, Ntagkas, N., Siebenkäs, A., Mäenpää, M., Matsubara, S., et al. (2019). A meta-analysis of plant responses to light intensity for 70 traits ranging from molecules to whole plant performance. *New Phytol.* 223, 107–122. doi: 10.1111/nph.15754

Preiti, G., Calvi, A., Badagliacca, G., Presti, E. L., Monti, M., and Bacchi, M. (2024). Agronomic performances and seed yield components of lentil (lens culinaris medikus) germplasm in a semi-arid environment. *Agronomy* 14, 303. doi: 10.3390/agronomy14020303

Priti, P., Mishra, G. P., Dikshit, H. K., T., V., Tontang, M. T., Stobdan, T., et al. (2021). Diversity in phytochemical composition, antioxidant capacities, and nutrient contents among mungbean and lentil microgreens when grown at plain-altitude region (delhi) and high-altitude region (leh-ladakh), India. *Front. Plant Sci.* 12. doi: 10.3389/fpls.2021.710812

Qiao, M.-Y., Zhang, Y.-J., Liu, L.-A., Shi, L., Ma, Q.-H., Chow, W. S., et al. (2021). Do rapid photosynthetic responses protect maize leaves against photoinhibition under fluctuating light? *Photosynthesis Res.* 149, 57–68. doi: 10.1007/s11120-020-00780-5

Saini, S., Sharma, P., Sharma, J., Pooja, P., and Sharma, A. (2024). Drought stress in lens culinaris: effects, tolerance mechanism, and its smart reprogramming by using modern biotechnological approaches. *Physiol. Mol. Biol. Plants* 30, 227–247. doi: 10.1007/s12298-024-01417-w

Schneider, C. A., Rasband, W. S., and Eliceiri, K. W. (2012). Nih image to imagej: 25 years of image analysis. *Nat. Methods* 9, 671–675. doi: 10.1038/nmeth.2089

Smith, H. L., McAusland, L., and Murchie, E. H. (2017). Don't ignore the green light: exploring diverse roles in plant processes. *J. Exp. Bot.* 68, 2099–2110. doi: 10.1093/jxb/erx098

Stamford, J. D., Hofmann, T. A., and Lawson, T. (2024). Sinusoidal led light recipes can improve rocket edible biomass and reduce electricity costs in indoor growth environments. *Front. Plant Sci.* 15. doi: 10.3389/fpls.2024.1447368

Tang, G., Wang, Y., Lu, Z., Cheng, S., Hu, Z., Chen, S., et al. (2024). Effects of combined nitrogen–phosphorus on biomass accumulation, allocation, and allometric growth relationships in pinus yunnanensis seedlings after top pruning. *Plants* 13, 2450. doi: 10.3390/plants13172450

Teng, Z., Luo, Y., Sun, J., Li, Y., Pearlstein, D. J., Oehler, M. A., et al. (2024). Effect of far-red light on biomass accumulation, plant morphology, and phytonutrient composition of ruby streaks mustard at microgreen, baby leaf, and flowering stages. *J. Agric. Food Chem.* 72, 9587–9598. doi: 10.1021/acs.jafc.3c06834

Toscano, S., Cavallaro, V., Ferrante, A., Romano, D., and Patané, C. (2021). Effects of different light spectra on final biomass production and nutritional quality of two microgreens. *Plants* 10, 1584. doi: 10.3390/plants10081584

Toyomasu, T., Tsuji, H., Yamane, H., Nakayama, M., Yamaguchi, I., Murofushi, N., et al. (1993). Light effects on endogenous levels of gibberellins in photoblastic lettuce seeds. *J. Plant Growth Regul.* 12, 85–93. doi: 10.1007/BF00193238

van Delden, S. H., SharathKumar, M., Butturini, M., Graamans, L. J. A., Heuvelink, E., Kacira, M., et al. (2021). Current status and future challenges in implementing and upscaling vertical farming systems. *Nat. Food* 2, 944–956. doi: 10.1038/s43016-021-00402-w

Vialet-Chabrand, S., Matsubara, S., and Lawson, T. (2024). Editorial: Dynamic photosynthesis under non-steady conditions. *Front. Plant Sci.* 15. doi: 10.3389/fpls.2024.1489818

Wang, T., Sun, Q., Zheng, Y., Xu, Y., Liu, B., and Li, Q. (2024). Effects of red and blue light on the growth, photosynthesis, and subsequent growth under fluctuating light of cucumber seedlings. *Plants* 13, 1668. doi: 10.3390/plants13121668

Wei, Y., Wang, S., and Yu, D. (2023). The role of light quality in regulating early seedling development. *Plants* 12, 2746. doi: 10.3390/plants12142746

Wellburn, A. R. (1994). The spectral determination of chlorophylls a and b, as well as total carotenoids, using various solvents with spectrophotometers of different resolution. *J. Plant Physiol.* 144, 307–313. doi: 10.1016/S0176-1617(11)81192-2

Yousef, A. F., Ali, M. M., Rizwan, H. M., Tadda, S. A., Kalaji, H. M., Yang, H., et al. (2021). Photosynthetic apparatus performance of tomato seedlings grown under various combinations of led illumination. *PloS One* 16, 1–17. doi: 10.1371/journal.pone.0249373

Yudina, L., Sukhova, E., Gromova, E., Mudrilov, M., Zolin, Y., Popova, A., et al. (2023). Effectofdurationof led lighting on growth, photosynthesis and respiration in lettuce. *Plants* 12, 442. doi: 10.3390/plants12030442

Zhang, X., Bian, Z., Yuan, X., Chen, X., and Lu, C. (2020). A review on the effects of light-emitting diode (led) light on the nutrients of sprouts and microgreens. *Trends Food Sci. Technol.* 99, 203–216. doi: 10.1016/j.tifs.2020.02.031

Zhang, S., Guo, X., Li, J., Zhang, Y., Yang, Y., Zheng, W., et al. (2022). Effects of light-emitting diode spectral combinations on growth and quality of pea sprouts under long photoperiod. *Front. Plant Sci.* 13. doi: 10.3389/fpls.2022.978462. This article is part of the Research Topic: Advanced Technologies for Energy Saving

Zukauskas, A., Bliznikas, Z., Breivė, K., Novičkovas, A., Samuolienė, G., Urbonavičiūtė, A., et al. (2011). Effect of supplementary pre-harvest led lighting on the antioxidant properties of lettuce cultivars. *Acta Hortic.* 907, 87–90. doi: 10.17660/ActaHortic.2011.907.8

3 Um Sistema de Agricultura Vertical de Precisão com Arquitetura Aberta para Microverdes de Gergelim: Telemetria Auditável para Iluminação Dinâmica e Avaliação Energia–Biomassa

Este capítulo apresenta o artigo intitulado *An Open-Architecture Precision Vertical Farming System for Sesame Microgreens: Audit-Ready Telemetry for Dynamic Lighting and Energy–Biomass Benchmarking*, aceito para publicação no periódico *Smart Agricultural Technology*.

Título em português: Um Sistema de Agricultura Vertical de Precisão com Arquitetura Aberta para Microverdes de Gergelim: Telemetria Auditável para Iluminação Dinâmica e Avaliação Energia–Biomassa.

DOI: <https://doi.org/10.1016/j.atech.2026.102105>

Periódico: *Smart Agricultural Technology*.

Indicadores do periódico: Impact Factor 5.7, CiteScore 7.7 e periódico *open access*.

O artigo apresenta o desenvolvimento e a validação de um *Precision Vertical Farming System* (PVFS) de arquitetura aberta, aplicado ao cultivo de microverdes de gergelim sob perfis temporais constantes e gaussianos de iluminação. A abordagem integra controle dinâmico de PPFD, telemetria auditável, monitoramento ambiental, consumo energético e desempenho biomássico, contribuindo para a rastreabilidade experimental e para a avaliação da eficiência energia–biomassa em sistemas de agricultura vertical.

Smart Agricultural Technology 14 (2026) 102105

Contents lists available at ScienceDirect

Smart Agricultural Technology

journal homepage: www.journals.elsevier.com/smart-agricultural-technology

An open-architecture precision vertical farming system for sesame microgreens: Audit-ready telemetry for dynamic lighting and energy–biomass benchmarking

Marlus Dias Silva [a,*], Jaqueline Martins Vasconcelos [a], Fábia Barbosa da Silva [a], Adriano Soares de Oliveira Bailão [b], Ítalo Moraes Rocha Guedes [c], Márcio da Silva Vilela [d], Adriano Carvalho Costa [a], Márcio Rosa [e], Lucas Loram Lourenço [a], Fabiano Guimarães Silva [a,*]

[a] Laboratory of Advanced Studies in Vertical Farming, Federal Institute of Education, Science and Technology Goiano (IF Goiano), Rio Verde Campus, Rio Verde, Goiás, Brazil
[b] Laboratory of Computational Intelligence, Federal Institute of Education, Science and Technology Goiano (IF Goiano), Rio Verde Campus, Rio Verde, Goiás, Brazil
[c] Brazilian Agricultural Research Corporation (EMBRAPA), Embrapa Vegetables (Embrapa Hortaliças), Brasília, Federal District, Brazil
[d] Laboratory of Automation, Simulation and Control, Federal Institute of Education, Science and Technology Goiano (IF Goiano), Rio Verde Campus, Rio Verde, Goiás, Brazil
[e] Graduate Program in Plant Production, University of Rio Verde (UniRV), Rio Verde, Goiás, Brazil

ARTICLE INFO

Keywords:
Precision vertical farming
Plant factory with artificial lighting (PFAL)
Internet of things (IoT)
Dynamic lighting
Energy use efficiency
Sesame microgreens
Reproducibility

ABSTRACT

The reproducibility of lighting protocols in *Plant Factories with Artificial Lighting* (PFALs) is frequently constrained by the scarcity of auditable operational data. This study presents and validates an open-architecture *Precision Vertical Farming System* (PVFS) capable of executing dynamic photosynthetic photon flux density (PPFD) profiles under controlled Daily Light Integral (DLI), ensuring traceability via IoT telemetry. The system was applied to sesame microgreens grown using a 2×4 factorial design, combining temporal profiles (Constant vs. Gaussian) and light spectra (White, Blue, Red, and RBW), with DLI equalized at $10.8\,\mathrm{mol\,m^{-2}\,d^{-1}}$. Telemetric validation demonstrated high stability (jitter ≈ 0) and data completeness ($> 98\%$), enabling the precise calculation of Specific Energy Consumption (SEC) and Energy-to-Mass Efficiency (EEMS). Results indicated that, under equivalent DLI, the Gaussian profile increased energy costs (higher SEC) without proportional biomass gains for most spectra. The Red–Constant treatment achieved the highest efficiency ($10.02\,\mathrm{g\,kWh^{-1}}$), whereas white light exhibited the highest energy cost. Principal Component Analysis (PCA) reinforced that energy performance (SEC/EEMS) was more strongly associated with production outcomes (biomass) than with instantaneous photosynthetic metrics (e.g., F_v/F_m), underscoring the importance of continuous monitoring of energy use and yield. The PVFS proved to be a robust tool for energy benchmarking and the standardization of lighting recipes in vertical farming.

1. Introduction

Global population growth and rapid urbanization impose increasing pressure on food production, necessitating agricultural systems that are more sustainable, efficient, and resilient. In this context, vertical farms—or *plant factories with artificial lighting* (PFALs), within the broader scope of controlled-environment agriculture (CEA)—have emerged as a promising alternative. They enable the production of high-value leafy crops and microgreens in tightly controlled environments, optimizing the use of space, water, and inputs while reducing dependence on external climatic conditions [1–3].

Despite this potential, the technical and economic feasibility of indoor agriculture relies heavily on the control and efficiency of artificial lighting. Lighting often accounts for a substantial share of energy use in PFALs and is a key determinant of photosynthesis, growth, and product quality [4–8]. Beyond spectral composition, the *temporal profile* of photosynthetic photon flux density (PPFD) delivery—such as Constant versus Gaussian profiles—may alter physiological responses and, crucially, the energy–biomass relationship, even when the daily light integral (DLI) remains equivalent. Therefore, evaluating temporal profiles requires moving beyond physiological *proxies* to incorporate energy–production metrics, such as specific energy consumption (SEC; $\mathrm{kWh\,g^{-1}}$)

* Corresponding authors.
E-mail addresses: marlus.silva@ifgoiano.edu.br (M. Dias Silva), fabiano.silva@ifgoiano.edu.br (F. Guimarães Silva).

https://doi.org/10.1016/j.atech.2026.102105
Received 14 February 2026; Received in revised form 11 April 2026; Accepted 11 April 2026
Available online 7 May 2026

and energy-to-mass efficiency (EEMS; g kWh^{-1}), supported by traceable electrical monitoring.

Advances in digital technologies, IoT, and data analytics have accelerated the development of intelligent solutions for CEA, integrating sensors, actuators, and analytical platforms in near real-time [9–11,42]. Recent studies exemplify this trend by combining monitoring and computational modeling for decision support. Examples include approaches based on spectral indices and computer vision for crop monitoring in vertical farms [12,13], dynamic protocols to improve resource-use efficiency in soilless systems [14], and open platforms for control and automation [15]. Existing indoor-farming and smart-agriculture platforms already provide important capabilities such as modular sensing, remote dashboards, actuator control, automated logging, cloud-enabled analytics, and adaptive lighting control [43,49,50,52,53]. However, these systems are typically oriented toward usability, affordability, scalability, automation, or communication responsiveness, rather than toward experimentally auditable execution of lighting protocols. Smart-farming literature also highlights persistent challenges related to fragmented, inconsistent, and heterogeneous IoT data, lack of standards, and the need to ensure the accuracy of transmitted data [48,51]. In indoor cultivation, this distinction is especially relevant because DLI directly influences biomass accumulation and energy-use efficiency [47]; thus, assuming treatment equivalence from nominal setpoints alone, without validating the delivered PPFD trajectory over time, may limit reproducibility and cross-study benchmarking. Nevertheless, solutions that integrate (i) programmable temporal profiles under a target DLI, (ii) continuous electrical measurement (power/energy), (iii) an analytical *pipeline* (statistical and multivariate) oriented toward energy–biomass indicators, and (iv) telemetry-based verification of timestamp coherence, data integrity, and achieved DLI equivalence in a unified and reproducible manner remain scarce. This gap is particularly relevant given the need for benchmarking and standardization of energy metrics in vertical farms [5] and the demand for integrated instrumentation in multi-objective optimization strategies under dynamic lighting [16]. Unlike existing indoor-farming platforms that primarily emphasize monitoring, automation, or cloud analytics, the PVFS was specifically designed to make dynamic lighting protocols experimentally auditable by coupling edge-executed setpoints with time-synchronized telemetry, QA/QC metrics for sampling regularity and completeness, and telemetry-derived validation of achieved DLI equivalence.

Due to their short growth cycle and high density of bioactive compounds, microgreens have gained prominence as a crop of interest, with increasing demand and the potential to enhance the nutritional value of diets [17–19]. Sesame (*Sesamum indicum* L.), although traditionally cultivated as an oilseed crop, is also a promising candidate for microgreen production due to the functional and nutritional value of its foliage. Young sesame leaves have been reported to contain diverse iridoids and polyphenols, including acteoside, with marked antioxidant and antiglycation activity, and acteoside accumulation in leaves has reached up to 12.9% of dry weight at specific growth stages [20]. In addition, sesame leaves have been described as a nutrient-rich edible leafy vegetable, with balanced amino acid composition and high levels of minerals and vitamins, including Ca, Se, and vitamins A, C, D, and B_2, in some cases exceeding values reported for commonly consumed vegetables [46]. These attributes make sesame especially attractive for PFAL-based microgreen production, where rapid-cycle crops with high functional value are of particular interest. However, knowledge gaps persist regarding how temporal PPFD profiles and different light spectra affect the growth, photochemistry, and productivity of sesame microgreens when energy performance is jointly evaluated with physiological responses.

This study presents and experimentally validates a *Precision Vertical Farming System* (PVFS) for PFAL research, where lighting protocols shift from purely textual descriptions to executable and auditable prescriptions supported by telemetry. The PVFS combines programmable control of temporal PPFD profiles under a target DLI, continuous logging of environmental and electrical variables, and an integrated analytical workflow to relate physiological performance and production to energy costs. To ensure reproducibility and auditability, the source code and associated services are made openly available.

Accordingly, the objective of this study was to develop and validate the PVFS and apply it to sesame microgreens production using a 2×4 factorial design (Constant and Gaussian profiles × four spectra), maintaining a fixed photoperiod and equivalent DLI. Operational compliance was verified via telemetry, and the effects of profile and spectrum were assessed on growth, pigments, chlorophyll fluorescence, and energy–biomass metrics (specific energy per area, AEC; dry mass yield per area, MSA; SEC/EEMS) using ANOVA and PCA.

2. Materials and methods

The experiment was conducted under controlled conditions using a 2×4 factorial design (Constant vs. Gaussian × four spectra), with equivalent DLI and six trays per treatment ($n = 6$; 48 experimental units). The PVFS executed the lighting protocols and logged environmental and electrical telemetry to ensure traceability. Growth, biomass, pigments, and chlorophyll fluorescence were evaluated, as well as AEC, MSA, SEC, and EEMS. Effects were tested by ANOVA/Tukey ($\alpha = 0.05$) and PCA, and operational compliance was verified through telemetry validation.

2.1. Overview and relevance of the PVFS architecture

The *Precision Vertical Farming System* (PVFS) was designed as a five-layer architecture (Fig. 1) that follows a common IoT platform view of layered separation of concerns-physical assets, edge devices, infrastructure services, communication interfaces, and applications-and adapts it to PFAL experimentation to make protocol execution and data provenance verifiable via telemetry [21,22]. In the PVFS, each control action (e.g., per-channel dimming/PPFD) is recorded with a reliable timestamp and is traceably linked to environmental and energy variables measured over the same interval, enabling audit-ready reconstruction of the executed lighting trajectory and its corresponding system response.

As illustrated in Fig. 1, localizing sensing, actuation, and local control at the edge reduces command-to-record latency and improves responsiveness, which is a core motivation for edge computing in smart agriculture [23,24]. Control and telemetry exchange follow an asynchronous publish/subscribe model over MQTT, a lightweight protocol widely used in IoT deployments [25–27]. To ensure temporal coherence across control events and measurements, PVFS timestamps messages in UTC and disciplines device clocks using the Network Time Protocol (NTP), enabling consistent time-series reconstruction (e.g., PPFD trajectories and DLI integration) and automated detection of gaps or anomalies [28]. Where bidirectional streaming is required (e.g., live telemetry dashboards), WebSocket provides a standardized full-duplex transport [29].

Overall, this architecture enables the PVFS to operate not only as an instrumented growth chamber but also as an evidence-oriented experimental infrastructure: protocol reproducibility becomes testable against persisted telemetry, and agronomic outcomes can be interpreted alongside operational and energy metrics (e.g., SEC and EEMS) derived from the same auditable record.

2.2. Experimental setup and cultivation conditions

The experiment was conducted under controlled conditions in a controlled-environment agriculture facility in Brazil. In each experimental unit, 1.28 g of sesame seeds (*Sesamum indicum* L.; ~480 seeds) were sown in trays (20 cm × 14 cm × 6.5 cm) filled with 100 g of a commercial substrate moistened with 25 mL of water and kept in the dark for 12 h. The trays were then transferred to a growth chamber with four shelves (Fig. 2) and four spectral compositions: cool white 6500 K

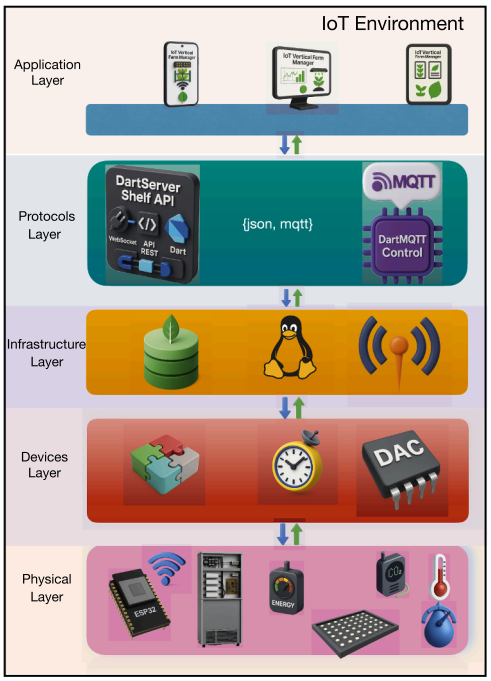

Fig. 1. PVFS five-layer architecture for PFAL experimentation. The Physical layer comprises the growth chamber, LED fixtures, environmental sensors, and electrical metering. The Devices layer executes lighting setpoints at the edge and acquires synchronized telemetry, including UTC timestamping and scheduled multi-channel dimming. The Infrastructure layer hosts messaging and persistence services (MQTT broker and a document-oriented database), storing raw telemetry and derived aggregations for querying and analysis. The Protocols layer defines standardized message interfaces for control and telemetry (e.g., JSON over MQTT) and exposes query/notification services (e.g., REST/WebSocket). The Application layer (IoT Vertical Farm Manager) supports treatment configuration, near real-time monitoring, and data export. Implementation details are provided in the Supplementary Material (Sections S1–S6).

(400–700 nm), red (peak 660 nm), blue (peak 440 nm), and RBW (70.5% red, 8.5% green, and 21.0% blue).

Microgreens were cultivated under a 12 h photoperiod (06:30–18:30) using two temporal lighting profiles: Constant (PPFD = 250 µmol m^{-2} s^{-1}) and Gaussian (PPFD = 85 µmol m^{-2} s^{-1} to 500 µmol m^{-2} s^{-1}, with automatic dimming via PVFS), while maintaining equivalent DLI (10.80 mol m^{-2} d^{-1}). PPFD and spectrum were verified using an LI-180 spectroradiometer (LI-COR, USA). Profiles were conducted in two consecutive 10-day trials.

Irrigation was adjusted to crop water demand (25 mL/d up to 7 DAS and 35 mL/d from 8 DAS onward). Environmental variables, including air temperature, relative humidity, and CO_2 concentration, were continuously logged throughout both experimental windows. Time-series stability analyses for these variables are presented in Supplementary Section S8 to document the chamber microclimate under the Constant and Gaussian windows. The 2 × 4 design (profile × spectrum) included six trays per combination ($n = 6$; 48 experimental units). At 10 DAS, chlorophyll *a* fluorescence, pigments, and biomass were evaluated; the tray was considered the experimental unit, and plant-level measurements were averaged per tray.

2.3. Growth and biomass assessment

For growth assessment, each replicate consisted of multiple seedlings. Fifteen plants were selected per replicate to measure hypocotyl length (CHL) and total leaf area (CTLA). These variables were obtained from images analyzed in ImageJ, as described by [30]. For statistical inference, plant-level measurements were aggregated as tray means (subsamples), preserving the tray as the independent experimental unit.

Fig. 2. Representation of the controlled growth environment.

The remaining plants in each replicate were used to determine fresh and dry mass of hypocotyls and leaves. Samples were weighed on an analytical balance to obtain fresh mass and then dried in a forced-air circulation oven (Tecnal, TE-394/1, Brazil) at 65 °C for 48 h to determine dry mass.

2.4. Chlorophyll a fluorescence

Chlorophyll *a* fluorescence parameters were obtained using an IMAGING-PAM fluorometer (MAXI version) and Imaging Win software (Heinz Walz GmbH, Effeltrich, Germany). Seedlings were individually fixed on a holder at 18.5 cm from a CCD camera coupled to the instrument. Fluorescence was measured on the adaxial leaf surface after 30 min of dark adaptation to ensure full opening of reaction centers. Under this condition, tissues were exposed to a low-intensity measuring light (0.03 μmol m^{-2} s^{-1}) to determine initial fluorescence (Fo). Next, a saturating light pulse (> 6000 μmol m^{-2} s^{-1}) was applied for 0.8 s to determine maximal fluorescence (Fm), and the maximum quantum yield of PSII was computed (Fv/Fm = (Fm – Fo) / Fm) [31].

After illuminating the sample for 40 s, fluorescence under light-adapted conditions was recorded to obtain actinic-light variables such as the effective quantum yield of PSII, Y(II), and non-photochemical quenching (NPQ) [32]. The photochemical quenching coefficient was calculated using standard PAM definitions, $q_P = (F'_m - F_s)/(F'_m - F'_0)$, as implemented in ImagingWin. Electron transport rate (ETR) was calculated as $\mathrm{ETR} = \mathrm{Y(II)} \times \mathrm{PAR} \times A_{\mathrm{leaf}} \times 0.5$ [33], where PAR is photosynthetically active radiation (photon flux density), A_{leaf} is the fraction of incident light absorbed by leaves, and 0.5 is the fraction of excitation energy assumed to be equally distributed between PSII and PSI [34]. When not directly measured, A_{leaf} and actinic irradiance followed the equipment/software settings used in ImagingWin.

2.5. Photosynthetic pigments

Pigment concentrations were determined after extraction with dimethyl sulfoxide (DMSO) saturated with calcium carbonate ($CaCO_3$) [35]. Chlorophyll *a* (Chl*a*), chlorophyll *b* (Chl*b*), and carotenoids (Cart) were quantified using a UV–vis spectrophotometer (Evolution 60S, Thermo Fisher Scientific Inc., MA, USA) at 665, 649, and 480 nm, respectively. Calculations followed the equations proposed by [36], and results were expressed as $\mu g\ g^{-1}$ of leaf fresh mass.

2.6. Calculation of specific energy consumption (SEC) and energy mass efficiency (EEMS)

Specific energy consumption (SEC) was calculated from areal energy consumption (AEC, kWh m^{-2}) and dry mass yield per area (MSA, g m^{-2}).

Areal energy consumption was defined as:

$$\mathrm{AEC} = \frac{E_{\mathrm{tot}}}{A}, \tag{1}$$

where E_{tot} is the total electrical energy consumed during cultivation (kWh) and A is the illuminated area (m^2). When only mean power P (W) and time t (h) were available, we used:

$$E_{\mathrm{tot}} = \frac{P \cdot t}{1000}. \tag{2}$$

Dry mass yield per area was estimated as:

$$\mathrm{MSA} = M_{\mathrm{sec}} \cdot N_m, \tag{3}$$

where M_{sec} is the mean dry mass per seedling (g) and N_m is seedling density (seedlings m^{-2}).

Specific energy consumption was then computed as:

$$\mathrm{SEC} = \frac{\mathrm{AEC}}{\mathrm{MSA}} \quad \left(\mathrm{kWh\,g^{-1}}\right). \tag{4}$$

From this relationship, energy mass efficiency (EEMS) was defined as the inverse of SEC, expressing the amount of dry biomass obtained per unit of consumed energy:

$$\mathrm{EEMS} = \frac{1}{\mathrm{SEC}} \quad \left(\mathrm{g\,kWh^{-1}}\right). \tag{5}$$

Thus, SEC and EEMS are complementary metrics: SEC indicates the energy cost per gram of dry mass produced, whereas EEMS represents biomass return per unit of electrical energy used.

For N_m, 480 seeds per tray (0.028 m^2) were considered, equivalent to 17 142 seeds m^{-2}, adjusted by the observed germination rate of 85%, resulting in 14 571 seedlings m^{-2}. The adopted thermal conditions (20–30 °C) agree with reports for *Sesamum indicum*, indicating high germination rates within this range, supporting the 85% adjustment [37–39].

2.7. Statistical analysis

All data processing and statistical analyses were performed in Python (v3.9.6) using widely adopted scientific libraries, including *pandas* for data handling, *statsmodels* for ANOVA and post-hoc comparisons, and *scikit-learn* for multivariate analysis. A fully reproducible workflow (code and datasets) will be made publicly available upon acceptance.

Data were first inspected by exploratory analysis. To mitigate the influence of outliers without excluding observations, extreme values were winsorized within each treatment cell (*Profile* × *Light*) using Tukey's IQR fences: values below $Q_1 - 1.5 \times IQR$ were set to the lower fence and values above $Q_3 + 1.5 \times IQR$ were set to the upper fence. Winsorization was applied only when $IQR > 0$ and the cell contained at least four non-missing observations.

For each response variable, a two-way factorial ANOVA was fitted with fixed effects of *Profile*, *Light*, and their interaction ($\alpha = 0.05$). Model assumptions were evaluated by residual diagnostics, including normality (Shapiro–Wilk test) and visual inspection of residuals versus fitted values and scale–location plots. When significant effects were detected, means were separated using Tukey's HSD as implemented in *statsmodels*. When the interaction term was significant, simple effects were evaluated (*Profile* within each *Light* and *Light* within each *Profile*).

Multiple comparisons were summarized using a compact letter display (CLD): uppercase letters compare *Profiles* within each *Light*, whereas lowercase letters compare *Lights* within each *Profile*. Results are reported as mean ± standard error (SE).

Multivariate patterns were assessed by principal component analysis (PCA) on tray-level observations ($n = 48$) after centering and unit-variance scaling (autoscaling). Pearson correlation coefficients were also computed. PCA scores, variable loadings, and the proportion of variance explained by each component are reported.

2.8. Telemetry validation and PVFS operational compliance

Operational compliance of the *Precision Vertical Farming System* (PVFS) was verified in both experimental windows (Constant: 08–18 March 2024; Gaussian: 22 March–01 April 2024) through (i) time-series quality control, (ii) DLI calculation from PPFD telemetry, and (iii) Gaussian-profile validation via model fitting.

2.8.1. Acquisition and preprocessing

Telemetry (per-channel PPFD and environmental variables) was collected via MQTT and persisted in MongoDB. Records were stored with UTC timestamps (ISO-8601) and converted to the local time zone (`America/Sao_Paulo`) only for photoperiod segmentation. For summary metrics and comparative plots, series were resampled to a fixed 10 s step using mean aggregation. In addition to the PPFD-focused validation reported below, environmental time series for air temperature, relative humidity, and CO_2 concentration were examined to document chamber microclimate stability across the Constant and Gaussian windows; these complementary analyses are summarized in Supplementary Section S8.

2.8.2. Time-series QA/QC (integrity, jitter, and gaps)

Quality Assurance (QA) and Quality Control (QC) procedures were applied to verify telemetry integrity and sampling-interval regularity. Evaluation was conducted on raw series (without resampling) using forward differences $\Delta t_i = t_{i+1} - t_i$. For each topic, the median interval, the IQR of Δt (sampling-interval variability; *jitter*), and the largest gap were reported; gaps were defined when $\Delta t_i > 60$ s. Completeness was estimated as the ratio between the number of observed samples and the expected number, given the observed duration and nominal interval. Metrics were also computed *per day* within the light window (06:30–18:30, local time), to report daily completeness and identify days with partial data loss.

2.8.3. Telemetry-derived DLI

Daily light integral (DLI; mol $m^{-2}\,d^{-1}$) was calculated by integrating instantaneous PPFD (μmol $m^{-2}\,s^{-1}$) over the photoperiod:

$$\mathrm{DLI} = \frac{1}{10^6} \sum_i \mathrm{PPFD}_i \cdot \Delta t_i, \tag{6}$$

where Δt_i is the time step (s) and the summation spans the light window. To reduce bias due to missing data, Δt_i was capped at 120 s during integration, and integration was clipped to the photoperiod end to avoid night-gap inflation (see Supplementary S7 for the sensitivity analysis and formulation). Equivalence of daily DLI relative to the nominal target was assessed using TOST, with equivalence bounds of ±5% of the target and $\alpha = 0.05$ (90% CI) [40].

2.8.4. Inter-channel uniformity

Inter-channel uniformity (ch1–ch4) was quantified by: (i) instantaneous CV% across channels at each resampled point during the photoperiod; and (ii) daily CV% across channels for daily DLI.

2.8.5. Gaussian-profile validation via model fitting

Under the Gaussian profile, temporal compliance was assessed by fitting a Gaussian function to the measured PPFD series for each channel, per day, within the photoperiod. Local time was normalized to $x \in [0, 1]$ and the following model was fitted:

$$\hat{y}(x) = c_0 + c_1 \exp\left(-\frac{1}{2}\left(\frac{x-\mu}{\sigma}\right)^2\right). \quad (7)$$

For fitting, PPFD was resampled to 30 s (mean). On a predefined grid of (μ, σ), c_0 and c_1 were estimated by linear least squares, and the best fit was selected by the lowest RMSE (*root mean square error*). Fit quality was summarized by RMSE, MAE (*mean absolute error*), and R^2, defined as:

$$\mathrm{RMSE} = \sqrt{\frac{1}{n}\sum_{i=1}^{n}(y_i - \hat{y}_i)^2}, \qquad \mathrm{MAE} = \frac{1}{n}\sum_{i=1}^{n}|y_i - \hat{y}_i|, \quad (8)$$

where y_i and $\hat{y}_i$ are the observed and fitted PPFD values, respectively. Peak time was derived from μ and the photoperiod limits; the procedure was repeated daily to identify days with operational deviations.

3. Results

Three sets of variables were evaluated: (i) photosynthetic pigments—chlorophyll *a* (*Chla*), chlorophyll *b* (*Chlb*), carotenoids (*Cart*), and the *Chla* : *Chlb* ratio; (ii) growth and morphology—hypocotyl length (*CHL*), total leaf area (*CTLA*), hypocotyl fresh weight (*HFW*), leaf fresh weight (*LFW*), leaf dry mass (*LMD*), total dry mass (*TMD*), and hypocotyl dry mass (*HMD*); and (iii) PSII photochemical parameters and energy-performance metrics—effective quantum yield $Y(\mathrm{II})$, maximum quantum efficiency F_v/F_m, non-photochemical quenching (NPQ), photochemical quenching coefficient (q_P), electron transport rate (ETR), specific energy consumption (SEC, $\mathrm{kWh\,g^{-1}}$), and its inverse, Energy-to-Mass Efficiency (EEMS, $\mathrm{g\,kWh^{-1}}$). Analyses considered the effects of lighting profiles (Constant and Gaussian), light spectra (blue, RBW, red, and white), and their interaction. Unless otherwise stated, values represent tray means (experimental unit; $n = 6$ per treatment), with plant-level measurements treated as subsamples aggregated by tray.

Photosynthetic pigment concentrations (Fig. 3) showed a significant *profile* × *light spectrum* interaction. Higher chlorophyll *a* (*Chla*) values (Fig. 3a) were observed under white, RBW, and blue light in the Constant profile. In contrast, under red light, the pattern was reversed, with *Chla* higher in the Gaussian than in the Constant profile. Within each profile, there were no differences among white, RBW, and blue, but all differed from red. In the Constant profile, red light resulted in significantly lower *Chla* than the other treatments, whereas in the Gaussian profile, red light produced the highest *Chla* compared with the other light spectra.

For chlorophyll *b* (*Chlb*) (Fig. 3b), the highest values occurred under white and red light in the Gaussian profile, whereas under RBW the highest values occurred in the Constant profile. Under blue light, no significant differences between profiles were detected.

Carotenoids (*Cart*) (Fig. 3c) differed between profiles under white, RBW, and red light, always with higher values in the Gaussian profile. Under blue light, no significant differences were observed.

The *Chla* : *Chlb* ratio (Fig. 3d) was higher in the Constant profile under white, RBW, and red light, whereas under blue light there was no significant difference between profiles.

Under white and red light, *Chlb* showed higher values in the Gaussian profile, whereas *Cart* also showed higher values in the Gaussian profile under white and red light (Fig. 3).

Electron transport rate (ETR) (Fig. 4d) differed significantly only under white light, with higher values in the Constant profile compared with the Gaussian profile.

The F_v/F_m ratio (Fig. 4a) differed between profiles under RBW and blue light, with higher values in the Gaussian profile. Under white and red light, there were no significant differences between profiles. Within the Constant profile, white and blue did not differ from each other, but both were higher than RBW, and red was lower than all other light spectra.

Non-photochemical quenching (NPQ) (Fig. 4e) differed only under white light, with higher values in the Gaussian profile. In the Constant profile, NPQ was higher under blue and red light than under white and RBW.

The effective quantum yield of PSII, $Y(\mathrm{II})$, and the photochemical quenching coefficient, q_P (Fig. 4(b) and (c), also differed under white light, with higher values in the Constant profile. Lower $Y(\mathrm{II})$ and q_P values were observed under blue and red light in the Constant profile, whereas in the Gaussian profile q_P was reduced under blue light.

Specific energy consumption (SEC; $\mathrm{kWh\,g^{-1}}$) (Fig. 4f) differed between profiles under RBW, blue, and red light, with higher values in the Gaussian profile. Under white light, there were no significant differences between profiles. Within the Constant profile, white light showed higher SEC than RBW, blue, and red, which did not differ from each other. Within the Gaussian profile, white light showed higher SEC than blue light, and blue light was higher than RBW and red, which did not differ from each other.

Hypocotyl length (CHL) (Fig. 5a) differed between profiles only under blue light, with higher values in the Constant profile than in the Gaussian profile. Within the Constant profile, white, blue, and red did not differ from each other and all were higher than RBW. In the Gaussian profile, white and red (not differing from each other) were higher than RBW and blue, which in turn did not differ from each other.

Total leaf area (CTLA) (Fig. 5b) showed no significant differences between profiles; within each profile, comparisons among light spectra were limited.

Hypocotyl fresh weight (HFW) (Fig. 5c) was higher in the Constant profile for all light spectra except RBW, for which there was no difference between profiles. Within the Constant profile, red showed the highest HFW, whereas white and RBW showed the lowest values. In the Gaussian profile, RBW showed lower HFW than the other light spectra.

Leaf fresh weight (LFW) (Fig. 5d) differed under white light, with higher values in the Gaussian profile. Under RBW, blue, and red light, there were no significant differences between profiles. Within the Constant profile, LFW under white light was lower than under the other light spectra.

Leaf dry mass (LMD) (Fig. 5e) differed under blue and red light, with higher values in the Constant profile. Under white and RBW light, there were no significant differences between profiles. Within the Constant profile, LMD was lower under white light than under the other light spectra.

Total dry mass (TMD) (Fig. 5f) differed under RBW, blue, and red light, always with higher values in the Constant profile. Under white light, there was no significant difference. Within the Constant profile, TMD was lower under white and RBW than under blue and red.

Hypocotyl dry mass (HMD) (Figure 5g) was higher in the Constant profile under RBW, blue, and red light. Under white light, there was no significant difference between profiles. The highest HMD values occurred under red light compared with the other light spectra.

In the Constant profile (Table 1), the red spectrum showed the lowest SEC ($0.0998\ \mathrm{kWh\,g^{-1}}$) and the highest EEMS ($10.02\ \mathrm{g\,kWh^{-1}}$). In the same profile, white light showed the highest SEC ($0.2341\ \mathrm{kWh\,g^{-1}}$) and the lowest EEMS ($4.27\ \mathrm{g\,kWh^{-1}}$).

In the Gaussian profile, SEC ranged from $0.1585\ \mathrm{kW\,h\,g^{-1}}$ to $0.2744\ \mathrm{kW\,h\,g^{-1}}$, whereas EEMS ranged from $3.64\ \mathrm{g\,kW^{-1}\,h}$ to $6.31\ \mathrm{g\,kW^{-1}\,h}$ (Table 1). Red light showed the lowest SEC ($0.1585\ \mathrm{kW\,h\,g^{-1}}$) and the highest EEMS ($6.31\ \mathrm{g\,kW^{-1}\,h}$), whereas white light showed the highest SEC ($0.2744\ \mathrm{kW\,h\,g^{-1}}$) and the lowest EEMS ($3.64\ \mathrm{g\,kW^{-1}\,h}$).

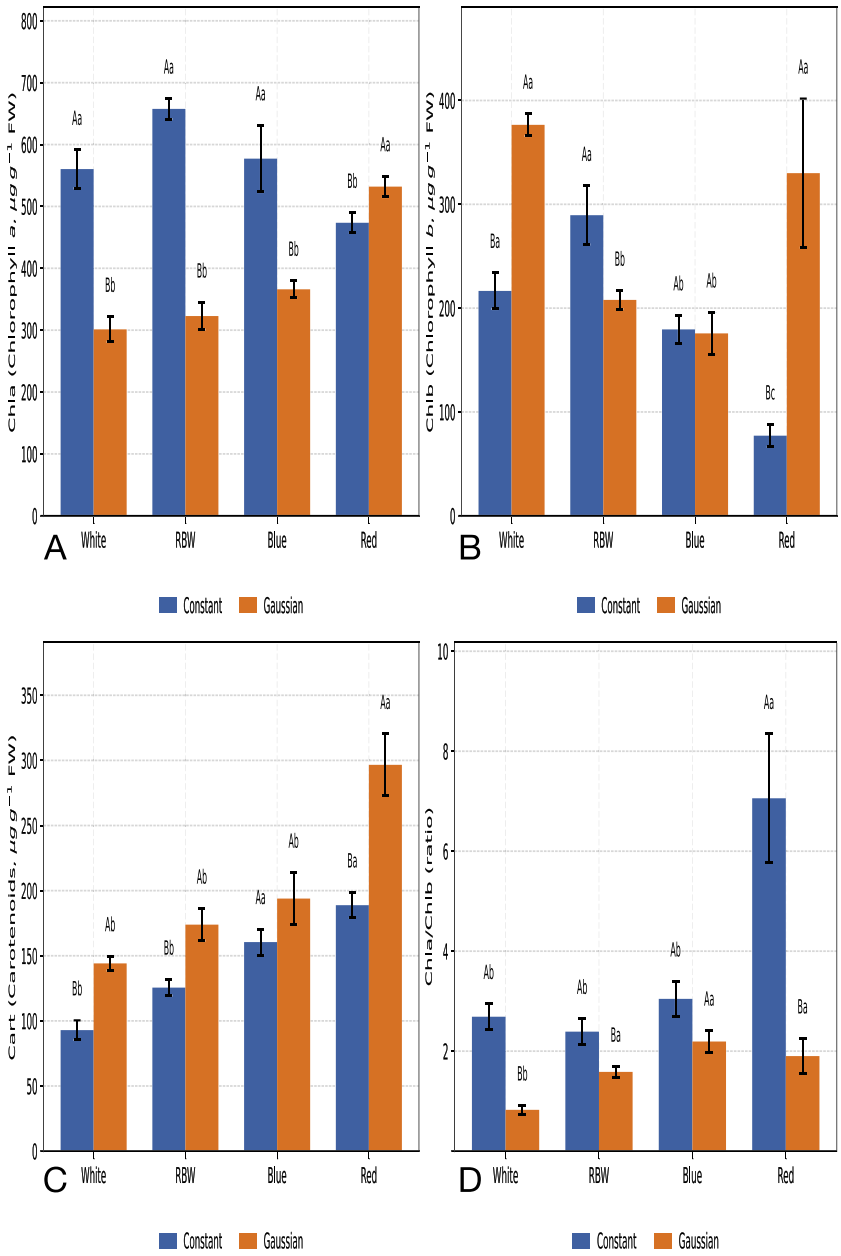

Fig. 3. Photosynthetic pigments and the *Chla* : *Chlb* ratio under two lighting profiles (Constant and Gaussian) and four light spectra (blue, RBW, red, and white; RBW = red–blue–white combination). Panels: (A) *Chla*; (B) *Chlb*; (C) *Cart*; (D) *Chla* : *Chlb*. Units: $\mu g\, g^{-1}$ fresh mass (A–C); dimensionless (D). Bars = mean ± SE. Uppercase letters compare *Profiles* within each *Light*; lowercase letters compare *Lights* within each *Profile*. (For interpretation of the references to colour in this figure legend, the reader is referred to the web version of this article.)

Table 1
Areal energy consumption (AEC), dry mass yield per area (MSA), specific energy consumption (SEC), and Energy-to-Mass Efficiency (EEMS) under different light spectra and lighting profiles. Seedling density was corrected based on the observed germination rate of 85%. SEC was calculated from full-precision AEC and MSA values prior to rounding.

	Constant				Gaussian			
Spectrum	AEC ($kWh\, m^{-2}$)	MSA ($g\, m^{-2}$)	SEC ($kWh\, g^{-1}$)	EEMS ($g\, kWh^{-1}$)	AEC ($kWh\, m^{-2}$)	MSA ($g\, m^{-2}$)	SEC ($kWh\, g^{-1}$)	EEMS ($g\, kWh^{-1}$)
Blue	13.51	104.33	0.1309	7.64	17.81	80.47	0.2232	4.48
RBW	12.24	96.09	0.1282	7.80	14.47	81.03	0.1793	5.58
Red	12.11	123.37	0.0998	10.02	13.25	83.95	0.1585	6.31
White	16.37	71.80	0.2341	4.27	23.09	84.43	0.2744	3.64

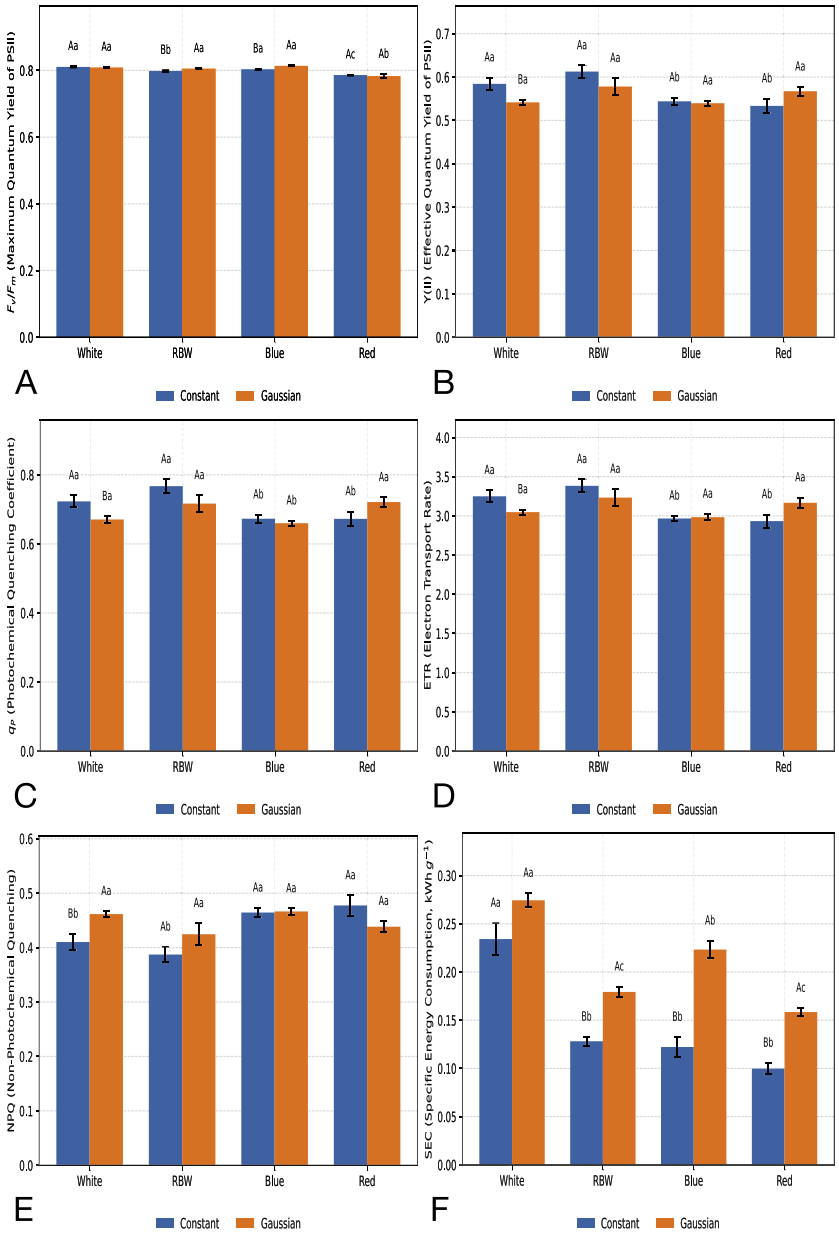

Fig. 4. PSII photochemical parameters and specific energy consumption (SEC) under Constant and Gaussian profiles across four light spectra (blue, RBW, red, and white). Panels: (A) F_v/F_m (maximum quantum yield of PSII); (B) $Y(II)$ (effective quantum yield of PSII); (C) q_P (photochemical quenching coefficient); (D) ETR (electron transport rate); (E) NPQ (non-photochemical quenching); (F) SEC, representing energy cost per unit biomass. Uppercase letters indicate differences between profiles within the same light, and lowercase letters indicate differences among lights within the same profile (Tukey, $\alpha = 0.05$). (For interpretation of the references to colour in this figure legend, the reader is referred to the web version of this article.)

Between profiles, differences in SEC were observed under RBW, blue, and red light, whereas under white light no significant difference between profiles was detected (Fig. 4f).

3.1. Multivariate analysis (PCA)

Principal Component Analysis (PCA) summarized the multivariate structure of morphological, physiological, pigment, and energy-performance variables. The first four components explained 76.47% of the total variance (PC1 = 34.37%, PC2 = 22.46%, PC3 = 11.30%, PC4 = 8.35%; Table 2).

PC1 showed strong correlations with NPQ ($r = -0.81$) and biomass traits (HFW: $r = -0.76$; HMD: $r = -0.77$; TMD: $r = -0.79$), and positive correlations with photochemical variables, including $Y(II)$ ($r = 0.78$), q_P ($r = 0.74$), and ETR ($r = 0.82$). SEC showed a moderate correlation with PC1 ($r = 0.53$) and a strong correlation with PC2 ($r = -0.76$).

PC2 showed positive correlations with *Chla* ($r = 0.67$), q_P ($r = 0.63$), $Y(II)$ ($r = 0.56$), and the *Chla* : *Chlb* ratio ($r = 0.54$), and a negative correlation with SEC ($r = -0.76$). PC3 was associated with leaf mass variables (LFW: $r = 0.84$; LMD: $r = 0.71$). PC4 showed correlation with F_v/F_m ($r = -0.70$) and *Chlb* ($r = 0.63$).

In the biplot (Fig. 6), vectors for $Y(II)$, q_P, and ETR showed similar directions, whereas NPQ pointed in the opposite direction. Biomass variables projected on the negative side of PC1, and SEC projected in the opposite direction to biomass variables. Treatments showed partial overlap in the scores on the first two components.

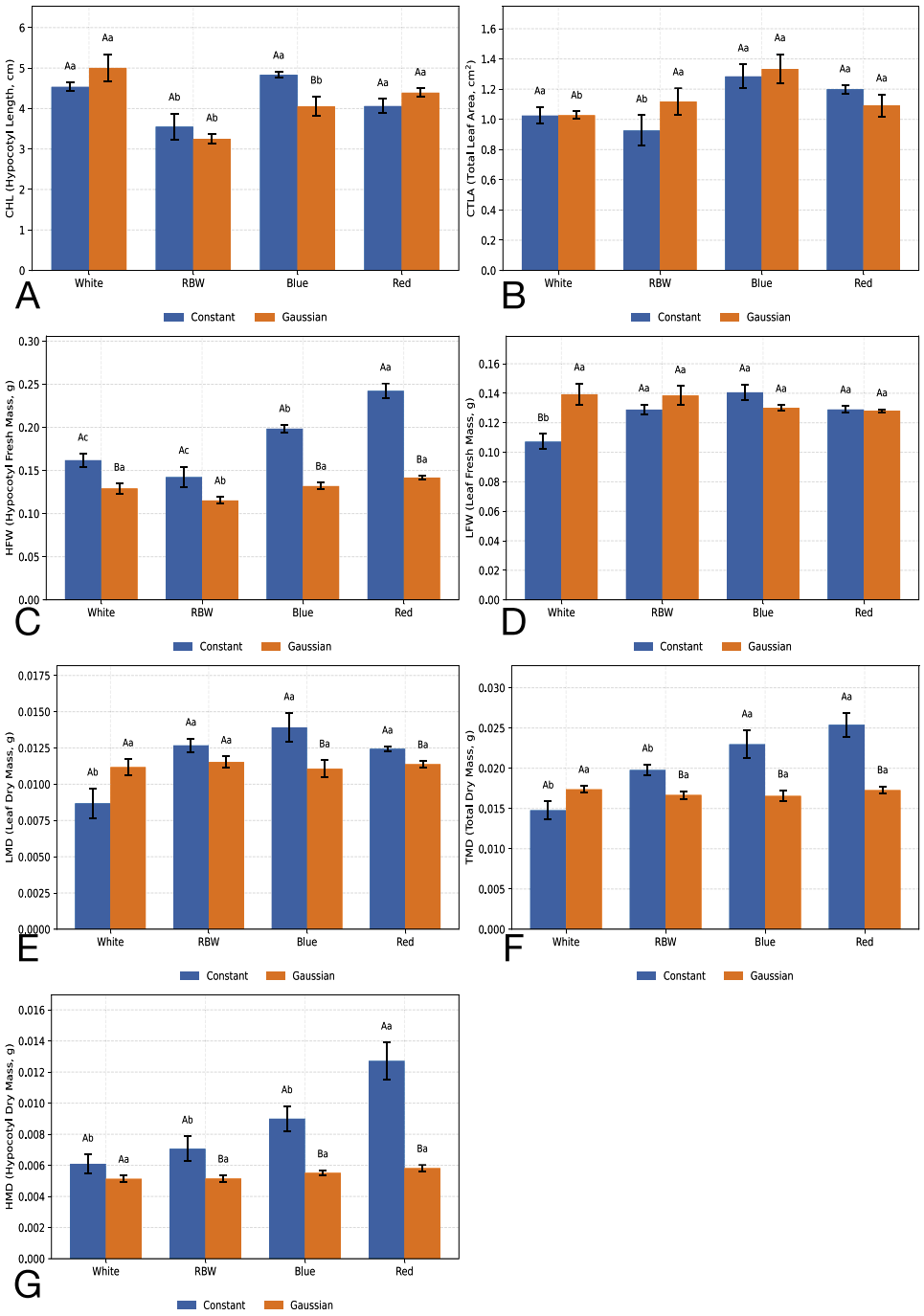

Fig. 5. Growth and morphology under Constant and Gaussian profiles across four light spectra (blue, RBW, red, and white). Panels: (A) CHL; (B) CTLA; (C) HFW; (D) LFW; (E) LMD; (F) TMD; (G) HMD. Bars = mean ± SE. Letters indicate differences by Tukey's test ($\alpha = 0.05$), with uppercase letters comparing *Profiles* and lowercase letters comparing *Light spectra*. (For interpretation of the references to colour in this figure legend, the reader is referred to the web version of this article.)

3.2. Correlation analysis

The Pearson correlation matrix (r) is shown in Fig. 7. All pairwise correlations are displayed (no significance filtering). Associations were classified as strong ($|r| \geq 0.70$), moderate ($0.30 \leq |r| < 0.70$), and weak ($|r| < 0.30$).

$Y(II)$ was strongly and positively correlated with q_P ($r = 0.98$) and ETR ($r = 0.97$), and strongly and negatively correlated with NPQ ($r = -0.99$). q_P and ETR were strongly and positively correlated ($r = 0.95$), and both were strongly and negatively correlated with NPQ ($r = -0.97$ for q_P vs. NPQ and $r = -0.97$ for ETR vs. NPQ). *Chla* showed a moderate correlation with q_P ($r = 0.43$) and a moderate negative correlation with NPQ ($r = -0.37$).

HFW and HMD were strongly correlated ($r = 0.86$). TMD was strongly correlated with HMD ($r = 0.88$), LMD ($r = 0.73$), and HFW ($r = 0.74$). LFW was strongly correlated with LMD ($r = 0.74$).

SEC showed a strong negative correlation with TMD ($r = -0.78$) and moderate negative correlations with HMD ($r = -0.69$), LMD ($r = -0.65$), and HFW ($r = -0.60$). Correlations of SEC with NPQ ($r = -0.04$), q_P ($r = -0.09$), and ETR ($r = 0.06$) were weak.

The *Chla* : *Chlb* ratio was moderately and negatively correlated with *Chlb* ($r = -0.68$) and weakly and positively correlated with *Chla*

Table 2
Correlation coefficients (r) between traits and the first four principal components (PC1–PC4). Values in **bold** indicate strong correlation ($|r| \geq 0.70$).

Variable (full name)	PC1	PC2	PC3	PC4
HFW (*Hypocotyl fresh weight, g*)	**−0.76**	0.39	−0.35	0.09
LFW (*Leaf fresh weight, g*)	−0.34	−0.08	**0.84**	−0.18
HMD (*Hypocotyl dry mass, g*)	**−0.77**	0.45	−0.16	−0.01
LMD (*Leaf dry mass, g*)	−0.50	0.34	**0.71**	−0.13
F_v/F_m (*Maximum quantum yield of PSII*)	0.23	−0.50	−0.06	**−0.70**
$Y(II)$ (*Effective quantum yield of PSII*)	**0.78**	0.56	0.09	−0.11
NPQ (*Non-photochemical quenching*)	**−0.81**	−0.51	−0.05	0.12
q_P (*Photochemical quenching coefficient*)	**0.74**	0.63	0.09	0.04
ETR (*Electron transport rate*)	**0.82**	0.48	0.14	−0.08
Chla (*Chlorophyll a*; µg g^{-1} FM)	0.08	0.67	−0.23	0.28
Chlb (*Chlorophyll b*; µg g^{-1} FM)	0.47	−0.30	0.32	0.63
Cart (*Carotenoids*; µg g^{-1} FM)	−0.24	0.01	0.26	0.38
TMD (*Total dry mass, g*)	**−0.79**	0.45	0.23	−0.06
SEC (*Specific energy consumption*; kWh g^{-1})	0.53	**−0.76**	−0.20	−0.04
CTLA (*Total leaf area, cm^2*)	−0.53	−0.29	0.06	−0.17
CHL (*Hypocotyl length, cm*)	−0.28	−0.45	−0.10	0.40
Chla_Chlb (*Chla* : *Chlb* ratio)	−0.48	0.54	−0.43	−0.18
Eigenvalue	5.842	3.818	1.920	1.420
Variance (%)	34.37	22.46	11.30	8.35
Cumulative (%)	34.37	56.83	68.12	76.47

($r = 0.29$). The ratio showed moderate correlations with HFW ($r = 0.64$) and HMD ($r = 0.57$), and a moderate negative correlation with SEC ($r = -0.49$). Correlations involving *Cart* were mostly weak.

3.3. Telemetry validation and PVFS operational compliance

PVFS telemetry showed high temporal regularity and high data availability across both experimental windows (Constant: 08–18/03/2024; Gaussian: 22/03–01/04/2024). Across PPFD channels ch1–ch4, the median sampling interval was 10.0 s under both profiles, with near-zero jitter (IQR of sampling intervals = 0.000–0.002 s for both profiles). The proportion of inter-sample intervals at the expected 10 s step was 99.92–99.95% (Constant) and 99.94% (Gaussian), and overall completeness was 99.80–99.86% under the Constant profile and 98.82% under the Gaussian profile (Table 3). In telemetry terms, these windows comprise 11 *photoperiod days* (inclusive dates: 08–18/03/2024 and 22/03/2024–01/04/2024), while agronomic time is reported as DAS (Day 0 = sowing on 08/03/2024 and 22/03/2024), and the crop timeline is described up to 10 DAS (i.e., through 18/03/2024 and 01/04/2024, respectively). Complementary environmental telemetry indicated that air temperature remained close to the nominal setpoint in both windows, whereas relative humidity showed a more pronounced midday depression under the Gaussian profile; these time-series stability analyses are provided in Supplementary Section S8.

In the daily assessment restricted to the photoperiod (06:30–18:30, local time), the lowest availability under the Constant profile occurred on 2024-03-12, ranging from 98.70–98.94% across channels. On that day, the largest within-photoperiod inter-sample interval reached 190–200 s, corresponding to outage gaps above 60 s (Table 3). Under the Gaussian profile, the lowest photoperiod availability was observed on 2024-03-30 (85.65%). Notably, the reduced availability on this day occurred as dispersed sample losses, because the largest inter-sample interval remained 20 s and no outage gaps above 60 s were observed on that date (Table 3). Across the Gaussian window, occasional within-photoperiod outage gaps ($\Delta t > 60$ s) were observed on a few days, with a maximum gap of approximately 137 s (e.g., 2024-04-01).

Daily DLI was estimated by integrating PPFD during the photoperiod. Mean DLI values were 10.33–10.42 mol m^{-2} d^{-1} under the Constant profile and 10.75–10.77 mol m^{-2} d^{-1} under the Gaussian profile (Table 3). The lowest daily DLI values were observed on 2024-03-08 (Constant: 10.05–10.14 mol m^{-2} d^{-1}) and 2024-03-30 (Gaussian: 10.14–10.15 mol m^{-2} d^{-1}) (Table 3). Equivalence of daily DLI relative to the target was assessed by TOST with a ±5% margin and a 90% CI criterion; equivalence was supported for all channels under both profiles when considering the distribution of daily DLI across the window (Table 3), despite these isolated low-DLI days falling slightly below the lower equivalence bound.

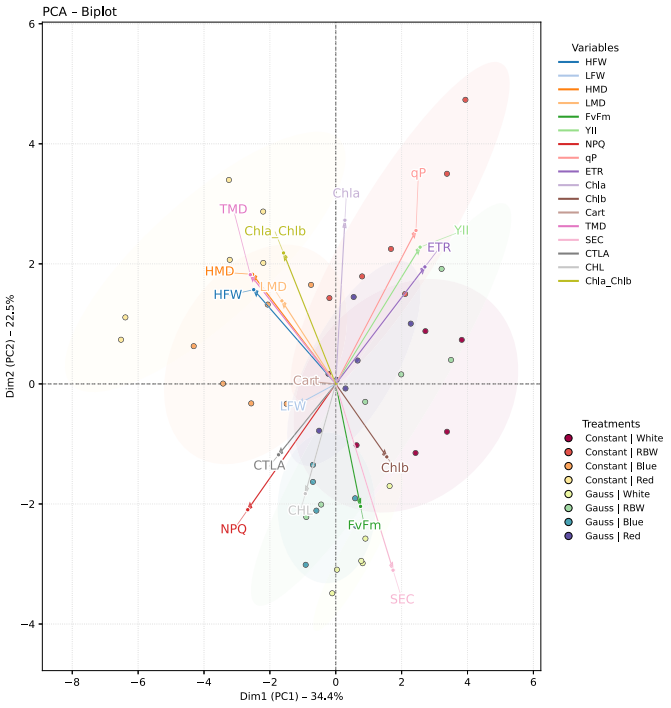

Fig. 6. PCA biplot considering morphological, photosynthetic, pigment, and energy-cost variables under different combinations of lighting profiles (Constant and Gaussian) and light spectra (blue, RBW, red, and white). Arrows represent trait vectors, with direction and length proportional to correlations with the components. Treatments are shown as points, with 90% confidence ellipses for each group. PC1 (34.37%) contrasts biomass traits and NPQ (negative scores) with photochemical performance ($Y(II)$, q_P, and ETR; positive scores). PC2 (22.46%) is mainly driven by a negative association with SEC and a positive association with *Chla* and photochemical-use indicators. (For interpretation of the references to colour in this figure legend, the reader is referred to the web version of this article.)

Daily inter-channel uniformity, quantified by the CV% of DLI across channels, was 0.37% under the Constant profile and 0.08% under the Gaussian profile (Table 3). Under the Gaussian profile, model fitting from telemetry yielded $\mu \approx 0.500$ and $\sigma \approx 0.150$–0.152, with $R^2 \approx 0.9997$–0.9998 and RMSE ≈ 1.84–2.25 across the four channels (Table 3).

4. Discussion

This study integrates two primary contributions: (i) the validation of a Precision Vertical Farming System (PVFS) capable of executing temporal lighting profiles under a target DLI, logging environmental/electrical telemetry in near real-time, and structuring data for ANOVA/Tukey and multivariate analysis; and (ii) evidence that, in sesame microgreens, the temporal shape of PPFD delivery (Constant vs. Gaussian) is associated with differences in the energy–biomass relationship, even when the daily DLI is maintained close to, and statistically equivalent to, the target across profiles.

From an engineering standpoint, the PVFS integrates control, traceability, and an analytical *pipeline* within an auditable and extensible architecture, aligning with recent advances in controlled-environment cultivation platforms and dynamic protocols [12–14]. The distinctive contribution here is coupling (a) programmable temporal profiles with setpoint-to-execution traceability, (b) continuous electrical metrology,

Table 3
Summary of key indicators for telemetry validation and PVFS operational compliance, based on PPFD channels ch1–ch4. Values reported as ranges reflect variation across channels.

Indicator	Constant (08–18/03/2024)	Gaussian (22/03–01/04/2024)
Validated PPFD channels	ch1–ch4	ch1–ch4
Sampling interval (median, s)	10.0	10.0
Jitter (IQR of sampling intervals, s)	0.000–0.002	0.000–0.002
Samples at expected step (%)	99.92–99.95	99.94
Overall completeness (% of expected samples)	99.80–99.86	98.82
Worst day within photoperiod (local)	2024-03-12	2024-03-30
Photoperiod availability on worst day (%)	98.70–98.94	85.65
Largest inter-sample interval on worst day (s)	190–200	20
Largest outage gap on worst day ($\Delta t > 60$ s) (s)	190–200	—[a]
Mean DLI (mol m^{-2} d^{-1})	10.33–10.42	10.75–10.77
DLI on worst-availability day (mol m^{-2} d^{-1})	10.34–10.43 (2024-03-12)	10.14–10.15 (2024-03-30)
Lowest daily DLI observed (mol m^{-2} d^{-1})	10.05–10.14 (2024-03-08)[d]	10.14–10.15 (2024-03-30)
DLI equivalence vs target (TOST, $\Delta = \pm 5\%$)	Equivalent (all ch, 90% CI)[b]	Equivalent (all ch, 90% CI)[b]
Daily inter-channel uniformity (CV% of DLI)	0.37	0.08
Gaussian fit : μ	—	0.500 (peak ≈ 12:30, local)[c]
Gaussian fit : σ	—	0.150–0.152
Fit quality: R^2	—	0.9997–0.9998
Fit quality: RMSE (PPFD)	—	1.84–2.25

[a] On 2024-03-30 (Gaussian profile), reduced photoperiod availability occurred as dispersed sample losses (max inter-sample interval = 20 s), without outage gaps above 60 s.

[b] TOST applied to daily DLI values with equivalence defined as $\Delta = 0.54$ mol m^{-2} d^{-1} (i.e., ±5% around 10.8 mol m^{-2} d^{-1}), using a 90% CI criterion.

[c] μ is reported on a normalized time scale over the 06:30–18:30 photoperiod (local); the peak time is estimated as 06:30 + $\mu \times 12$ h.

[d] On 2024-03-08 (Constant profile), daily DLI was slightly below the lower ±5% equivalence bound (10.26 mol m^{-2} d^{-1}), indicating an isolated low-DLI day within the Constant window.

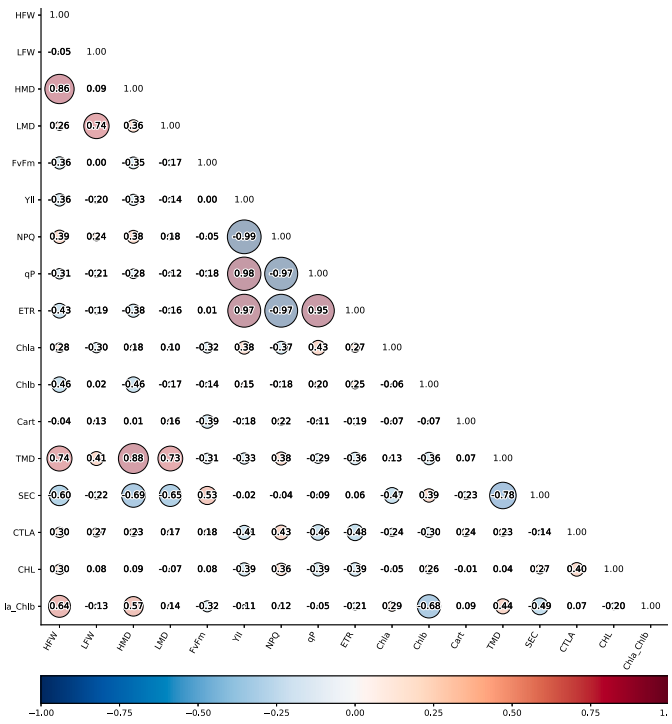

Fig. 7. Pearson correlation matrix (r) among physiological, morphological, pigment, and energy-performance variables under different combinations of lighting profiles (Constant and Gaussian) and light spectra (blue, RBW, red, and white). Red circles indicate positive correlations and blue circles indicate negative correlations, with size proportional to $|r|$. SEC represents specific energy consumption (energy cost per unit biomass). (For interpretation of the references to colour in this figure legend, the reader is referred to the web version of this article.)

and (c) actionable efficiency metrics (SEC/EEMS), providing a practical basis for multi-objective optimization and future extensions (e.g., telemetry-updated digital models) [41].

Telemetry underpins the operational comparability between profiles by documenting high temporal regularity (10 s median; IQR ≈ 0 s) and high data availability across four channels (ch1–ch4) in both experimental windows (Constant: 08–18/03/2024; Gaussian: 22/03–01/04/2024), with high overall completeness (Table 3). Restricting assessment to the photoperiod enabled the identification of days with lower availability (12/03/2024 in Constant; 30/03/2024 in Gaussian) and the quantification of gaps, making deviations explicit and auditable (Table 3). The DLI derived directly from telemetry was equivalent to the target (TOST; $\Delta = \pm 5\%$; 90% CI) and showed high inter-channel uniformity (low CV%), while in the Gaussian profile, the temporal shape was well described by a Gaussian model (high R^2 and low RMSE; Table 3). This reduces the likelihood that differences in SEC/EEMS are driven by unverified discrepancies in the daily light dose.

Complementary analyses of environmental telemetry showed that air temperature remained close to the nominal setpoint in both windows, supporting the thermal stability of the chamber during the experiment. Relative humidity exhibited greater intradiurnal variation than temperature and showed a more pronounced midday depression under the Gaussian window, consistent with stronger transient evaporative demand under dynamic PPFD. Thus, although the experiment was conducted under a stable thermal regime, the temporal shape of light delivery may also have modulated the chamber microenvironment through humidity-related responses. CO_2 was also monitored continuously; however, its interpretation was treated more cautiously because the cleaned time series frequently reached the upper analytical threshold adopted for supplementary visualization (2000 ppm). Therefore, CO_2 telemetry was retained as a monitored contextual variable rather than the primary basis for inferring environmental stability between the Constant and Gaussian windows; these complementary analyses are presented in Supplementary Section S8.

Regarding the energy–production relationship, the Constant profile showed lower SEC and higher EEMS than the Gaussian profile under RBW, blue, and red light (Fig. 4F; Table 1), whereas under white light there was no significant between-profile difference in SEC. Moreover, Areal Energy Consumption (AEC) was higher in the Gaussian profile for all spectra (Table 1), suggesting a higher electrical cost to deliver the protocol despite DLI equivalence. These results are consistent with two complementary factors, particularly under white light: (i) modulation may increase the fraction of time spent in states of higher photoprotective demand, reducing effective photosynthetic efficiency over the day, and (ii) modulation may shift the electrical operating point of the driver–LED system, affecting the wall-plug efficiency and the real cost per delivered photon [4,14,16].

Although the present study did not include a natural-light or conventional cultivation control, this omission should be interpreted in light of the study scope. The objective here was not to compare PFAL production directly against open-field or greenhouse systems, but rather to benchmark alternative lighting strategies within the same instrumented PFAL platform under controlled and auditable conditions. This distinction is important because broader literature indicates that PFAL and vertical-farming systems are substantially more electricity-dependent than greenhouse or open-field cultivation, while benchmarking itself remains a major challenge in the sector [5,45]. Therefore, the SEC and EEMS values reported here should be interpreted as within-system performance indicators for dynamic lighting management in PFALs, rather than as absolute evidence of superiority over conventional cultivation. Future studies should extend this comparison to daylight-assisted greenhouse or conventional references under harmonized crop, yield, and system-boundary criteria.

PSII photochemistry indicated that between-profile differences were most evident under white light: in the Constant profile, $Y(II)$ and q_P were higher and NPQ was lower, whereas in the Gaussian profile NPQ increased (Fig. 4B,C,E); ETR differed between profiles only under white light (Fig. 4D). However, energy cost per unit of biomass was not explained by instantaneous PSII variables: SEC correlated strongly with TMD ($r = -0.78$) and moderately with biomass traits, but showed weak correlations with NPQ, q_P, and ETR (Fig. 7). Thus, energy performance was dominated by time-integrated outcomes (harvested biomass) and by the effective electrical consumption of the protocol.

Across spectra, red light under the Constant profile was the most efficient energy–production combination, showing the lowest SEC (0.0998 $kWh\,g^{-1}$) and highest EEMS (10.02 $g\,kWh^{-1}$), consistent with higher dry mass yield per area (MSA) (Table 1) and greater dry biomass traits (Figure 5E–G). This pattern is mechanistically consistent with two complementary factors. First, red-centric horticultural lighting can achieve favorable photon efficacy, and dedicated 660 nm LED panels measured under plant-growth conditions have been reported to deliver higher photon efficacy than several white LED panels [4,44]. Second, red photons coincide with a major chlorophyll absorption region and can support biomass accumulation efficiently when daily light delivery is stable, a tendency also consistent with previous microgreen evidence under constant red lighting [6]. At the same time, this interpretation should be kept appropriately cautious: the present study did not directly measure the real-time relationship between delivered PPFD and electrical power consumption for each treatment (i.e., treatment-specific $\mu mol\,J^{-1}$), nor did it isolate luminaire-level wall-plug efficiency as an independent response variable. Therefore, the explanation for the superior Red–Constant performance should be interpreted as literature-consistent and mechanistically plausible, rather than as a direct demonstration of treatment-specific photon efficacy in the present experiment. In contrast, white light exhibited the highest SEC in both profiles and the lowest EEMS, indicating the highest energy cost per unit of dry biomass (Table 1).

Pigments exhibited a *profile* × *spectrum* interaction (Fig. 3). In the Constant profile, *Chla* was higher under white, RBW, and blue, whereas under red light, *Chla* was higher in the Gaussian profile. Carotenoids increased in the Gaussian profile under white, RBW, and red, and *Chlb* was higher in the Gaussian profile under white and red. Under RBW, *Chlb* was higher in the Constant profile, whereas under blue there was no difference between profiles (Fig. 3B). The *Chla*:*Chlb* ratio was higher in the Constant profile under white, RBW, and red, with no difference under blue. Taken together, these patterns suggest spectrum-dependent adjustments in light harvesting and photoprotection, with signals of greater photoprotective investment under modulation in specific conditions (e.g., white) [7,16].

Regarding growth traits, the Constant profile increased dry biomass (LMD, HMD, and TMD) under RBW, blue, and red and increased HFW for most spectra (except RBW), consistent with the lower SEC and higher EEMS observed in those combinations (Fig. 5; Table 1). Under white light, the Gaussian profile increased LFW (Fig. 5D), and TMD did not differ between profiles, offering no advantage in SEC/EEMS (Table 1). In microgreens, this decoupling is relevant because fresh mass may reflect expansion/hydration, whereas dry mass represents effective matter accumulation [17,18].

PCA reinforced the separation between energy performance and instantaneous variables: SEC loaded strongly on PC2 ($r = -0.76$), opposite to biomass variables, whereas PC1 contrasted biomass variables and NPQ (negative scores) with photochemical performance ($Y(II)$, q_P, and ETR; positive scores) (Fig. 6; Table 2). This supports the interpretation that SEC/EEMS better synthesize the trade-off between electrical cost and production than point-in-time PSII measurements.

As a limitation, the present conclusions are based on a single photoperiod, a specific daily light dose range, and a short cultivation cycle typical of sesame microgreens. Therefore, the relative performance of Constant and Gaussian light delivery should be interpreted within this experimental scope and not automatically extrapolated to longer crop cycles, other developmental stages, different DLI and photoperiod combinations, or other crop species [17]. Because plant responses to temporal light distribution can vary with canopy development, biomass accumulation, and source–sink dynamics over time, future studies should test these lighting strategies across broader phenological stages and under multiple DLI levels and photoperiod regimes.

In summary, the PVFS enabled auditable execution and verification of dynamic lighting protocols under controlled DLI, providing a robust basis for energy benchmarking in PFAL research. Within this experimental scope, the Constant profile improved energy–biomass efficiency under RBW, blue, and red light, and the Red–Constant treatment was the most efficient strategy (lowest SEC and highest EEMS), whereas white light incurred the highest energy cost per unit biomass (Table 1).

5. Conclusion

This study demonstrates that the *Precision Vertical Farming System* (PVFS) enables the reproducible execution and auditing of lighting protocols in PFALs by integrating (i) programmable temporal profiles under a target DLI, (ii) near real-time environmental and electrical telemetry, and (iii) an analytical *pipeline* (ANOVA/Tukey and PCA) to relate physiological and production responses to energy costs. Telemetry-based validation confirmed high sampling regularity and data completeness, verified DLI equivalence derived from recorded PPFD, and demonstrated the strong adherence of the Gaussian profile to its modeled shape, thereby minimizing operational uncertainty during treatment comparison.

Under a fixed photoperiod (12 h) and equivalent DLI (~ 10.8 $mol\,m^{-2}\,d^{-1}$), the temporal shape of PPFD delivery significantly influenced the energy–biomass trade-off in sesame microgreens. The Constant profile achieved superior energy-to-mass efficiency (lower SEC and higher EEMS) under RBW, blue, and red light, whereas the Gaussian profile increased Areal Energy Consumption (AEC) across all spectra. Among the evaluated treatments, the Red–Constant combination proved to be the most energy-efficient strategy, yielding the highest dry mass per unit of consumed energy, whereas white light exhibited the

highest energy cost per unit biomass. Multivariate analysis confirmed that SEC and EEMS aligned primarily with integrated biomass variables, reinforcing the conclusion that energy–production metrics capture operational system performance more effectively than instantaneous PSII photochemical measurements.

In terms of future perspectives, the PVFS provides a robust technical foundation for energy benchmarking and multi-objective optimization of lighting protocols. The system is extensible to experiments spanning multiple DLI levels, photoperiods, planting densities, and developmental stages, and supports integration with experimental planning routines, operational diagnostics, and the automated benchmarking of light "recipes" in dynamic scenarios.

Glossary / Abbreviations

PVFS: Precision Vertical Farming System: Open-architecture layered platform that executes lighting protocols and logs environmental/electrical telemetry for auditable, reproducible PFAL experiments.
PFAL: Plant Factory with Artificial Lighting: Indoor cultivation system in which artificial lighting is the primary driver of photosynthesis and production.
CEA: Controlled-Environment Agriculture: Production under controlled conditions (e.g., temperature, humidity, CO_2, and lighting), typically indoors.
PPFD: Photosynthetic Photon Flux Density (μmol m^{-2} s^{-1}): Photon flux (400–700 nm) incident on the crop canopy; used here as the time-varying lighting setpoint.
DLI: Daily Light Integral (mol m^{-2} d^{-1}): Time integral of PPFD over the photoperiod; used as the target daily light dose (equalized across treatments).
Constant profile: PPFD delivery with approximately constant intensity over the photoperiod (flat setpoint).
Gaussian profile: PPFD delivery described by a Gaussian-shaped curve over the photoperiod; compliance can be evaluated by goodness-of-fit metrics (e.g., R^2, RMSE).
RBW: Combined spectrum consisting of red, blue, and white components (reported proportions: 70.5% red, 21.0% blue, and 8.5% green from the white channel).
IoT: Internet of Things: Networked sensors/actuators enabling near real-time measurement (telemetry) and control in the growth chamber.
Telemetry: Time-stamped operational measurements (e.g., environmental variables, power/energy, and lighting control signals) transmitted and persisted for auditability and time-series analysis.
MQTT: Message Queuing Telemetry Transport: Lightweight publish/subscribe protocol used for device–server communication (telemetry and control).
JSON: JavaScript Object Notation: Structured payload format used to transmit messages (e.g., identifier, timestamp, metric, value, unit, status).
UTC: Coordinated Universal Time: Reference time zone used to timestamp telemetry records for traceability and comparability.
ISO-8601: International date-time format used for telemetry timestamps (e.g., 2024-03-08T12:00:00Z).
MongoDB: Document-oriented database used to persist raw telemetry records (with UTC timestamps) and support time-series queries/aggregations.
Docker / Docker Compose: Container-based deployment used to run infrastructure services with persistent volumes and version-controlled configurations.
ESP32: Wi-Fi-enabled microcontroller used as the embedded controller to acquire sensor data and apply lighting setpoints.
FreeRTOS: Real-time operating system supporting non-blocking embedded acquisition/control routines.
NTP: Network Time Protocol: Used for time synchronization, with RTC failover to increase tolerance to outages.
RTC: Real-Time Clock: Local clock module supporting timekeeping during connectivity/power interruptions.
DS3231: RTC module (I^2C) used for time synchronization/failover.
DAC: Digital-to-Analog Converter: Used to generate analog dimming signals for lighting control.
MCP4725: 12-bit I^2C DAC used to control LED driver dimming/PPFD output.
DHT22: Digital temperature/humidity sensor used in the chamber.
MH-Z14: NDIR CO_2 sensor used to measure CO_2 concentration in the chamber.
kWh: Kilowatt-hour: Energy unit used to quantify total electrical consumption during each treatment.
Power factor: Ratio of real to apparent power, used to characterize electrical load behavior.
AEC: Areal Energy Consumption (kWh m^{-2}): Total electrical energy consumed normalized by illuminated area.
MSA: Dry mass yield per area (g m^{-2}), estimated from mean dry mass per seedling and seedling density.
SEC: Specific Energy Consumption (kWh g^{-1}): Energy cost per gram of dry mass produced, computed as SEC = AEC/MSA.
EEMS: Energy-to-Mass Efficiency (g kWh^{-1}): Dry-mass return per unit of energy, defined as EEMS = 1/SEC.
REST: Representational State Transfer: API endpoints used for queries and control-service integration.
WebSocket: Bidirectional communication channel used for near real-time queries/notifications.
ANOVA: Analysis of Variance: Statistical framework used to test factor and interaction effects in the factorial design.
Tukey HSD: Tukey Honestly Significant Difference: Post-hoc multiple-comparison test used after ANOVA.
CLD: Compact Letter Display: Letter-based grouping that summarizes Tukey HSD results; groups sharing a letter are not significantly different at $\alpha = 0.05$.
PCA: Principal Component Analysis: Multivariate method used to summarize covariance structure and relate energy-performance metrics (SEC/EEMS) to dry-mass and photosynthetic variables.
TOST: Two One-Sided Tests: Equivalence testing applied to daily DLI values; equivalence margin defined as $\Delta = \pm 5\%$ around the target DLI using a 90% CI criterion.
CI: Confidence interval: Interval estimate used in inference and equivalence testing (e.g., 90% CI in TOST).
CV: Coefficient of variation (%): Relative dispersion measure, used e.g. to evaluate inter-channel uniformity.
R^2: Coefficient of determination: Goodness-of-fit metric for Gaussian-model compliance.
RMSE: Root mean square error (PPFD units): Fit error metric used to quantify Gaussian-model compliance.
MAE: Mean absolute error (PPFD units): Fit error metric used alongside RMSE.
IQR: Interquartile range: Robust dispersion metric used to guide winsorization.
Winsorization: Robust preprocessing replacing extreme values based on a rule (here, IQR-based) to reduce undue influence while preserving sample size.
PAM fluorometry: Pulse-amplitude modulated fluorometry used to obtain chlorophyll *a* fluorescence parameters with an IMAGING-PAM fluorometer.
Fo: Minimal fluorescence measured after dark adaptation under weak measuring light.
Fm: Maximal fluorescence induced by a saturating pulse after dark adaptation.
Fv/Fm: Maximum quantum yield of PSII, computed as $(F_m - F_o)/F_m$.
Y(II): Effective quantum yield of PSII under actinic light (light-adapted conditions).
NPQ: Non-photochemical quenching: Fluorescence-derived indicator of energy dissipation as heat under light-adapted conditions.
qP: Photochemical quenching coefficient under light-adapted conditions.
ETR: Electron transport rate, estimated as $\mathrm{ETR} = \mathrm{Y(II)} \times \mathrm{PAR} \times A_{\mathrm{leaf}} \times 0.5$.
PAR: Photosynthetically active radiation term used in ETR estimation.
A_{leaf}: Fraction of incident radiation absorbed by leaves; used in ETR calculation.

Funding

The author(s) declare that financial support was received for the research, authorship, and/or publication of this article. This project was funded by the National Council for Scientific and Technological Development (CNPq; Grant Nos. #408285/2021-4, #421052/2023-6, and #153369/2023-0) and by the Funding Authority for Studies and Projects/Research Support Foundation of the State of Goiás (FINEP/FAPEG; Tecnova II Grant No. #202010267000346).

Declaration of generative AI and AI-assisted technologies in the writing process

During the preparation of this work, the authors used ChatGPT to improve language clarity and readability. After using this tool, the authors reviewed and edited the content as needed and take full responsibility for the content of the publication.

CRediT authorship contribution statement

Marlus Dias Silva: Writing – review & editing, Writing – original draft, Visualization, Validation, Software, Methodology, Formal analysis, Data curation, Conceptualization; **Jaqueline Martins Vasconcelos:** Writing – review & editing, Supervision, Resources, Project administration, Methodology, Investigation; **Fábia Barbosa da Silva:** Writing – review & editing, Supervision, Project administration, Methodology, Funding acquisition, Conceptualization; **Adriano Soares de Oliveira Bailão:** Writing – review & editing, Validation, Software, Methodology; **Ítalo Moraes Rocha Guedes:** Writing – review & editing, Visualization, Methodology, Formal analysis, Data curation; **Márcio da Silva Vilela:** Writing – review & editing, Supervision, Resources; **Adriano Carvalho Costa:** Writing – review & editing, Supervision, Resources; **Márcio Rosa:** Writing – review & editing, Supervision, Resources; **Lucas Loram Lourenço:** Writing – review & editing, Investigation, Data curation; **Fabiano Guimarães Silva:** Writing – review & editing, Supervision, Project administration, Methodology, Funding acquisition, Conceptualization.

Data availability

The data generated and analyzed in this study are publicly available. The source code used in this study is available in the GitHub repository: https://github.com/marlussilva/pvfs-sesame-microgreens-cea.

Declaration of competing interest

The authors declare the following financial interests/personal relationships which may be considered as potential competing interests: Fabiano Guimaraes Silva reports financial support was provided by Goiano Federal Institute. If there are other authors, they declare that they have no known competing financial interests or personal relationships that could have appeared to influence the work reported in this paper.

Acknowledgments

The authors thank the Goiano Federal Institute of Education, Science and Technology - Rio Verde CAMPUS, the Pro-Rectory of Research, Postgraduate Studies, and Innovation of the Goiano Federal Institute, the National Council for Scientific and Technological Development (CNPq), and the Financier of Studies and Projects (FINEP), as well as the Research Support Foundation of the State of Goiás (FAPEG) for the funding.

Supplementary material

Supplementary material associated with this article can be found in the online version at 10.1016/j.atech.2026.102105.

References

[1] S.R. Jaeger, Vertical farming (plant factory with artificial lighting) and its produce: consumer insights, Curr. Opin. Food Sci. 56 (2024) 101145. https://doi.org/10.1016/j.cofs.2024.101145
[2] S. Oh, C. Lu, Vertical farming: smart urban agriculture for enhancing resilience and sustainability in food security, J. Hortic. Sci. Biotechnol. 98 (2) (2023) 133–140. https://doi.org/10.1080/14620316.2022.2141666
[3] M. Guo, Z. Jin, L. Ma, S. Ou, Application of plant factory with artificial lighting in horticultural production: current progress and future trends, Hortic. Plant J. (2025). https://doi.org/10.1016/j.hpj.2025.04.005
[4] P. Kusuma, P.M. Pattison, B. Bugbee, From physics to fixtures to food: current and potential LED efficacy, Hortic. Res. 7 (1) (2020) 56. https://doi.org/10.1038/s41438-020-0283-7
[5] L. Miserocchi, A. Franco, Benchmarking energy efficiency in vertical farming: status and prospects, Therm. Sci. Eng. Prog. 58 (2025) 103165. https://doi.org/10.1016/j.tsep.2024.103165
[6] M.D. Silva, J.M. Vasconcelos, F.B. da Silva, A.S. de Oliveira Bailão, Í.M.R. Guedes, M. da Silva Vilela, A.C. Costa, M. Rosa, F.G. Silva, Growing in red: impact of different light spectra and lighting conditions on lentil microgreens growth in vertical farming, Front. Plant Sci. 15 (2024). https://doi.org/10.3389/fpls.2024.1515457
[7] K.R. Susilo, A. Eu, B. Besemer, E. Heuvelink, R.C.H. de Vos, L.F.M. Marcelis, Extended photoperiod improves growth and nutritional quality of pak choi under constant daily light integral, Front. Plant Sci. 16 (2025). https://doi.org/10.3389/fpls.2025.1621513
[8] L.F. Lozano-Castellanos, L.M. Navas-Gracia, I.C. Lozano-Castellanos, A. Correa-Guimaraes, Technologies applied to artificial lighting in indoor agriculture: a review, Sustainability 17 (7) (2025) 3196. https://doi.org/10.3390/su17073196
[9] T. Miller, G. Mikiciuk, I. Durlik, M. Mikiciuk, A. Łobodzińska, M. Śnieg, The IoT and AI in agriculture: the time is now–A systematic review of smart sensing technologies, Sensors 25 (12) (2025). https://doi.org/10.3390/s25123583
[10] V.H.U. Eze, E.C. Eze, G.U. Alaneme, P.E. Bubu, E.O.E. Nnadi, M.B. Okon, Integrating IoT sensors and machine learning for sustainable precision agroecology: enhancing crop resilience and resource efficiency through data-driven strategies, challenges, and future prospects, Discov. Agric. 3 (1) (2025) 83. https://doi.org/10.1007/s44279-025-00247-y
[11] V. Choudhary, P. Guha, G. Pau, S. Mishra, An overview of smart agriculture using internet of things (IoT) and web services, Environ. Sustain. Indic. 26 (2025) 100607. https://doi.org/10.1016/j.indic.2025.100607
[12] Z. Wei, W. Fang, UV-NDVI for real-time crop health monitoring in vertical farms, Smart Agric. Technol. 8 (2024) 100462. https://doi.org/10.1016/j.atech.2024.100462
[13] M. Landolfo, F. Perotti, A. Pistillo, G. Pennisi, G. Gianquinto, F. Orsini, Optimizing artificial lighting for convolutional neural network-based crop monitoring with low-cost RGB imaging in indoor cultivation, Smart Agric. Technol. 13 (2026) 101677. https://doi.org/10.1016/j.atech.2025.101677
[14] N. Grasso, B. Fasciolo, G. Bruno, P. Chiabert, Development of a dynamic protocol for improving the productivity of soilless farming systems, Smart Agric. Technol. 12 (2025) 101264. https://doi.org/10.1016/j.atech.2025.101264
[15] J. Morales-Guerra, S. Suarez-Cortez, J. Morales-Duran, E. Reyes-Vera, J. Botero-Valencia, SmartGrow datacontrol: an IoT architecture for the acquisition of environmental physiological parameters in Cannabis sativa cultivations, SoftwareX 27 (2024) 101880. https://doi.org/10.1016/j.softx.2024.101880
[16] Kaiser, et al., Vertical farming goes dynamic, Front. Sci. 2 (2024) 1411259. https://doi.org/10.3389/fsci.2024.1411259
[17] J.K. Lone, R. Pandey, Gayacharan, Microgreens on the rise: expanding our horizons from farm to fork, Heliyon 10 (4) (2024) e25870. https://doi.org/10.1016/j.heliyon.2024.e25870
[18] M. Bhaswant, D.K. Shanmugam, T. Miyazawa, C. Abe, T. Miyazawa, Microgreens-A comprehensive review of bioactive molecules and health benefits, Molecules 28 (2) (2023) 867. https://doi.org/10.3390/molecules28020867
[19] E.R. Turner, Y. Luo, R.L. Buchanan, Microgreen nutrition, food safety, and shelf life: a review, J. Food Sci. (2020). https://doi.org/10.1111/1750-3841.15049
[20] Y. Fuji, A. Uchida, K. Fukahori, M. Chino, T. Ohtsuki, H. Matsufuji, Chemical characterization and biological activity in young sesame leaves (Sesamum indicum L.) and changes in iridoid and polyphenol content at different growth stages, PLOS ONE 13 (3) (2018) e0194449. https://doi.org/10.1371/journal.pone.0194449
[21] T. Domínguez-Bolaño, O. Campos, V. Barral, C.J. Escudero, J.A. García-Naya, An overview of IoT architectures, technologies, and existing open-source projects, Internet Things 20 (2022) 100626. https://doi.org/10.1016/j.iot.2022.100626
[22] H. Mrabet, S. Belguith, A. Alhomoud, A. Jemai, A survey of IoT security based on a layered architecture of sensing and data analysis, Sensors 20 (13) (2020) 3625. https://doi.org/10.3390/s20133625
[23] R. Gong, H. Zhang, G. Li, J. He, Edge computing-enabled smart agriculture: technical architectures, practical evolution, and bottleneck breakthroughs, Sensors 25 (17) (2025) 5302. https://doi.org/10.3390/s25175302
[24] P. Yu, F. Teng, W. Zhu, C. Shen, Z. Chen, J. Song, Cloud–edge–device collaborative computing in smart agriculture: architectures, applications, and future perspectives, Front. Plant Sci. 16 (2025) 1668545. https://doi.org/10.3389/fpls.2025.1668545
[25] J. Wytrębowicz, K. Cabaj, J. Krawiec, Messaging protocols for IoT systems–A pragmatic comparison, Sensors 21 (20) (2021) 6904. https://doi.org/10.3390/s21206904
[26] D. Silva, L.I. Carvalho, J. Soares, R.C. Sofia, A performance analysis of internet of things networking protocols: evaluating MQTT, CoAP, OPC UA, Appl. Sci. 11 (11) (2021) 4879. https://doi.org/10.3390/app11114879
[27] A. Larmo, A. Ratilainen, J. Saarinen, Impact of CoAP and MQTT on NB-IoT system performance, Sensors 19 (1) (2019) 7. https://doi.org/10.3390/s19010007
[28] J. Martin, J. Burbank, W. Kasch, D.L. Mills, Network time protocol version 4: protocol and algorithms specification, 2010, (RFC 5905). https://doi.org/10.17487/RFC5905
[29] I. Fette, A. Melnikov, The WebSocket protocol, 2011, (RFC 6455). https://doi.org/10.17487/RFC6455
[30] C.A. Schneider, W.S. Rasband, K.W. Eliceiri, NIH Image to ImageJ: 25 years of image analysis, Nat. Methods 9 (7) (2012) 671–675. https://doi.org/10.1038/nmeth.2089
[31] B. Genty, J.-M. Briantais, N.R. Baker, The relationship between the quantum yield of photosynthetic electron transport and quenching of chlorophyll fluorescence, Biochim. Biophys. Acta - Gen. Subj. 990 (1) (1989) 87–92. https://doi.org/10.1016/S0304-4165(89)80016-9
[32] T. Lawson, D.M. Kramer, C.A. Raines, Improving yield by exploiting mechanisms underlying natural variation of photosynthesis, Curr. Opin. Biotechnol. 23 (2) (2012) 215–220. https://doi.org/10.1016/j.copbio.2011.12.012

[33] W. Bilger, U. Schreiber, M. Bock, Determination of the quantum efficiency of photosystem II and of non-photochemical quenching of chlorophyll fluorescence in the field, Oecologia 102 (4) (1995) 425–432. https://doi.org/10.1007/BF00341354
[34] A. Laisk, F. Loreto, Determining photosynthetic parameters from leaf CO2 exchange and chlorophyll fluorescence (Ribulose-1,5-Bisphosphate carboxylase/oxygenase specificity factor, dark respiration in the light, excitation distribution between photosystems, alternative electron transport rate, and mesophyll diffusion resistance), Plant Physiol. 110 (3) (1996) 903–912. https://doi.org/10.1104/pp.110.3.903
[35] J.N. de Castro, C. Müller, G.M. Almeida, A.C. Costa, Physiological tolerance to drought under high temperature in soybean cultivars, Aust. J. Crop Sci. 13 (2019) 976–987. https://doi.org/10.21475/AJCS.19.13.06.P1767
[36] A.R. Wellburn, The spectral determination of chlorophylls a and b, as well as total carotenoids, using various solvents with spectrophotometers of different resolution, J. Plant Physiol. 144 (3) (1994) 307–313. https://doi.org/10.1016/S0176-1617(11)81192-2
[37] H. Kyauk, N.W. Hopper, R.D. Brigham, Effects of temperature and presoaking on germination, root length and shoot length of sesame (Sesamum indicum L.), Environ. Exp. Bot. 35 (3) (1995) 345–351. https://doi.org/10.1016/0098-8472(95)00013-X
[38] H. Balouchi, V.S. Khankahdani, A. Moradi, M. Gholamhoseini, R. Piri, S.Z. Heydari, B. Dedicova, Seed fatty acid changes germination response to temperature and water potentials in six sesame (Sesamum indicum L.) cultivars: estimating the cardinal temperatures, Agriculture 13 (10) (2023) 1936. https://doi.org/10.3390/agriculture13101936
[39] G. Parmoon, S.A. Moosavi, A. Poshtdar, S.A. Siadat, Effects of cadmium toxicity on sesame seed germination explained by various nonlinear growth models, Ocl 27 (2020) 57. https://doi.org/10.1051/ocl/2020053
[40] D. Lakens, Equivalence tests: a practical primer for t tests, correlations, and meta-analyses, Soc. Psychol. Personal. Sci. (2017). Open access (PMC), https://doi.org/10.1177/1948550617697177
[41] W. Du, P. Jin, W. Jin, Smart farm digital twin model based on edge-cloud architecture for tomato monitoring and detection, Smart Agric. Technol. 12 (2025) 101254. https://doi.org/10.1016/j.atech.2025.101254
[42] A.S. Rathor, S. Choudhury, A. Sharma, P. Nautiyal, G. Shah, Empowering vertical farming through IoT and AI-Driven technologies: a comprehensive review, Heliyon 10 (15) (2024) e34998. https://doi.org/10.1016/j.heliyon.2024.e34998
[43] L.-D. Van, Y.-B. Lin, T.-H. Wu, Y.-W. Lin, S.-R. Peng, L.-H. Kao, C.-H. Chang, PlantTalk: a smartphone-based intelligent hydroponic plant box, Sensors 19 (8) (2019) 1763. https://doi.org/10.3390/s19081763
[44] T.I. Wong, X. Zhou, Photon efficacy and cost investigation of LEDs at different wavelengths and color temperatures for horticulture, Discov. Agric. 2 (2024) 125. https://doi.org/10.1007/s44279-024-00137-9
[45] C. Stanghellini, D. Katzin, The dark side of lighting: a critical analysis of vertical farms' environmental impact, J. Clean. Prod. 458 (2024) 142359. https://doi.org/10.1016/j.jclepro.2024.142359
[46] H. Liu, F. Zhou, T. Zhou, Y. Yang, Y. Zhao, A novel wrinkled-leaf sesame mutant as a potential edible leafy vegetable rich in nutrients, Sci. Rep. 12 (2022) 18478. https://doi.org/10.1038/s41598-022-23263-0
[47] K.P. Gavhane, M. Hasan, D.K. Singh, et al., Determination of optimal daily light integral (DLI) for indoor cultivation of iceberg lettuce in an indigenous vertical hydroponic system, Sci. Rep. 13 (2023) 10923. https://doi.org/10.1038/s41598-023-36997-2
[48] G. Alturif, W. Saleh, A.A. El-Bary, R.A. Osman, Towards efficient IoT communication for smart agriculture: a deep learning framework, PLOS ONE (2024). https://doi.org/10.1371/journal.pone.0311601
[49] N. Kharraz, A. Revoly, I. Szabó, IoT-based adaptive lighting framework for optimizing energy efficiency and crop yield in indoor farming, J. Sens. Actuator Netw. 14 (3) (2025) 59. https://doi.org/10.3390/jsan14030059
[50] N. Kharraz, I. Szabó, Cloud-driven data analytics for growing plants indoor, AgriEngineering 7 (4) (2025) 101. https://doi.org/10.3390/agriengineering7040101
[51] K. Dineva, T. Atanasova, Cloud data-driven intelligent monitoring system for interactive smart farming, Sensors 22 (17) (2022) 6566. https://doi.org/10.3390/s22176566
[52] V. Wichitwechkarn, W. Rohde, R. Choudhary, Design and validation of an open-sourced automation system for vertical farming, HardwareX 16 (2023) e00497. https://doi.org/10.1016/j.ohx.2023.e00497
[53] N.N. Thilakarathne, M.S. Abu Bakar, P.E. Abas, H. Yassin, Towards making the fields talks: a real-time cloud enabled IoT crop management platform for smart agriculture, Front. Plant Sci. 13 (2023). https://doi.org/10.3389/fpls.2022.1030168

Supplementary Material — PVFS Architecture and Implementation

Supplementary Material — PVFS implementation

S1. PVFS architecture

The *Precision Vertical Farming System* (PVFS) was implemented using a five-layer architecture (Figure 1) — *Physical*, *Devices*, *Infrastructure*, *Protocols*, and *Application* — to systematically manage lighting control, acquire environmental and energy metrics, ensure telemetry persistence, and handle user interaction.

S2. Physical layer: sensing, electrical metering, and lighting control

The physical layer was built around the ESP32 microcontroller (Espressif Systems, Shanghai, China), widely used in IoT-based smart agriculture systems [1–3]. The ESP32 provided Wi-Fi connectivity and supported I^2C, SPI, and UART buses for interfacing sensors and actuators.

Temperature and relative humidity were measured using a DHT22 (AM2302) sensor, with a -40 to $80\,^{\circ}C$ operating range and typical accuracy of $\pm 0.5\,^{\circ}C$ [4]. CO_2 concentration was monitored using an MH-Z14 (NDIR) sensor via UART-TTL, with a typical 0 to 5000 ppm range and nominal specification of $\pm(50\text{ ppm} + 3\%\text{ of reading})$ [5, 6].

Time synchronization and tolerance to power interruptions were supported by a DS3231 RTC with a backup battery (I^2C) [7–10]. Electrical consumption was measured with a PZEM-004T V3 module (voltage, current, power, and energy) via UART-TTL [11]. Lighting control used four channels driven by an MCP4725 DAC (12-bit) via I^2C, utilizing EEPROM to restore the last setpoint [12, 13].

The main interconnections were SPI (microSD), I^2C (RTC/DAC), and UART/TTL (sensors/electrical metering). Figure 2 summarizes module interconnections and the physical segregation of the electronics compartment.

1

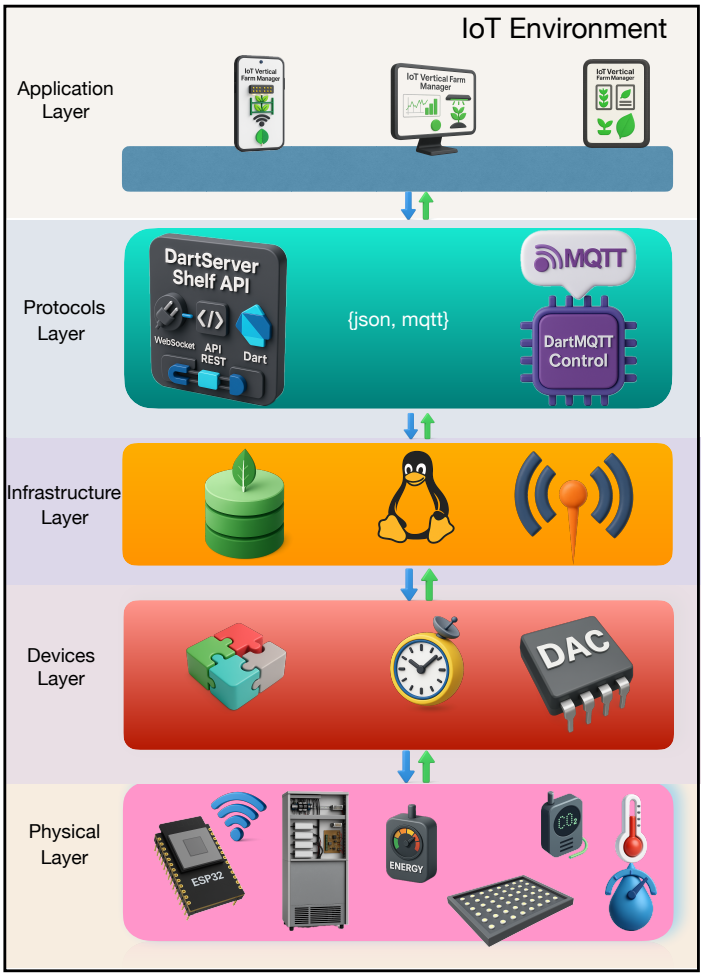

Figure 1: PVFS five-layer architecture. **Physical**: ESP32, environmental sensors (temperature, relative humidity, and CO_2), electrical metering, and LED fixtures. **Devices**: non-blocking firmware (FreeRTOS), NTP time synchronization with RTC fallback, and dimming via MCP4725 DAC (12-bit; 0–100%). **Infrastructure**: Mosquitto (publish/subscribe model) and MongoDB (document-oriented storage and aggregations). **Protocols**: DartMQTT Control and server-side Dart Shelf API. **Application**: *IoT Vertical Farm Manager* for configuration, near real-time telemetry, and data export.

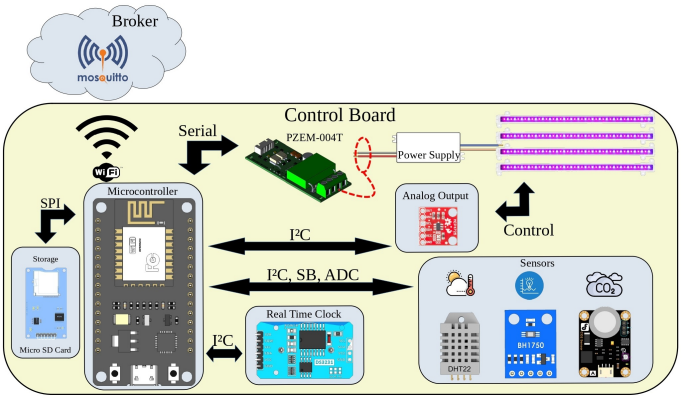

Figure 2: PVFS hardware architecture. Interconnections: SPI (microSD), I²C (DS3231/RTC and MCP4725/DAC), UART/TTL (PZEM-004T V3), and analog outputs for dimming. The electronics compartment was isolated from the cultivation area to reduce interference and improve operational safety.

The growth chamber was adapted from an upright freezer, with an external upper compartment dedicated to the electronics assembly (Figure 3).

S3. Devices layer: firmware, time synchronization, and message format

ESP32 controllers ran non-blocking firmware under FreeRTOS for the continuous acquisition of environmental variables and application of lighting setpoints. Time was synchronized via NTP with RTC fallback; records were timestamped in UTC using ISO-8601 format.

Device–server communication used MQTT in a publish/subscribe model. Messages were transmitted as `JSON` with a structured *payload*, including device/topic identifier, `timestamp`, `metric`, `value`, `unit`, and `status`. The physical integration of the growth chamber and embedded system, including an overview of the chamber and the electronics panel, is shown in Figure 3.

S4. Infrastructure layer: messaging and data persistence

The infrastructure layer provided messaging and persistence through Mosquitto (MQTT *broker*) and MongoDB (document-oriented database). Services ran in

(a) Overview of the growth chamber.

(b) Electronics panel with ESP32 and control modules.

Figure 3: Integration between the growth chamber structure and the embedded system.

Docker containers (Docker Compose), with configuration files and persistent volumes under version control.

Telemetry was persisted in MongoDB with UTC timestamps (ISO-8601), preserving raw records for auditing and time-based queries. Database aggregations supported summarization and queries at multiple granularities. Mosquitto mediated telemetry and commands via publish/subscribe, with access control and TLS support where applicable.

S5. Protocols layer: Dart modules, aggregation, and reconnection

The *Protocols* layer integrated two *Dart* modules: *DartMQTT Control* (MQTT collection/publication and session management) and the server-side *Dart Shelf API* (application services and persistence). Telemetry was aggregated using mean values over 10 s windows, reducing traffic and producing series suitable for visualization and analysis; during disconnections, automatic reconnection with *exponential backoff* was applied. The API provided REST and WebSocket endpoints for near real-time queries and notifications.

S6. Application layer: treatment setup, monitoring, and export

The application layer was implemented in the *IoT Vertical Farm Manager* software, developed in *Flutter* (*Dart*) (Figure 4). The app was used to (i) configure lighting protocols, (ii) monitor near real-time telemetry, and (iii) export data (`CSV/JSON`). Historical queries and events were accessed via REST and WebSocket, and configuration commands were transmitted via MQTT. For each experimental treatment, the app generated a per-channel schedule $[t, \mathrm{dim}\%]$ and transmitted it to the controllers.

The source code for firmware, services, application, and analysis scripts will be made publicly available on GitHub upon completion of the peer-review process.

S7. Sensitivity of daily DLI to the Δt integration cap

Rationale.. Daily light integral (DLI) was computed by integrating PPFD telemetry over the photoperiod. Because real-world IoT streams may contain occasional sampling dropouts, the forward time step Δt between consecutive samples can become artificially large. A common mitigation is to cap Δt to a maximum value, limiting the implicit "sample-and-hold" assumption across long gaps. However, for time-varying profiles (e.g., Gaussian), an overly strict cap could, in principle, underestimate DLI. To quantify this potential bias, we performed a sensitivity analysis using alternative Δt caps.

Methods.. Using the Gaussian-profile telemetry window (2024-03-22 to 2024-04-01; photoperiod 06:30–18:30, local time), we recomputed daily DLI for each PPFD channel under three settings: cap = 60 s, cap = 120 s (main analysis), and no cap. In all cases, integration was clipped to the photoperiod end to avoid night-gap inflation. Daily DLI was computed as:

$$\mathrm{DLI} = \sum_i \mathrm{PPFD}_i \cdot \min(\Delta t_i, \Delta t_{\max})/10^6,$$

with $\Delta t_{\max} \in \{60\ \mathrm{s}, 120\ \mathrm{s}, \infty\}$.

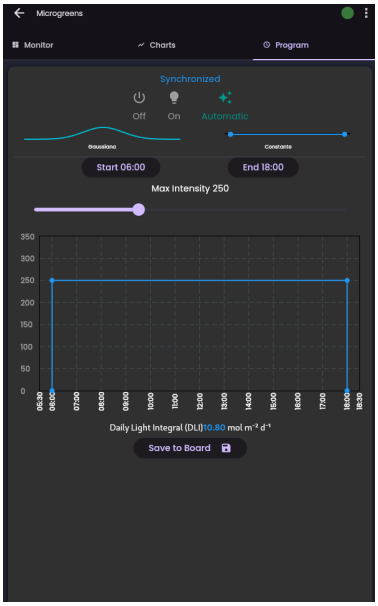

(a) Constant profile.

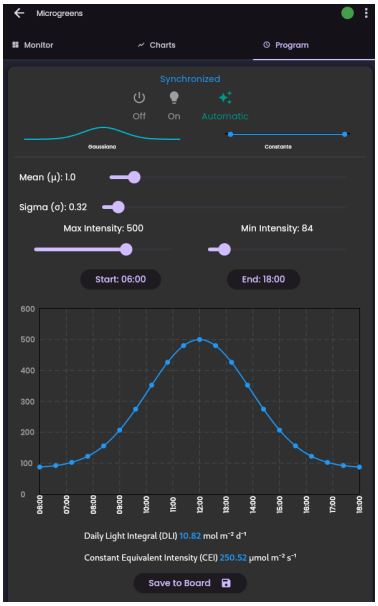

(b) Gaussian profile.

(c) Real-time telemetry dashboard.

Figure 4: *IoT Vertical Farm Manager* interface: (A) Constant profile; (B) Gaussian profile; (C) real-time telemetry (per-channel dimming, PPFD, temperature, relative humidity, CO_2, power, energy, power factor, and Wi-Fi signal strength; RSSI, dBm).

Across all channels and days (44 channel-days), the absolute percent difference between cap = 120 s and cap = 60 s had a median of 0.0000% and a maximum of 0.1801% (i.e., ≤ 0.0195 mol m^{-2} d^{-1}), with no channel-day exceeding 0.5% (Table 1). Relative to the no-cap baseline, cap = 120 s showed a median absolute difference of 0.0000%. The maximum difference (6.9773%) occurred on a single day (2024-03-30) when photoperiod completeness dropped to 3701 samples (approximately 85.7% of the expected 10 s cadence), indicating a severe dropout. In this case, the no-cap formulation effectively extends the last observation across long gaps (sample-and-hold), inflating DLI, whereas the capped integration yields a conservative estimate that does not over-credit DLI during telemetry outages. Excluding this dropout day, the maximum absolute difference between no-cap and cap = 120 s was $\leq 0.0188\%$ (approximately 0.0020 mol m^{-2} d^{-1}).

Finally, equivalence testing (TOST) versus the target DLI (10.8 mol m^{-2} d^{-1} with a $\pm 5\%$ margin) was satisfied for all cap settings across channels (Table 2), indicating that the study conclusions regarding DLI compliance are robust to the choice of the Δt cap within the observed telemetry quality regime.

Table 1: Sensitivity of daily DLI to the integration cap on Δt. Values report absolute percent differences between cap settings.

MQTT topic	Channel	Days	Median $\lvert\%\Delta\rvert$ (120 vs 60)	Max $\lvert\%\Delta\rvert$ (120 vs 60)	Days $\lvert\%\Delta\rvert > 0.5$ (120 vs 60)	Median $\lvert\%\Delta\rvert$ (no-cap vs 120)	Max $\lvert\%\Delta\rvert$ (no-cap vs 120)	Days $\lvert\%\Delta\rvert > 0.5$ (no-cap vs 120)
sc5/ppfd_total_ch1	ch1	11	0.0000	0.1790	0.0000	0.0000	6.8968	1.0000
sc5/ppfd_total_ch2	ch2	11	0.0000	0.1798	0.0000	0.0000	6.9467	1.0000
sc5/ppfd_total_ch3	ch3	11	0.0000	0.1801	0.0000	0.0000	6.9773	1.0000
sc5/ppfd_total_ch4	ch4	11	0.0000	0.1793	0.0000	0.0000	6.9361	1.0000

S8. Environmental microclimate stability during the experimental windows

Rationale.. To complement the telemetry-based validation of PPFD execution and address the potential influence of lighting dynamics on the chamber microenvironment, we examined the stability of air temperature, relative humidity, and CO_2 concentration during the Constant and Gaussian experimental windows. Because dynamic PPFD profiles may alter transpiration demand and, consequently, the chamber microclimate, these variables were evaluated as additional

Table 2: Equivalence (TOST) of daily DLI versus the target across Δt cap settings.

MQTT topic	Channel	Cap	Target	Δ	n	Mean	SD	$CI_{90,low}$	$CI_{90,high}$	p_{equiv}	Equivalent
sc5/ppfd_total_ch1	ch1	nocap	10.8000	0.5400	11.0000	10.8100	0.0273	10.7951	10.8249	0.0000	1.0000
sc5/ppfd_total_ch1	ch1	cap60	10.8000	0.5400	11.0000	10.7367	0.2002	10.6273	10.8461	0.0000	1.0000
sc5/ppfd_total_ch1	ch1	cap120	10.8000	0.5400	11.0000	10.7414	0.1991	10.6326	10.8502	0.0000	1.0000
sc5/ppfd_total_ch2	ch2	nocap	10.8000	0.5400	11.0000	10.8114	0.0281	10.7960	10.8267	0.0000	1.0000
sc5/ppfd_total_ch2	ch2	cap60	10.8000	0.5400	11.0000	10.7375	0.2011	10.6276	10.8474	0.0000	1.0000
sc5/ppfd_total_ch2	ch2	cap120	10.8000	0.5400	11.0000	10.7422	0.2000	10.6329	10.8515	0.0000	1.0000
sc5/ppfd_total_ch3	ch3	nocap	10.8000	0.5400	11.0000	10.8131	0.0299	10.7968	10.8294	0.0000	1.0000
sc5/ppfd_total_ch3	ch3	cap60	10.8000	0.5400	11.0000	10.7389	0.2005	10.6293	10.8485	0.0000	1.0000
sc5/ppfd_total_ch3	ch3	cap120	10.8000	0.5400	11.0000	10.7436	0.1994	10.6346	10.8526	0.0000	1.0000
sc5/ppfd_total_ch4	ch4	nocap	10.8000	0.5400	11.0000	10.8275	0.0262	10.8132	10.8419	0.0000	1.0000
sc5/ppfd_total_ch4	ch4	cap60	10.8000	0.5400	11.0000	10.7537	0.2028	10.6429	10.8646	0.0000	1.0000
sc5/ppfd_total_ch4	ch4	cap120	10.8000	0.5400	11.0000	10.7584	0.2018	10.6481	10.8687	0.0000	1.0000

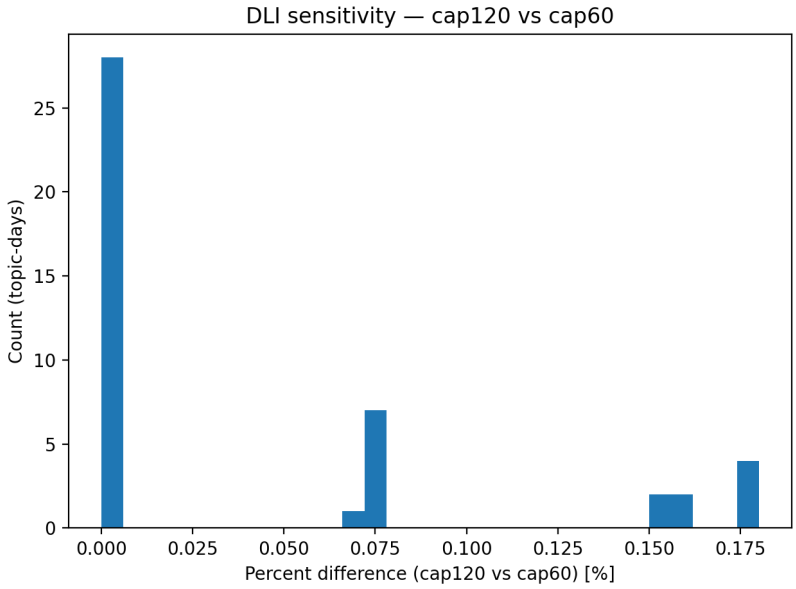

Figure 5: Distribution of absolute percent differences in daily DLI between cap = 120 s and cap = 60 s across all channels and days.

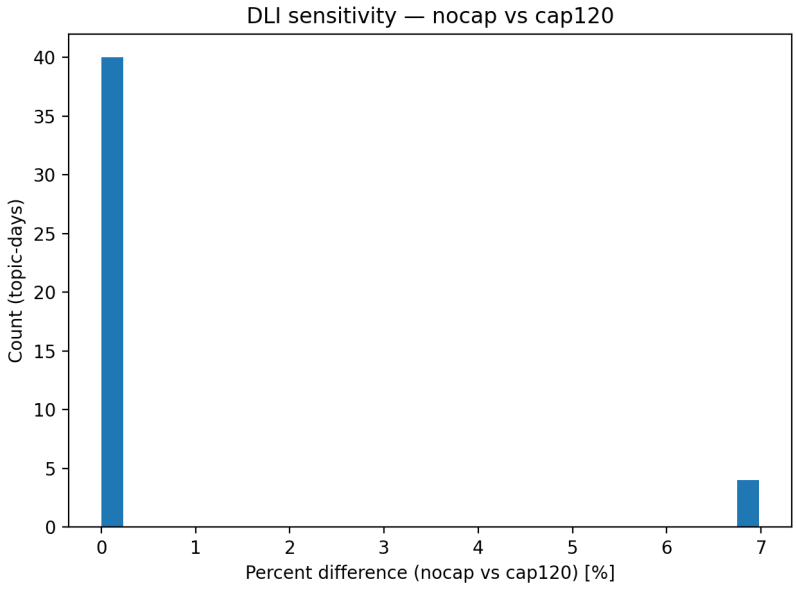

Figure 6: Distribution of absolute percent differences in daily DLI between no-cap and cap = 120 s across all channels and days. The tail is driven by a single day with a severe telemetry dropout (2024-03-30).

contextual descriptors of the experimental conditions.

Methods.. Environmental telemetry was extracted from the same PVFS database used for the main validation workflow. For visualization purposes, time series were resampled and screened using predefined validity bounds, followed by a rolling median/MAD despiking procedure to reduce the influence of obvious sensor artifacts while preserving the original temporal structure of the data. We then summarized the cleaned telemetry by window using central tendency and dispersion metrics and generated two complementary visualizations: (i) daily median with P5–P95 envelopes, and (ii) photoperiod diurnal profiles expressed as median ± IQR. These analyses were intended to document the stability of the chamber microenvironment during the two lighting windows rather than to infer causal effects independently of the lighting treatment. For the cleaned visualization workflow used in this section, CO_2 telemetry was evaluated using an operational upper screening threshold of 2000 ppm; therefore, the 2000 ppm limit discussed below refers to the analytical threshold adopted for visualization and window-level stability summaries, not to the nominal hardware range of the MH-Z14 sensor described in Section S2. Raw telemetry remained archived and was not overwritten.

Results and interpretation.. Air temperature remained close to the nominal setpoint in both windows, with highly similar mean values (24.67 °C under Constant and 24.68 °C under Gaussian) and low coefficients of variation (1.19 % and 1.53 %, respectively), indicating stable thermal control throughout the experiment. The photoperiod profiles also showed only modest intradiurnal variation, although the Gaussian window exhibited a slightly broader thermal excursion around midday.

Relative humidity was continuously monitored in both windows and showed greater intradiurnal variation than temperature. Under the Constant window, mean relative humidity was 86.84 % (CV = 9.54 %), whereas under the Gaussian window it was 86.25 % (CV = 15.89 %). The diurnal overlays revealed a more pronounced midday depression in relative humidity during the Gaussian window,

consistent with a stronger transient evaporative demand under dynamic PPFD. Thus, although the thermal regime remained stable, the humidity profiles suggest that the temporal shape of light delivery may have influenced the chamber microenvironment during the photoperiod.

CO_2 concentration was also logged throughout both windows. However, its interpretation was limited by the frequent occurrence of readings at the upper analytical threshold (2000 ppm), which represented approximately 52.0 % of the cleaned records under Constant and 51.6 % under Gaussian. For this reason, CO_2 telemetry is presented here as a monitored contextual variable, but not as the primary basis for claiming environmental stability between lighting windows.

Overall, these supplementary analyses indicate that the experiment was conducted under a stable thermal regime, while relative humidity displayed structured intradiurnal variation that was more pronounced under the Gaussian profile. This supports the interpretation that the observed treatment effects were generated under monitored and documented chamber conditions, while also acknowledging that dynamic lighting may modulate the microenvironment through humidity-related responses.

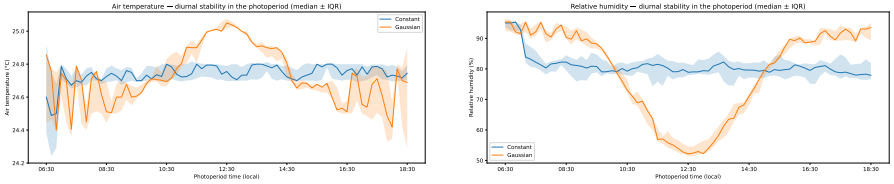

(a) Air temperature during the photoperiod (median ± IQR).

(b) Relative humidity during the photoperiod (median ± IQR).

Figure 7: Supplementary characterization of chamber microclimate during the Constant and Gaussian windows. Temperature remained close to the nominal setpoint in both windows, whereas relative humidity showed a stronger intradiurnal depression under the Gaussian profile, especially around midday.

Table 3: Summary of cleaned environmental telemetry by experimental window. Temperature and relative humidity are emphasized as primary descriptors of chamber stability, whereas CO_2 interpretation is limited by frequent readings at the upper analytical threshold used in the cleaned visualization workflow.

Variable	Window	Mean	SD	CV (%)	Notes
Air temperature (°C)	Constant	24.67	0.29	1.19	Stable around setpoint
Air temperature (°C)	Gaussian	24.68	0.38	1.53	Slightly broader midday excursion
Relative humidity (%)	Constant	86.84	8.28	9.54	Moderate intradiurnal variation
Relative humidity (%)	Gaussian	86.25	13.71	15.89	Stronger midday depression
CO_2 (ppm)	Constant	1372.89	784.03	57.11	52.0% at upper threshold (2000 ppm)
CO_2 (ppm)	Gaussian	1493.90	676.74	45.30	51.6% at upper threshold (2000 ppm)

References

[1] A. Morchid, R. Jebabra, H. M. Khalid, R. El Alami, H. Qjidaa, M. Ouazzani Jamil, Iot-based smart irrigation management system to enhance agricultural water security using embedded systems, telemetry data, and cloud computing, Results in Engineering 23 (2024) 102829. doi:https://doi.org/10.1016/j.rineng.2024.102829.
URL https://www.sciencedirect.com/science/article/pii/S2590123024010843

[2] T. S. Gunawan, N. N. Kamarudin, M. Kartiwi, M. R. Effendi, Automatic watering system for smart agriculture using esp32 platform, in: 2022 IEEE 8th International Conference on Smart Instrumentation, Measurement and Applications (ICSIMA), Melaka, Malaysia, 2022, pp. 185–189. doi:10.1109/ICSIMA55652.2022.9928950.

[3] A. Saxena, A. Agarwal, B. Nagrath, C. S. Jayavanth, S. Thulasidoss, S. Maheswari, P. Sasikumar, Deep learning-driven iot solution for smart tomato farming, Scientific Reports 15 (2025) 31092. doi:10.1038/s41598-025-15615-3.
URL https://doi.org/10.1038/s41598-025-15615-3

[4] J. A. Abdinoor, Z. K. Hashim, B. Horváth, S. Zsebő, D. Stencinger, G. Hegedüs, L. Bede, A. Ijaz, I. M. Kulmány, Performance of low-cost air temperature sensors and applied calibration techniques—a systematic review, Atmosphere 16 (7) (2025) 842. doi:10.3390/atmos16070842.
URL https://doi.org/10.3390/atmos16070842

[5] R. Macagga, M. Asante, G. Sossa, D. Antonijević, M. Dubbert, M. Hoffmann, Validation and field application of a low-cost device to measure co_2 and evapotranspiration (et) fluxes, Atmospheric Measurement Techniques 17 (4) (2024) 1317–1332. doi:10.5194/amt-17-1317-2024.
URL https://amt.copernicus.org/articles/17/1317/2024/

[6] M. Dalvai Ragnoli, G. Singer, The river runner: a low-cost sensor prototype for continuous dissolved greenhouse gas measurements, Journal of Sensors and Sensor Systems 13 (2024) 41–61. doi:10.5194/jsss-13-41-2024.

[7] S. Wang, Z. Li, et al., A wireless real-time continuous monitoring system for the internal movements of mountain glaciers using sensor networks, Sensors 22 (23) (2022) 9061. doi:10.3390/s22239061.
URL https://www.mdpi.com/1424-8220/22/23/9061

[8] M. Romoli, et al., A wireless gamma-ray monitoring system for cemented radwaste drums, Sensors 24 (7) (2024) 2332. doi:10.3390/s24072332.
URL https://www.mdpi.com/1424-8220/24/7/2332

[9] B. Nguyen, B. Goto, J. S. Selker, C. Udell, Hypnos board: A low-cost all-in-one solution for environment sensor power management, data storage, and task scheduling, HardwareX 10 (2021) e00213. doi:10.1016/j.ohx.2021.e00213.
URL https://pmc.ncbi.nlm.nih.gov/articles/PMC9123445/

[10] H. J. Jumaah, et al., Development of uav-based $pm_{2.5}$ monitoring system, Drones 5 (3) (2021) 60. doi:10.3390/drones5030060.
URL https://www.mdpi.com/2504-446X/5/3/60

[11] G. B, S. George, Iot based smart energy management system using pzem-004t sensor & node mcu, International Journal of Engineering Research & Technology (IJERT) 9 (7) (2021) 45–48. doi:10.17577/IJERTCONV9IS07011.
URL https://www.ijert.org/iot-based-smart-energy-management-system-using-pzem-004t-sensor-node-mcu

[12] M. T. Inc., Mcp4725 12-bit digital-to-analog converter with eeprom (2024).
URL https://www.alldatasheet.com/datasheet-pdf/view/233449/MICROCHIP/MCP4725.html

[13] C. G. C. Carducci, A. Monti, M. H. Schraven, M. Schumacher, D. Mueller, Enabling esp32-based iot applications in building automation systems, in: 2019 II Workshop on Metrology for Industry 4.0 and IoT (MetroInd4.0&IoT), Naples, Italy, 2019, pp. 306–311. doi:10.1109/METROI4.2019.8792852.

4 Registros de software associados ao desenvolvimento da tese

Os trabalhos científicos que compõem esta tese estão diretamente vinculados à produção tecnológica desenvolvida ao longo da pesquisa. Além da avaliação agronômica dos efeitos da iluminação artificial sobre microverdes, o estudo exigiu a concepção e a aplicação de soluções computacionais voltadas ao controle, monitoramento, aquisição, armazenamento e análise de dados em sistemas de agricultura vertical de precisão.

Esses softwares constituem parte integrante da contribuição metodológica e tecnológica da tese, pois permitiram executar protocolos de cultivo com maior precisão, registrar variáveis ambientais e operacionais e assegurar a rastreabilidade dos dados experimentais. Assim, os registros apresentados neste capítulo não devem ser entendidos como produtos acessórios, mas como componentes que sustentaram a condução dos experimentos e a consolidação da arquitetura proposta.

No artigo *Growing in red: impact of different light spectra and lighting conditions on lentil microgreens growth in vertical farming*, foram investigados os efeitos de diferentes espectros luminosos e regimes temporais de iluminação sobre o crescimento, a fisiologia, a produção de biomassa, os pigmentos fotossintéticos e a eficiência energética de microverdes de lentilha cultivados em ambiente vertical controlado. Os resultados demonstraram que o manejo da luz interfere significativamente nas respostas morfofisiológicas e produtivas das plantas, reforçando a necessidade de sistemas capazes de executar tratamentos luminosos com precisão, repetibilidade e rastreabilidade.

No artigo *An open-architecture precision vertical farming system for sesame microgreens: Audit-ready telemetry for dynamic lighting and energy–biomass benchmarking*, essa abordagem foi ampliada por meio do desenvolvimento e da validação de uma arquitetura aberta de agricultura vertical de precisão. A arquitetura integrou controle ambiental, execução de perfis dinâmicos de PPFD, aquisição de telemetria auditável, armazenamento estruturado de dados e avaliação de métricas agronômicas e energéticas. Com isso, a pesquisa avançou de uma análise centrada apenas na resposta vegetal para uma abordagem integrada entre planta, energia, automação, dados e rastreabilidade operacional.

Nesse contexto, os registros de software formalizam os principais componentes digitais desenvolvidos no âmbito da tese. O *IoT Vertical Farm Manager* foi criado para o gerenciamento e a configuração de ambientes de cultivo protegido, apoiando o acompanhamento de variáveis ambientais e a condução de protocolos experimentais. A *IoT Control API* viabilizou a comunicação entre dispositivos, serviços e aplicações, fortalecendo a integração entre sensores, atuadores,

banco de dados e interfaces de supervisão.

A *Plataforma Avançada de Gerenciamento e Monitoramento IoT com MQTT e Registro Dinâmico de Dados Ambientais* consolidou a camada de comunicação e registro das variáveis ambientais, utilizando MQTT para organizar o fluxo de mensagens entre os dispositivos e a infraestrutura de armazenamento. De forma complementar, o *Dashboard Inteligente para Dispositivos IoT Utilizando Linux* contribuiu para a visualização e supervisão das informações coletadas, enquanto o *Software de gerenciamento e registro de ambientes de internet das coisas* reforçou a organização dos dados provenientes dos dispositivos conectados.

Além dos softwares voltados ao controle e monitoramento do ambiente, o *ImagingWin-GigE Data Analyzer: Potencializando Insights com Médias Dinâmicas* ampliou a dimensão analítica da pesquisa, apoiando o processamento, a interpretação e a extração de informações a partir dos dados gerados. Em conjunto, esses produtos demonstram que o desenvolvimento tecnológico da tese envolveu não apenas o controle físico do ambiente de cultivo, mas também a aquisição, organização, visualização e análise das informações experimentais.

A relevância desses registros está na transformação da estrutura física de cultivo em uma plataforma experimental inteligente, modular e reprodutível. A integração entre sensores, atuadores, comunicação em rede, armazenamento persistente e interfaces de usuário permitiu maior controle sobre a execução dos tratamentos e maior confiabilidade na interpretação dos resultados, especialmente em experimentos com iluminação dinâmica.

Assim, os registros de software apresentados neste capítulo materializam a dimensão aplicada e inovadora da tese. Eles evidenciam que a pesquisa resultou não apenas em conhecimento agronômico sobre microverdes, mas também em produtos tecnológicos voltados à automação, ao monitoramento, à gestão e à análise de sistemas de agricultura vertical de precisão.

A seguir, são apresentados os certificados de registro de programa de computador associados aos produtos tecnológicos desenvolvidos no contexto desta tese. Esses documentos comprovam a formalização institucional dos softwares e reforçam o caráter aplicado, tecnológico e interdisciplinar da arquitetura proposta.

REPÚBLICA FEDERATIVA DO BRASIL
MINISTÉRIO DO DESENVOLVIMENTO, INDÚSTRIA, COMÉRCIO E SERVIÇOS
INSTITUTO NACIONAL DA PROPRIEDADE INDUSTRIAL
DIRETORIA DE PATENTES, PROGRAMAS DE COMPUTADOR E TOPOGRAFIAS DE CIRCUITOS

Certificado de Registro de Programa de Computador

Processo Nº: **BR512024002843-9**

O Instituto Nacional da Propriedade Industrial expede o presente certificado de registro de programa de computador, válido por 50 anos a partir de 1° de janeiro subsequente à data de 03/10/2023, em conformidade com o §2°, art. 2° da Lei 9.609, de 19 de Fevereiro de 1998.

Título: Software de gerenciamento e registro de ambientes de internet das coisas

Data de publicação: 03/10/2023

Data de criação: 02/10/2023

Titular(es): INSTITUTO FEDERAL DE EDUCAÇÃO, CIÊNCIA E TECNOLOGIA GOIANO

Autor(es): VINÍCIUS MAGALHÃES DE QUEIROZ; RAFAEL CARVALHO DE MENDONÇA; MARLUS DIAS SILVA; ADRIANO SOARES DE OLIVEIRA BAILÃO; FABIANO GUIMARÃES SILVA; FÁBIA BARBOSA DA SILVA

Linguagem: OUTROS

Campo de aplicação: AG-06

Tipo de programa: GI-01

Algoritmo hash: SHA-512

Resumo digital hash:
6df75af65531504179b42c7e28c6e868906358e811b5bf5bfeff800ecea0f6118c002512a045119e7aad4a5ab13636a9d08
97962b70bcf83aef624552d362622

Expedido em: 13/08/2024

Aprovado por:
Carlos Alexandre Fernandes Silva
Chefe da DIPTO

REPÚBLICA FEDERATIVA DO BRASIL
MINISTÉRIO DO DESENVOLVIMENTO, INDÚSTRIA, COMÉRCIO E SERVIÇOS
INSTITUTO NACIONAL DA PROPRIEDADE INDUSTRIAL
DIRETORIA DE PATENTES, PROGRAMAS DE COMPUTADOR E TOPOGRAFIAS DE CIRCUITOS

Certificado de Registro de Programa de Computador

Processo Nº: **BR512024003275-4**

O Instituto Nacional da Propriedade Industrial expede o presente certificado de registro de programa de computador, válido por 50 anos a partir de 1° de janeiro subsequente à data de 10/02/2024, em conformidade com o §2°, art. 2° da Lei 9.609, de 19 de Fevereiro de 1998.

Título: Dashboard Inteligente para Dispositivos IoT Utilizando Linux

Data de publicação: 10/02/2024

Data de criação: 01/02/2024

Titular(es): INSTITUTO FEDERAL DE EDUCAÇÃO, CIÊNCIA E TECNOLOGIA GOIANO

Autor(es): MARLUS DIAS SILVA; ADRIANO SOARES DE OLIVEIRA BAILÃO; FABIANO GUIMARÃES SILVA; BRUNO ANTUNES MARTINS

Linguagem: OUTROS

Campo de aplicação: AG-05

Tipo de programa: GI-01

Algoritmo hash: SHA-512

Resumo digital hash:
09dd85c344fd9e8ab17cdcd7cd82d660a060fdbfd2c4fa951b32a2e552b048a17115e50c5bde43e715a8789c14de8ab95c559d7841aef75f509e80ef9aa4b56d

Expedido em: 17/09/2024

Aprovado por:
Carlos Alexandre Fernandes Silva
Chefe da DIPTO

REPÚBLICA FEDERATIVA DO BRASIL
MINISTÉRIO DO DESENVOLVIMENTO, INDÚSTRIA, COMÉRCIO E SERVIÇOS
INSTITUTO NACIONAL DA PROPRIEDADE INDUSTRIAL
DIRETORIA DE PATENTES, PROGRAMAS DE COMPUTADOR E TOPOGRAFIAS DE CIRCUITOS

Certificado de Registro de Programa de Computador

Processo Nº: **BR512024003278-9**

O Instituto Nacional da Propriedade Industrial expede o presente certificado de registro de programa de computador, válido por 50 anos a partir de 1° de janeiro subsequente à data de 20/02/2024, em conformidade com o §2°, art. 2° da Lei 9.609, de 19 de Fevereiro de 1998.

Título: Plataforma Avançada de Gerenciamento e Monitoramento IoT com MQTT e Registro Dinâmico de Dados Ambientais

Data de publicação: 20/02/2024

Data de criação: 10/02/2024

Titular(es): INSTITUTO FEDERAL DE EDUCAÇÃO, CIÊNCIA E TECNOLOGIA GOIANO

Autor(es): LEANDRO RODRIGUES DA SILVA SOUZA; MARLUS DIAS SILVA; ADRIANO SOARES DE OLIVEIRA BAILÃO; FABIANO GUIMARÃES SILVA

Linguagem: OUTROS

Campo de aplicação: IF-10

Tipo de programa: AT-06

Algoritmo hash: SHA-512

Resumo digital hash:
e3be6a4011ce135874907c12dd4a387e56e24d4841996f7a8cedda771d3029ce0253a8717f16cd064ccf1a6c25afb7b424a13bc63e0f25e6b9852a8a57ec39fa

Expedido em: 17/09/2024

Aprovado por:
Carlos Alexandre Fernandes Silva
Chefe da DIPTO

REPÚBLICA FEDERATIVA DO BRASIL
MINISTÉRIO DO DESENVOLVIMENTO, INDÚSTRIA, COMÉRCIO E SERVIÇOS
INSTITUTO NACIONAL DA PROPRIEDADE INDUSTRIAL
DIRETORIA DE PATENTES, PROGRAMAS DE COMPUTADOR E TOPOGRAFIAS DE CIRCUITOS

Certificado de Registro de Programa de Computador

Processo Nº: **BR512024003310-6**

O Instituto Nacional da Propriedade Industrial expede o presente certificado de registro de programa de computador, válido por 50 anos a partir de 1° de janeiro subsequente à data de 10/02/2024, em conformidade com o §2°, art. 2° da Lei 9.609, de 19 de Fevereiro de 1998.

Título: IoT Control API

Data de publicação: 10/02/2024

Data de criação: 01/02/2024

Titular(es): INSTITUTO FEDERAL DE EDUCAÇÃO, CIÊNCIA E TECNOLOGIA GOIANO

Autor(es): MARLUS DIAS SILVA; ADRIANO SOARES DE OLIVEIRA BAILÃO; FABIANO GUIMARÃES SILVA; FÁBIA BARBOSA DA SILVA; JAQUELINE MARTINS VASCONCELOS

Linguagem: OUTROS

Campo de aplicação: IF-10

Tipo de programa: IA-02

Algoritmo hash: SHA-512

Resumo digital hash:
a846426a73f8836c525743591fbd49eba572c77c80496c041b135f35217f046c7b472b921e4935b8fd98bcebab6b7cbb48d92e8a7a339461576c399de745198a

Expedido em: 17/09/2024

Aprovado por:
Carlos Alexandre Fernandes Silva
Chefe da DIPTO

REPÚBLICA FEDERATIVA DO BRASIL
MINISTÉRIO DO DESENVOLVIMENTO, INDÚSTRIA, COMÉRCIO E SERVIÇOS
INSTITUTO NACIONAL DA PROPRIEDADE INDUSTRIAL
DIRETORIA DE PATENTES, PROGRAMAS DE COMPUTADOR E TOPOGRAFIAS DE CIRCUITOS

Certificado de Registro de Programa de Computador

Processo Nº: **BR512025001070-2**

O Instituto Nacional da Propriedade Industrial expede o presente certificado de registro de programa de computador, válido por 50 anos a partir de 1° de janeiro subsequente à data de 01/02/2024, em conformidade com o §2°, art. 2° da Lei 9.609, de 19 de Fevereiro de 1998.

Título: IoT Vertical Farm Manager: Aplicativo Android para Agricultura Vertical

Data de publicação: 01/02/2024

Data de criação: 20/01/2024

Titular(es): INSTITUTO FEDERAL DE EDUCAÇÃO, CIÊNCIA E TECNOLOGIA GOIANO

Autor(es): MARLUS DIAS SILVA; ADRIANO SOARES DE OLIVEIRA BAILÃO; FABIANO GUIMARÃES SILVA; FÁBIA BARBOSA DA SILVA; JAQUELINE MARTINS VASCONCELOS; ÍTALO MORAES ROCHA GUEDES; MARCIO ROSA

Linguagem: OUTROS

Campo de aplicação: IF-10

Tipo de programa: AP-01

Algoritmo hash: SHA-512

Resumo digital hash:
7f2176ea2cc9cd97f4d6ecf4132aa64cafefcf3fc3441b12b583684d1430d6f97dcae0f1b6924506ce709d8d220c7c26f0ae59cfdc79e204eb020c700f0e1b57

Expedido em: 25/03/2025

Aprovado por:
Carlos Alexandre Fernandes Silva
Chefe da DIPTO

REPÚBLICA FEDERATIVA DO BRASIL
MINISTÉRIO DO DESENVOLVIMENTO, INDÚSTRIA, COMÉRCIO E SERVIÇOS
INSTITUTO NACIONAL DA PROPRIEDADE INDUSTRIAL
DIRETORIA DE PATENTES, PROGRAMAS DE COMPUTADOR E TOPOGRAFIAS DE CIRCUITOS

Certificado de Registro de Programa de Computador

Processo Nº: **BR512026001117-5**

O Instituto Nacional da Propriedade Industrial expede o presente certificado de registro de programa de computador, válido por 50 anos a partir de 1° de janeiro subsequente à data de 26/04/2024, em conformidade com o §2°, art. 2° da Lei 9.609, de 19 de Fevereiro de 1998.

Título: ImagingWinGigE Data Analyzer: Potencializando Insights com Médias Dinâmicas

Data de publicação: 26/04/2024

Data de criação: 25/04/2024

Titular(es): INSTITUTO FEDERAL DE EDUCAÇÃO, CIÊNCIA E TECNOLOGIA GOIANO

Autor(es): MARLUS DIAS SILVA; ADRIANO SOARES DE OLIVEIRA BAILÃO; FABIANO GUIMARÃES SILVA; FÁBIA BARBOSA DA SILVA; JAQUELINE MARTINS VASCONCELOS; MÁRCIO ROSA; ITALO MORAES ROCHA GUEDES

Linguagem: OUTROS

Campo de aplicação: BT-01

Tipo de programa: FA-01

Algoritmo hash: SHA-512

Resumo digital hash:
8835a1c087c6c3296891ca44064ae363127eec2c6885177ae4922e323db83972afec8e07fac2dbdc03746c484c77c9df34f1b564e9e10e1f1073117a55ebb864

Expedido em: 03/03/2026

Aprovado por:
ERICA GUIMARAES CORREA
Chefe da Divisão de Programas de Computador e Topografias de Circuitos Integrados

5 Conclusão

Esta tese demonstrou que o avanço da agricultura vertical de precisão depende da integração entre resposta biológica, eficiência energética e infraestrutura digital auditável. Os resultados obtidos indicam que, em sistemas de produção vegetal em ambiente controlado, não é suficiente identificar estratégias capazes de promover crescimento vegetal; é necessário verificar, com rastreabilidade operacional e critério energético, quais estratégias apresentam melhor relação entre desempenho agronômico e energia consumida.

No estudo com microverdes de lentilha, verificou-se que a interação entre qualidade espectral e regime temporal de fornecimento da luz influenciou diretamente o crescimento, a produção de biomassa, os pigmentos fotossintéticos e parâmetros associados ao desempenho fisiológico das plantas. De modo geral, os regimes constantes favoreceram maior produção de biomassa e melhor eficiência energética, especialmente sob luz vermelha, branca e RBW, enquanto o regime gaussiano apresentou maior potencial para estimular o acúmulo de carotenoides. Esses resultados evidenciam que a escolha da estratégia luminosa deve estar vinculada ao objetivo produtivo do sistema, seja ele maximizar biomassa, favorecer atributos funcionais ou melhorar a racionalidade energética do cultivo.

No estudo com microverdes de gergelim, a contribuição foi ampliada por meio do desenvolvimento e da validação do *Precision Vertical Farming System* (PVFS), uma arquitetura aberta voltada ao controle, monitoramento e registro auditável de experimentos em agricultura vertical. O sistema demonstrou capacidade de executar perfis dinâmicos de PPFD sob DLI controlado, registrar telemetria ambiental e elétrica com elevada completude de dados e integrar métricas energéticas à análise agronômica. Dessa forma, o PVFS permitiu transformar protocolos de iluminação em rotinas executáveis, monitoráveis e verificáveis, contribuindo para reduzir incertezas operacionais e fortalecer a reprodutibilidade experimental.

Um dos principais achados desta tese foi demonstrar que a equivalência de DLI não implica, necessariamente, equivalência de desempenho energético. Mesmo quando os tratamentos receberam integral luminosa diária equivalente, os perfis temporais de fornecimento da luz produziram relações distintas entre energia consumida e biomassa gerada. No estudo com gergelim, o perfil gaussiano aumentou o consumo energético por área e, em parte dos tratamentos, elevou o custo energético por biomassa sem gerar ganhos proporcionais de massa seca. Por outro lado, o tratamento Red–Constant apresentou o melhor desempenho energia–biomassa, enquanto a luz branca esteve associada aos maiores custos energéticos por unidade de biomassa.

Esses resultados reforçam que a avaliação de receitas de luz em *Plant Factories with Artificial Lighting* (PFALs) deve ir além da resposta fisiológica isolada. A pergunta central não deve ser apenas qual tratamento produz mais, mas qual tratamento apresenta melhor equilíbrio

entre produção vegetal, qualidade fisiológica, estabilidade operacional e energia consumida. Nesse sentido, métricas como *Areal Energy Consumption* (AEC), *Specific Energy Consumption* (SEC) e *Energy-to-Mass Efficiency* (EEMS) mostraram-se fundamentais para interpretar a eficiência real das estratégias de iluminação em sistemas de cultivo indoor.

A integração entre os dois artigos confirma que o manejo da luz em agricultura vertical deve ser orientado por critérios fisiológicos, produtivos, energéticos e operacionais. No estudo com lentilha, os resultados evidenciaram que diferentes combinações entre espectro e regime temporal alteram a biomassa, os pigmentos e o desempenho fisiológico das plantas. No estudo com gergelim, a instrumentação do PVFS permitiu quantificar com maior precisão a relação entre energia consumida e biomassa produzida, demonstrando que diferentes trajetórias temporais de PPFD, ainda que sob DLI equivalente, podem gerar custos energéticos e retornos produtivos distintos.

Outro aporte relevante desta tese é a demonstração de que a infraestrutura digital não constitui apenas um suporte técnico, mas parte integrante da qualidade científica do experimento. Ao integrar sensores, atuadores, controle programável, comunicação IoT, armazenamento de dados, telemetria contínua e análise energética, o PVFS ampliou a rastreabilidade, a auditabilidade e a confiabilidade dos experimentos conduzidos. Essa contribuição é especialmente importante em estudos com iluminação dinâmica, nos quais pequenas diferenças entre o protocolo planejado e o protocolo efetivamente executado podem comprometer a interpretação dos resultados.

Os registros de software associados ao desenvolvimento da tese reforçam o caráter aplicado e tecnológico da pesquisa. As ferramentas desenvolvidas e registradas demonstram que os resultados obtidos não se limitaram à análise agronômica, mas envolveram também a construção de soluções computacionais para controle, monitoramento, comunicação, armazenamento e interpretação de dados em sistemas de agricultura vertical de precisão. Dessa forma, a tese contribui tanto para o avanço científico no manejo da luz em microverdes quanto para o desenvolvimento de infraestrutura tecnológica aplicável a ambientes reais de pesquisa e produção.

As conclusões apresentadas devem ser interpretadas dentro do escopo experimental adotado, que envolveu microverdes cultivados em ciclos curtos, espécies específicas, condições controladas, fotoperíodo definido e níveis determinados de DLI. Portanto, a extrapolação dos resultados para outras espécies, estádios fenológicos, densidades de cultivo, arranjos espectrais, fotoperíodos ou intensidades luminosas deve ser realizada com cautela. Estudos futuros poderão ampliar essa abordagem por meio da avaliação de múltiplos níveis de DLI, diferentes durações de fotoperíodo, novos perfis temporais de iluminação e outras espécies cultivadas em sistemas PFAL.

Como perspectiva futura, a arquitetura desenvolvida nesta tese oferece base para a incorporação de inteligência computacional à agricultura vertical de precisão. A combinação entre telemetria contínua, histórico operacional, análise multivariada e métricas energia–biomassa pode subsidiar sistemas de recomendação de receitas de luz, detecção preditiva de falhas, ajuste

dinâmico de variáveis ambientais e otimização multicritério entre produtividade, qualidade e consumo energético.

Em síntese, esta tese oferece uma contribuição interdisciplinar ao campo da agricultura vertical de precisão ao demonstrar que a eficiência de sistemas indoor depende simultaneamente da resposta da planta, da energia necessária para produzi-la e da capacidade do sistema de registrar e validar o protocolo executado. Ao reunir evidências agronômicas, critérios energéticos, arquitetura IoT e produtos de software, o trabalho reafirma que a produção vegetal em ambiente controlado será mais robusta, eficiente e reprodutível quando for biologicamente orientada, energeticamente racional e digitalmente verificável.